Distribution Agreement

In presenting this thesis or dissertation as a partial fulfillment of the requirements for an advanced degree from Emory University, I hereby grant to Emory University and its agents the non-exclusive license to archive, make accessible, and display my thesis or dissertation in whole or in part in all forms of media, now or hereafter known, including display on the world wide web. I understand that I may select some access restrictions as part of the online submission of this thesis or dissertation. I retain all ownership rights to the copyright of the thesis or dissertation. I also retain the right to use in future works (such as articles or books) all or part of this thesis or dissertation.

Signature:

_____	_____
Gokul Raghunath	Date

Biophysics of Membrane Remodeling driven by Protein Crowding

By

Gokul Raghunath
Doctor of Philosophy

Chemistry

_____

R. Brian Dyer, Ph.D.
Advisor

_____

James T. Kindt, Ph.D.
Committee Member

_____

Khalid Salaita, Ph.D.
Committee Member

Accepted:

_____

Lisa A. Tedesco, Ph.D.
Dean of the James T. Laney School of Graduate Studies

_____

Date

Biophysics of Membrane Remodeling driven by Protein Crowding

By

Gokul Raghunath
B. Tech., Anna University, India, 2012

Advisor: R. Brian Dyer, Ph.D.

An abstract of
A dissertation submitted to the Faculty of the
James T. Laney School of Graduate Studies of Emory University
in partial fulfillment of the requirements for the degree of
Doctor of Philosophy in Chemistry
2019

Abstract

Biophysics of Membrane Remodeling driven by Protein Crowding
By Gokul Raghunath

Generation and stabilization of membrane curvature by proteins is considered to be indispensable for cellular function such as signaling, fusion and transport. Given the crowded nature of the interface, peripheral and trans-membrane proteins have been observed to trigger cellular shape changes as a consequence of their sheer density. Despite its prevalence in biology, key mechanistic details underlying membrane bending driven by protein crowding remain elusive.

In this thesis, a quantitative biophysical investigation of membrane bending driven by protein crowding is presented. We developed a quantitative fluorescence-based assay involving energy transfer between donor-tagged lipids (NBD-PE) and acceptor-tagged lipids (Rhodamine-PE) incorporated into the membrane surface. This approach provided a spectroscopic handle on membrane area expansion, thus enabling ensemble measurements in the bulk solution phase, instead of a conventional imaging-based approach. Using this methodology, we quantitatively determine the critical protein-lipid ratios at which membrane bending was triggered. We find strong coupling between the intrinsic vesicle curvature and the phase behavior of the liposomes used, indicating that curvature stress imposed by changing the vesicle diameters can affect membrane deformation. While these equilibrium measurements provide a handle over several experimental variables, little information could be obtained with regards to presence of structural intermediates that precede membrane deformation.

To address this, we quantified the association kinetics of protein binding to a liposome surface using Stopped-flow fluorescence quenching. Results from our study indicates that protein binding to lipid surface does not follow a simple bi-molecular association behavior. Instead, protein binding occurs through multiple, interconvertible conformations with varying packing densities. Finally, we extend our kinetic investigation to measure the timescales of membrane deformation using stopped-flow fluorescence. We report a complex multi-phasic behavior, with the vesicles sampling at least two intermediates before reaching its final deformed state. Subsequent biophysical investigation reveals that protein binding causes membrane thinning, before resulting in deformation of the vesicle structure. Together with the equilibrium data, our results greatly enhance the fundamental understanding of membrane deformation driven by protein crowding.

Biophysics of Membrane Remodeling driven by Protein Crowding

By

Gokul Raghunath
B. Tech., Anna University, India, 2012

Advisor: R. Brian Dyer, Ph.D.

A dissertation submitted to the Faculty of the
James T. Laney School of Graduate Studies of Emory University
in partial fulfillment of the requirements for the degree of
Doctor of Philosophy
in Chemistry
2019

Acknowledgements

First and foremost, I thank my advisor, Prof. R. Brian Dyer, for providing me with the creative freedom, resources and invaluable guidance that allowed me to grow and mature as a scientist. Managing a large group of students with a diverse set of ideas and backgrounds, spread across multiple sub-disciplines of Chemistry is no easy task. Yet, he manages to be extremely accessible in and outside of the lab- speaking volumes about his work ethic and dedication to his profession. His disciplined and principled approach to mentoring his students has offered me and other colleagues, a unique platform for accruing knowledge during graduate school. I am also grateful for help from Prof. James Kindt and Dr. Khalid Salaita, who have served on my committee for six long-years. Both of my committee members have engaged me with scientific discussions at several junctures, and challenged a number of my ideas which helped me shape and hone my scientific reasoning. Outside of my committee, I have also enjoyed having both academic and non-academic discussions with other faculty members at Emory including Dr. Weinert, Dr. Conticello, Dr. MacBeth, Dr. Hagen and Dr. Lutz.

I would also like to thank my parents Raghunath Srinivasan and Vathsala Raghunath for their love, affection and undeterred support throughout my life. I have fond memories of discussing my career path with my parents, who did not enjoy the same socio-economic freedom that they created for me with their hard work and perseverance. The innumerable sacrifices they made during the past three-decades, enabled me to achieve quality college education, and subsequently, a successful shot at graduate school. Also, thanks to my brother, Sriram and my sister-in-law Archana for offering moral support and for the consistent supply of cute photographs of their daughter Shravishta.

Additionally, I would like to thank my friends and present and former colleagues from Emory. Dr. Brandon Greene, for offering spirited mentorship, and for being a great friend and an inspiration. Dr. Bryant Chica for being great company, and partaking in intense scientific discussions no matter the time of the day. Dr. Erin Schuler for teaching me experimental techniques and helping me overcome my fear of public speaking and presentations. Morgan, Jessica, Zihao, Victor, Robert, AJ, Arshad, Wallace, Mooeung, Yimu, Ace and Keon for being great classmates. Samuel, Qun, Helen, Micah, Monica, Brooke, Rachel, Greg, Alexia, Tiffany and Sara for being great friends and even better colleagues. Misael, Radhika, and Aysha, for helping me see through my last year in graduate school smoothly. Palak, Arventh, and Sara for being the best roommates ever. Poornima, Kiran, Shikha, Badrinath, Pranay, Skanda, Anna Grace, Rohit, Sekhar, Aruni, Moyuk, etc., for providing me with friendship that allowed me to live a life outside graduate school.

I would also like to thank the people that inspired me to take up graduate school while I was in college. Prof. Gautam Pennathur, Prof. Sharmila Anishetty, Dr. Tamilselvan Kumaravelu and Prof. Karthe Ponnuraj identified my potential as a scientist and encouraged me to pursue a doctoral degree. Dr. Kamakoti Bhat, Dr. Preethi, Dr. Ramya, Dr. Shobana, Dr. Upasana, Dr. Revathi, Dr. Jemima, Ramaseshan and Vishwanathan for introducing me to the joys of academic research.

Finally, special thanks to Oak Ridge National Labs and Dr. Qian Shuo for help with Small angle X-Ray Scattering measurements. I am lucky to have been surrounded by such amazing people, and I dedicate this dissertation to all of their help.

Table of Contents

List of Figures

List of Tables

Chapter 1

Introduction to protein driven membrane curvature generation

1.1 Lipid membrane morphology and its significance

1.1.1 Lipid membranes as biological envelopes

Several critical biological processes happen on or within the spatially confined region dictated by the lipid membrane surface.[1] The presence of lipid membranes represents a hallmark feature of the cellular system, for the compartmentalization[2] and spatial segregation[3] of biomolecules in the form of enclosed organelles enables the cells to possess distinct spaces with a specific functionality.[4] By isolating the individual organelles from the cytosolic region of the cells, the lipid membranes are essential in retaining the functional complexity of biochemical systems. The ability of lipid membranes to restrict free motion of charged ions and metabolites across the hydrophobic region of the bilayer leads to several interesting biological consequences. For instance, most heterotrophs rely on the chemical energy produced via photosynthesis for their survival. [5-6] In plant cells, the initial steps of oxygenic photosynthesis involve Photosystem II, a membrane-bound protein complex. The antenna complex accepts photons from sunlight, leading to excitation of electrons to higher energy levels. The electrons are subsequently shuttled down the electron transport chain ultimately resulting in pumping of protons across the thylakoid membrane into the lumen. Due to the impermeability of ions and charged molecules across the lipid bilayer, the proton concentration on exterior of the membrane builds up relative to the interior.[6] This results in an electrochemical gradient, which ensures the flow of protons through the membrane bound enzyme ATP-synthase, culminating in the phosphorylation of ADP to ATP. Hence, the lipid membranes (acting as barriers to ions) play a vital role in the generation of a proton gradient across the bilayer, ultimately leading to the synthesis and production of ATP, the “molecular currency” of intracellular

energy transfer. [7] Phospholipid membranes also act as molecular gatekeepers that prevent free transport of metabolites, particularly, hydrophilic molecules, across the bilayer. This makes membrane structures a key player in maintaining controlled communication between the various components of a cell.[8]

1.1.2 Cellular traffic and membrane curvature

To maintain the tight regulation of molecular exchange between the cytosol and the organelles, cells usually possess transport proteins that facilitate the transfer of specific metabolites across the membrane. Intracellular transportation of bulky macromolecules, however, requires a completely different kind a machinery. [9] Transportation of such higher-order molecular structures is facilitated by the formation of large macromolecular complexes characterized by the formation of highly distinctive structural features.[10] Interestingly, several organelles have been observed to possess complex shapes usually characterized with regions of extremely high curvatures. For instance, the Endoplasmic Reticulum (ER) consists of membrane tubules with diameters ranging from 50-100nm (Figure 1.1). [11-12]

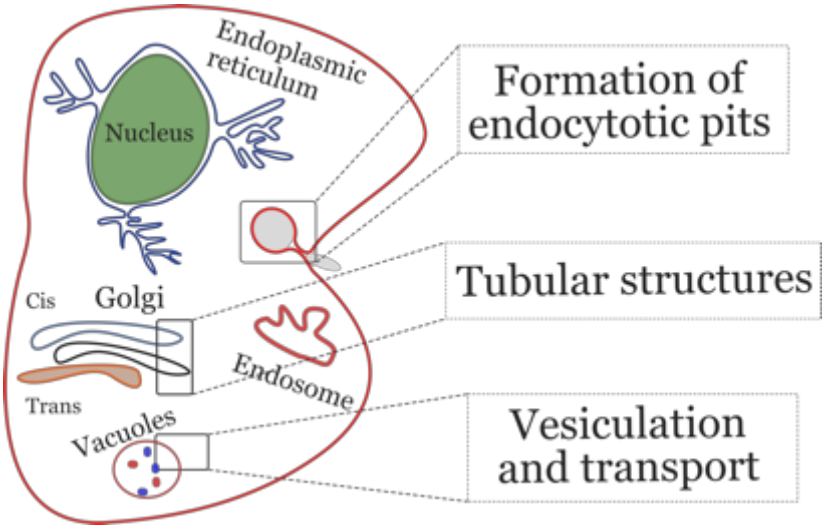

Figure 1.1. Key components of eukaryotic cells and membrane traffic facilitated by membrane curvature. Various organelles utilize structures with varying membrane curvatures. For instance, endocytosis requires the invagination of vesicles (lower mean curvatures) whereas tubular structures at the golgi complex exhibits highly curved regions.[11-12]

The tubules in the peripheral ER, in particular are interconnected into a

complex network that span the entire cytoplasmic space of the cell. Highly curved structures are found in Golgi complexes (GC) as well. The GC network possesses a number of stacked tubular structures that undergo fission and fusion to facilitate molecular exchange. Beyond the ER and GC, highly curved membranes have been found in mitochondria as well as at the plasma membrane level during cell division. Despite limited direct evidence, it is believed that the evolutionary reason for the prevalence of such structures, is to enable for rapid exchange of molecular and macromolecular cargo across the enveloped bodies within cytoplasmic space. [13]

1.1.3 Membrane curvature in pathophysiology

Besides enabling molecular transport across the cytoplasm, membrane curvature generation is vital in numerous viral and autoimmune diseases. Infectivity from pathogens such as Influenza, HIV, Shiga toxin, Ebola, etc., are all mediated through the initiation of membrane curvature leading to membrane fusion or budding.[13] In Influenza virus, this process is mediated by the viral surface protein- Hemagglutinin (HA). The surface proteins first recognize the sialic acid receptors on the cell surface. Subsequently, the viral particles are endocytosed and the sudden change in the pH upon the maturation of the endosome triggers a large-scale conformational re-arrangement, that is believed to cause membrane fusion, and ultimately the release of the viral genetic material into the host cell.[14] It is worthwhile noting that endocytosis is not unique to the infectivity of influenza virus. Rather, it is a key critical pathway for uptake of a number of pathogens. [12, 15-16] Hence, understanding the fundamentals of membrane curvature generation by various pathogens will enable for better rational design of treatment strategies that can target a multitude of diseases.[17]

1.1.4 Physicochemical properties that govern membrane curvature and protein binding

While the prevalence of highly curved structures in organelle membrane surfaces is well-established, the physical basis for generation of such structures is not completely understood. Specifically, the energy cost associated with membrane bending (~0.2-0.6 K_BT/nm^2) to shape flat lipid membranes into such intricate morphologies, makes this discussion, a complex yet fascinating one.[18] Owing to the presence of two acyl chains a large polar headgroup, most Phosphatidylcholine (PC) lipids exhibit a cylindrical shape. Hence, for maximal water exclusion (to protect the membrane's hydrophobic core) cellular membranes formed through self-assembly of lipids with a cylindrical architecture results in a membrane surface that initially exists in a flat, planar state.[19]

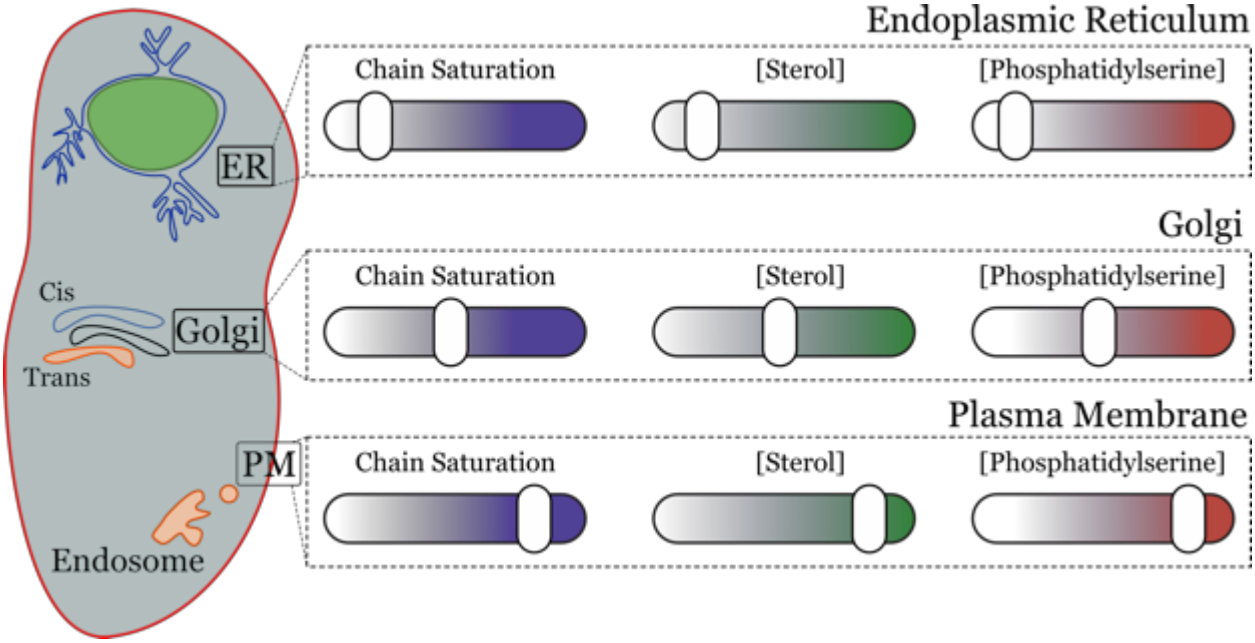

Figure 1.2. Examples of physicochemical parameters that influence membrane curvature and protein binding. Electrostatics play a role in regulating protein association. Packing defects, as a consequence of chain saturation and sterol concentration regulates protein hydrophobic insertion. Membrane curvature influences packing defects, but can indirectly play a role in controlling phase separation. This illustration was adapted from Bigay et al.[20]

Deformation of such structures leading to controlled, intricate shapes, therefore, is possible only upon climbing the steep energy barrier to membrane stretching, as well as bending.[18] A number of factors contribute to the barrier overall- including the lipid local curvature, membrane thickness, bending stiffness, etc. A number of mechanisms have been proposed to explain how cells manage to overcome such barriers. [20] The mechanisms vary from non-specific generation of highly curved structures driven through osmotic shock and thermal undulations, to specific mechanisms that utilize membrane binding proteins. The protein binding in turn, is dictated by the membrane's physicochemical properties, such as electrostatics, presence of packing defects, intrinsic mean curvature, membrane phase structure and the presence of specific receptors [20] (Figure 1.2)

Non-specific mechanisms such as osmotic pressure, has been shown to be an important driving force in regulating the bilayer structure. By transferring cells or vesicles into a hypotonic solution, substantial movement of water molecules to the interior of membranes was observed. This movement was coupled to an overall increase in cellular (or vesicular) volume, inducing lateral tension in the membrane surface. In-vitro studies have revealed that osmotic pressure can also regulate membrane fusion without any assistance from additional protein interactions. Osmotic stress was also found to affect the phase behavior of various lipid mixtures, highlighting the importance of considering the chemical potential of the solvent (water) in a cellular milieu. A thorough discussion of all non-specific mechanisms leading to membrane bending is beyond the scope of this thesis. Hence, a brief overview of intracellular membrane curvature generation by proteins will be presented in the following section.

1.2 **Protein driven membrane remodeling- The classic mechanisms**

1.2.1 Cytoskeletal protein driven shape changes

The prevalence of densely decorated membrane-associated motor proteins on the surface of the ER, GC and other organelles led to the assumption that cell membranes could be shaped by members of the motor protein superfamily, such as kinesin and dynein.[21] While mechanobiological generation of membrane tubules are certainly feasible, it is worthwhile noting that the protein anchors that connect such molecular motors to the membrane move freely along the surface plane, due to the fluid nature of the lipid membrane. As a consequence, the resulting force transmission is not orthogonal to the membrane surface; instead, is weak, transient, and transmitted in a tangential fashion.[22] This phenomenon, despite the concerted action of several proteins render such motor proteins incapable (by themselves) of sustaining the long-lasting elastic forces necessary to cause severe structural deformities in a complex crowded interface. Hence, a pre-requisite for efficient generation of membrane curvatures is for the interacting protein to transmit the forces in a direction perpendicular to bilayer plane and do so, non-uniformly to localized regions of the membrane surface.[14] Interestingly, motor proteins are able to accomplish this by acting in synergy with the cytoskeleton in the formation of tubular structures. It is worthwhile noting however, that such microtubules generated by motor proteins have to experience persistent force for maintaining a tubule structure, and should appear as straight lines during imaging. Given the bent nature of typical organelle membranes such as the ER and GC tubules, it is believed that the stabilization of such bent-membrane structures is accomplished through or with assistance from alternative mechanisms involving reticulons and DP1/Yop1p proteins.[23]

1.2.2 Modulation of lipid composition and asymmetry by protein association

Several reports of membrane curvature induced by proteins that promote lipid asymmetry has been published in the literature. A classic example for such behavior can be found in flippases that facilitate the transfer of phospholipids on the outer leaflet to the inner leaflet. In such cases, it is widely believed that the act of maintaining consistent asymmetry across the leaflets promotes curvature and ultimately budding and fission due to the difference in composition between the two bilayers. [24] It is worthwhile noting that such behavior is not restricted to proteins that enhance the lipid flip-flop rate. Lipid compositional asymmetry can also be generated by receptor clustering, as observed in cases of Cholera toxin B, Shiga Toxin B, etc.[25] In these cases, clustering of lipids such as gangliosides on one face of the membrane promotes negative curvature and ultimately leads to invagination and endocytosis.[26]

1.2.3 Insertion of hydrophobic regions of amphipathic proteins

Direct perturbation of the membrane structure can be accomplished by insertion of amphipathic proteins containing specific stretches of hydrophobic residues. Most proteins that penetrate the membrane surface have been observed to insert their hydrophobic motifs in a shallow fashion. As a result, the protein is able to partition itself in between the lipid headgroups in an efficient fashion, leading to an enhancement in curvature on the outer leaflet. [27,28] Interestingly, proteins that contain amphipathic helices, such as α-Synuclein are thought to detect defect sites within the membrane surface.[29] Upon detection of the defect sites, the disordered region of the protein undergoes a folding transition into an alpha helix, inserting into the membrane bilayer, thereby causing local disruption to membrane phase structure. The generation of

curvature by direct protein insertion into the membrane, is found to be more pronounced if several insertion events occur in close proximity to each other.[30]

1.2.4 Curvature sensing and scaffolding proteins

While curvature sensing is a common feature observed in a number of different membrane-protein attachment modalities, certain protein families containing specific curvature sensing domains are capable of recognizing regions of extreme curvature through well-defined scaffolding mechanisms.[31] The BAR domain in particular, is a great example for a nanoscale membrane scaffold. The BAR domain forms a crescent-shaped dimer, that has been identified to be one of the most conserved features of the protein-amphiphysin, usually found in synaptic vesicles.[32-33] The N-terminal BAR domain is thought to recognize highly curved structures on the membrane surface, and ultimately generate tubules and bend membranes to assist amphiphysin in its endocytotic function. The curvature sensing mechanism of BAR domains is particularly interesting as they are thought to interact with the membranes, by matching the areas of local curvature with their own concave face.[34] This promotes electrostatic attraction between the positively charged residues in the concave region of the protein and the negatively charged residues such as phosphatidylinositol phosphates, such as PtdIns(4,5)P_2. In addition to imposing its nanoscopic scaffolding on the membrane surface, BAR domains can oligomerize subsequently, leading to an enhancement of the local concentration of the interacting partners, resulting in membrane bending.

In addition to BAR domain proteins, peripheral membrane protein oligomerization has been implicated as an alternative membrane bending mechanism. Coat proteins such as clathrin, COPI and COPII have been shown to assist in vesicle fission by attaching themselves to the adaptor proteins, that possess membrane binding properties. Another

example for oligomerization driven generation of membrane curvature is dynamin GTPase superfamily.[35-36] These proteins assume a unique helical polymeric architecture, and is thought to self-associate with one another at tightly curved junctions, ultimately leading to the scission of vesicles. It is worthwhile noting that, high-local protein concentrations at the interface is observed irrespective of the specific mechanisms utilized by macromolecular complexes to trigger membrane bending. Implications for this observation will be discussed in the following section.

1.3 Membrane bending driven by protein crowding.

1.3.1 Ubiquity of the crowded membrane-protein interface

Cell membranes are usually populated by several trans and peripheral membrane proteins. Expression levels of membrane associated proteins are as high as 50% of the total mass of mammalian plasma membrane.[3] It has been estimated that the surface density of the bound proteins approach, if not exceed, 30,000 proteins per μm^2.[37] This results in limited surface area for other interacting partners, thereby resulting in larger scale structural re-organization to accommodate a biomolecular interaction that occurs within a restricted surface area. As a result of such drastic macromolecular confinement, number of interesting biochemical consequences arise due to volume exclusion. The distribution of the protein crystallin within the eyes is a classic example.[38] Crystallins are usually not translated postnatally, meaning that an organism born with this protein solution must retain its structural integrity throughout its lifespan to maintain the transparency of the eye lens. Interestingly, the protein is present within the cells in form of a solution of extremely high concentrations (~500mG/mL). In-vitro studies have revealed that the thermal stability of the proteins is enhanced by increasing the concentration indicating the stabilizing effects of crowding on the protein structure. The

macromolecular crowding inside the cell therefore, is believed to be confer the extreme thermal stability, that is necessary for the lens to retain its transparency over several decades.[39]

Another example to consider, is the internal surface of erythrocytes, where the concentration of hemoglobin is extremely high. [40]In specific conditions such as sickle cell hemoglobin, it is well known that oxygen binding of hemoglobin is linked to the oligomerization of the protein. Several studies have reported that the oxygen affinity to such complexes can be explained only by accounting for the volume exclusion effects.[41] Quantitative studies have revealed that macromolecular crowding is a critical parameter to account for, especially when considering the cell sickling kinetics.[42] While a thorough discussion of the importance of macromolecular crowding is beyond the scope of this thesis, the above-mentioned examples clearly demonstrate the important role it plays in influencing cellular traffic, communication and function.

1.3.2 Membrane curvature generation by protein crowding

Aside from volume exclusion events leading to changes in cellular biochemical pathways, protein crowding on the membrane surface has also been identified as an independent driver of membrane bending. Recent reports have indicated that membrane curvature can be generated even by non-specific attachment of proteins within confined regions of a liposome surface.[43] Multiple reports have shown that non-membrane associated proteins such as Green Fluorescence Protein (GFP) can drive membrane bending purely by the virtue of its sheer density, and steric repulsions at the membrane surface. While this model provides limited molecular detail, the ability of proteins to drive membrane deformations without the assistance of a physiologically relevant interface was attractive to many investigators.[44] In these studies, proteins

containing hexa-histidine tags were immobilized on the vesicle surface by utilizing the interaction between a synthetic lipid, Ni-NTA-DGS and the histidine tag of the protein. By controlling the lipid composition, specific binding of the proteins to individual phase-separated domains was achieved. It was found that when the local density of protein binding was increased by utilizing phase separation, the proteins were able to generate tubules of extremely high curvatures.

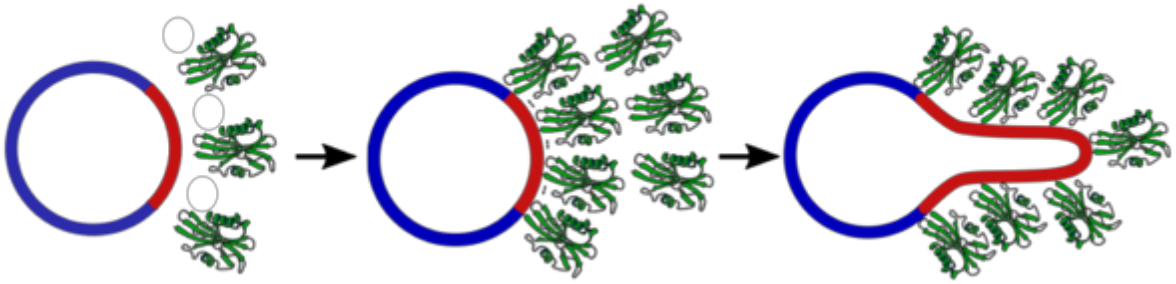

Figure 1.3. High local protein density drives membrane bending irrespective of the protein association mechanism. A schematic that illustrates the proposed origin of curvature generation by protein crowding is presented. Upon binding to the membrane surface, steric collisions between the bound protein complexes leads to curvature generation.[44]

The tubule formation frequency drastically decreased upon reducing the local protein density, indicating that the steric collisions between the laterally mobile membrane-bound proteins were responsible for the deformations. This colligative mechanism could be extended to more physiologically relevant systems, such as epsin1 and AP180.[45] This coupled with the ubiquity of macromolecular crowding at the cell surface (discussed in section 1.3.1), opened the doors for an alternative mechanism to be proposed; one that is universal, and conserved across all the families of curvature generating proteins.

1.3.3 Fluctuations in membrane bound protein structure and its role in curvature generation

A key feature of the protein crowding mechanism, is the steric bulk and the hydrodynamic occupation of proteins on a membrane surface. Both peripheral and trans-membrane proteins are extremely dynamic molecules, that sample several conformations and orientations that occupy different areas at the interface. α-Synuclein is a classic example, for its intrinsically disordered nature is more likely to cause a greater probability of steric collisions with the neighboring protein molecules as opposed to a compact, and a stable globular protein with a well-defined stokes radius. [46]Not surprisingly, several follow-up reports have confirmed that the membrane bending capacity of protein binding is greatly enhanced by adding intrinsically disordered domains to its soluble region.[47] The hydrodynamics of disordered proteins were also found to impact the ability of the individual proteins to sense and detect highly curved regions in the cell surface. [48]It was found that upon increasing vesicle curvature (decreasing vesicle sizes), the restriction to protein-chain conformational freedom enforced by the flat lipid membrane decreased, thereby easing the steric pressure on the membrane surface, subsequently leading to better binding. The ability of intrinsically disordered domains to cause morphological changes in membranes was observed both in the case of membrane-inserting Epsin proteins, as well as the non-natural Ni-NTA DGS containing membranes hinting at the broad applicability of the steric-crowding mechanism in driving membrane curvature.[48]

1.3.4 Membrane curvature generation accomplished by protein unfolding-folding transitions.

We sought to explore the possibility of membrane curvature generation by controlled unfolding of protein structures bound to the membrane surface peripherally.

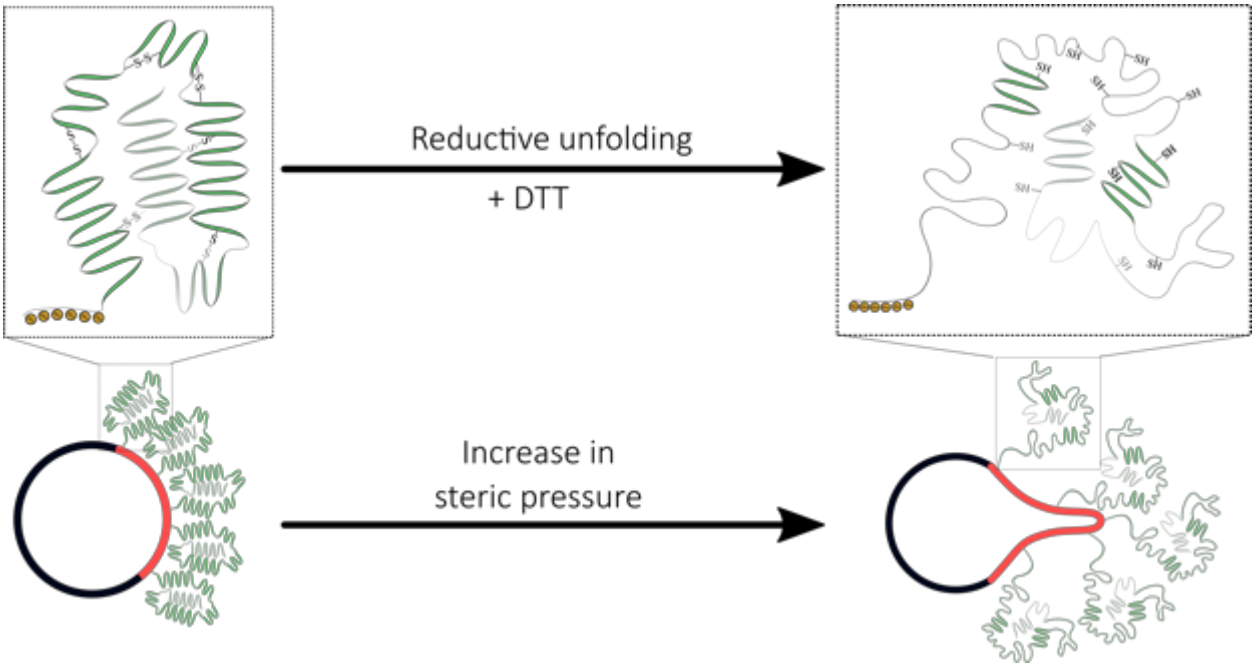

Figure 1.4: Proposed schematic for triggering membrane bending by protein unfolding. Histidine-tagged Human serum albumin (HSA) was tightly attached to the membrane surface utilizing Ni-NTA-DGS lipids incorporated into the liposomes. The increase in steric pressure is generated by reducing disulfide bonds stabilizing the protein structure.

The experimental design for studying the effects of the protein folding-unfolding transition on membrane curvature generation, was simple in concept: tightly bind a protein to the membrane surface with protein binding lipid (Ni-NTA-DGS), and then unfold it and probe the effect on membrane curvature. But, this was difficult in practice, since most protein unfolding methods directly perturb the membrane, including temperature, denaturants such as guanidine hydrochloride, and acid-induced unfolding.

We were able to accomplish this by utilizing His-tagged human serum albumin as a model for this study because the helical structure of HSA is stabilized by 17 disulfide bridges. Reduction of these disulfide bonds by 1,4-dithiothreitol (DTT) triggers partial unfolding of the protein and leads to an increase in the hydrodynamic radii by 1.2-fold, but DTT by itself does not perturb the membrane structure. We have used DTT-triggered unfolding of HSA to induce membrane bending, tubule formation, and budding in model membrane systems (Figure 1.4). The extent, and the frequency of tubule formation was found to be much higher upon unfolding of the membrane bound-proteins. The effect was found to be significantly more pronounced when using liposomes exhibiting phase separation, as opposed to uni-phasic vesicles, indicating that the steric pressure generated from protein unfolding in conjunction with the steric crowding at a localized region of the liposome surface, can drive membrane deformation. [49]

1.3.5 Debate in the literature and the need for mechanistic investigation

Several independent studies have confirmed that membrane bending can be triggered by protein crowding. However, a thorough, fundamental understanding of the mechanisms underlying this process remains elusive. Some groups have challenged the usage of bulky headgroups in the form of artificial lipids such as Ni-NTA-DGS due to its' ability to favor positive curvature.[11] The mechanism also faced criticism about the anomalously high density of proteins required to drive membrane bending. A critical point of contention, are the experimental results on membrane vesiculation by Epsin N-Terminal Homology domain (ENTH). It was observed that when the protein associated to the membrane via its natural interface, (i.e. direct insertion into the membrane) a significantly higher fraction of vesiculation was observed, as opposed to the histidine-

tagged variant (binding to Ni-NTA-DGS containing lipids) carrying an identical sequence.[12] Another independent study observed that far greater surface coverage was required when the proteins were anchored to the membrane using the artificial Ni-Hexa-His interaction, relative to the endophilin BAR domain proteins.[50]

However, despite the debate, crowding driven membrane curvature is an extremely attractive target of study for both biophysicists and cell biologists alike. Studying the changes in cellular membrane morphology is intrinsically a multi-variate problem, where fundamental investigation of individual parameters involved in controlling this process is rendered extremely complicated by how inter-connected some of the experimental variables are.[20, 51] For example, by changing a variable, as simple as cholesterol concentration, several parameters related to the experimental investigation are disrupted. Cholesterol can modulate lipid lateral mobility, influence the phase structure of the lipids under consideration, and can make the membrane stiffer or more fluid. Hence, minor changes to a single experimental variable (cholesterol concentration) usually manifests in a large-scale domino like effect, where multiple parameters are instantaneously disrupted. The colligative, universal nature of the proposed mechanism, enables for a simplified, reductionist approach to studying this complex problem. The prevalence of histidine tags in molecular biology, and the commercial availability of the lipid, Ni-NTA-DGS enables for quantitative biophysical investigation of parameters that were previously inaccessible to researchers. If performed carefully, it is possible to obtain crucial structural and fundamental insight into the mechanism underlying membrane bending by protein crowding. Such insights can then be naturally expanded to other curvature induction mechanisms as well.

1.4 Aims and scope of this thesis

As detailed above, protein crowding mediated membrane bending represents a universal mechanism through which membrane remodeling can be facilitated by protein attachment. To develop a thorough mechanistic picture of this process, a quantitative investigation of the structural and kinetic intermediates that lead to membrane remodeling is necessary. Central to solving such a complex multivariate problem, is a reductionist approach, which eliminates experimental variables in a systematic fashion to understand the role of individual factors that play an important role in regulating membrane deformation. In this thesis, we attempt to accomplish this by utilizing a multi-pronged approach. We utilize simple model proteins with well-understood structural features and trigger liposome deformation by using the Histidine-tag and Ni-NTA interaction. Chapter 2 details the development of a FRET-based assay, that enables quantification of the amount of protein necessary to drive membrane bending in an ensemble setting. In addition to exploring a number of key experimental variables, we were able to achieve valuable insights with regards to the curvature dependent phase behavior of the liposomes under investigation. Chapter 3 details a thorough kinetic investigation into the timescales of protein association to a liposome surface in a crowded milieu. By studying the kinetics of Histidine-tagged GFP binding to the membrane surface, we were able to show that that protein binding did not follow a simple bimolecular association behavior. Instead, it occurs multimodally with different orientations leading to varying protein footprint at the interface. In chapter 4, we provide a kinetic investigation of the membrane bending process utilizing the FRET assay developed in chapter 2. We report that the protein-driven membrane expansion process is multi-phasic and previously un-identified structural intermediates were

found in our stopped flow data. We utilized asymmetric vesicles to control the partitioning of the fluorophores to the individual leaflets of the liposomes. Subsequent spectroscopic and X-ray scattering analysis show that significant membrane thinning occurs upon protein binding, prior to membrane area expansion. The identification of membrane thinning as a kinetic intermediate in our studies, indicates that the membrane expansion mechanism is not purely just due to membrane stretching as previously thought. Instead, a more sophisticated model is required to adequately describe the mechanism. In chapter 5, we discuss the significance of our results and the new avenues for exploration that our data have opened up. We believe that our approach has provided novel insights pertaining to the physical basis of membrane bending driven by protein crowding and has greatly improved our fundamental understanding of the process.

1.5 References.

1. Shibata, Y.; Hu, J.; Kozlov, M. M.; Rapoport, T. A., Mechanisms shaping the membranes of cellular organelles. *Annu Rev Cell Dev Biol* **2009,** *25*, 329-54.

2. Krapf, D., Compartmentalization of the plasma membrane. *Curr Opin Cell Biol* **2018,** *53*, 15-21.

3. Busto, J. V.; Elting, A.; Haase, D.; Spira, F.; Kuhlman, J.; Schafer-Herte, M.; Wedlich-Soldner, R., Lateral plasma membrane compartmentalization links protein function and turnover. *EMBO J* **2018,** *37* (16).

4. Silhavy, T. J.; Kahne, D.; Walker, S., The bacterial cell envelope. *Cold Spring Harb Perspect Biol* **2010,** *2* (5), a000414.

5. Sojo, V.; Pomiankowski, A.; Lane, N., A bioenergetic basis for membrane divergence in archaea and bacteria. *PLoS Biol* **2014,** *12* (8), e1001926.

6. Flugge, U. I.; Westhoff, P.; Leister, D., Recent advances in understanding photosynthesis. *F1000Res* **2016,** *5*, 2890.

7. Hohmann-Marriott, M. F.; Blankenship, R. E., Evolution of photosynthesis. *Annu Rev Plant Biol* **2011,** *62*, 515-48.

8. Gonzalez, L., Jr.; Scheller, R. H., Regulation of membrane trafficking: structural insights from a Rab/effector complex. *Cell* **1999,** *96* (6), 755-8.

9. Yang, N. J.; Hinner, M. J., Getting across the cell membrane: an overview for small molecules, peptides, and proteins. *Methods Mol Biol* **2015,** *1266*, 29-53.

10. McMahon, H. T.; Gallop, J. L., Membrane curvature and mechanisms of dynamic cell membrane remodelling. *Nature* **2005,** *438* (7068), 590-6.

11. McMahon, H. T.; Boucrot, E., Membrane curvature at a glance. *J Cell Sci* **2015,** *128* (6), 1065-70.

12. Kozlov, M. M.; Campelo, F.; Liska, N.; Chernomordik, L. V.; Marrink, S. J.; McMahon, H. T., Mechanisms shaping cell membranes. *Curr Opin Cell Biol* **2014,** *29*, 53-60.

13. Mazzon, M.; Mercer, J., Lipid interactions during virus entry and infection. *Cell Microbiol* **2014,** *16* (10), 1493-502.

14. Samji, T., Influenza A: understanding the viral life cycle. *Yale J Biol Med* **2009,** *82* (4), 153-9.

15. Hansen, C. G.; Nichols, B. J., Molecular mechanisms of clathrin-independent endocytosis. *J Cell Sci* **2009,** *122* (Pt 11), 1713-21.

16. Doherty, G. J.; McMahon, H. T., Mechanisms of endocytosis. *Annu Rev Biochem* **2009,** *78*, 857-902.

17. Johannes, L.; Wunder, C.; Bassereau, P., Bending "on the rocks"--a cocktail of biophysical modules to build endocytic pathways. *Cold Spring Harb Perspect Biol* **2014,** *6* (1).

18. Stachowiak, J. C.; Brodsky, F. M.; Miller, E. A., A cost-benefit analysis of the physical mechanisms of membrane curvature. *Nat Cell Biol* **2013,** *15* (9), 1019-27.

19. Lipowsky, R., Coupling of bending and stretching deformations in vesicle membranes. *Adv Colloid Interface Sci* **2014,** *208*, 14-24.

20. Bigay, J.; Antonny, B., Curvature, lipid packing, and electrostatics of membrane organelles: defining cellular territories in determining specificity. *Dev Cell* **2012,** *23* (5), 886-95.

21. Akhmanova, A.; Hammer, J. A., 3rd, Linking molecular motors to membrane cargo. *Curr Opin Cell Biol* **2010,** *22* (4), 479-87.

22. Doherty, G. J.; McMahon, H. T., Mediation, modulation, and consequences of membrane-cytoskeleton interactions. *Annu Rev Biophys* **2008,** *37*, 65-95.

23. Voeltz, G. K.; Prinz, W. A.; Shibata, Y.; Rist, J. M.; Rapoport, T. A., A class of membrane proteins shaping the tubular endoplasmic reticulum. *Cell* **2006,** *124* (3), 573-86.

24. Daleke, D. L., Phospholipid flippases. *J Biol Chem* **2007,** *282* (2), 821-5.

25. Ewers, H.; Helenius, A., Lipid-mediated endocytosis. *Cold Spring Harb Perspect Biol* **2011,** *3* (8), a004721.

26. Shi, J.; Yang, T.; Kataoka, S.; Zhang, Y.; Diaz, A. J.; Cremer, P. S., GM1 clustering inhibits cholera toxin binding in supported phospholipid membranes. *J Am Chem Soc* **2007,** *129* (18), 5954-61.

27. Ford, M. G.; Mills, I. G.; Peter, B. J.; Vallis, Y.; Praefcke, G. J.; Evans, P. R.; McMahon, H. T., Curvature of clathrin-coated pits driven by epsin. *Nature* **2002,** *419* (6905), 361-6.

28. Varkey, J.; Isas, J. M.; Mizuno, N.; Jensen, M. B.; Bhatia, V. K.; Jao, C. C.; Petrlova, J.; Voss, J. C.; Stamou, D. G.; Steven, A. C.; Langen, R., Membrane curvature induction and tubulation are common features of synucleins and apolipoproteins. *J Biol Chem* **2010,** *285* (42), 32486-93.

29. Nuscher, B.; Kamp, F.; Mehnert, T.; Odoy, S.; Haass, C.; Kahle, P. J.; Beyer, K., Alpha-synuclein has a high affinity for packing defects in a bilayer membrane: a thermodynamics study. *J Biol Chem* **2004,** *279* (21), 21966-75.

30. Campelo, F.; McMahon, H. T.; Kozlov, M. M., The hydrophobic insertion mechanism of membrane curvature generation by proteins. *Biophys J* **2008,** *95* (5), 2325-39.

31. Jensen, D.; Schekman, R., COPII-mediated vesicle formation at a glance. *J Cell Sci* **2011,** *124* (Pt 1), 1-4.

32. Rao, Y.; Haucke, V., Membrane shaping by the Bin/amphiphysin/Rvs (BAR) domain protein superfamily. *Cell Mol Life Sci* **2011,** *68* (24), 3983-93.

33. Peter, B. J.; Kent, H. M.; Mills, I. G.; Vallis, Y.; Butler, P. J.; Evans, P. R.; McMahon, H. T., BAR domains as sensors of membrane curvature: the amphiphysin BAR structure. *Science* **2004,** *303* (5657), 495-9.

34. Mim, C.; Unger, V. M., Membrane curvature and its generation by BAR proteins. *Trends Biochem Sci* **2012,** *37* (12), 526-33.

35. Morlot, S.; Roux, A., Mechanics of dynamin-mediated membrane fission. *Annu Rev Biophys* **2013,** *42*, 629-49.

36. Ferguson, S. M.; De Camilli, P., Dynamin, a membrane-remodelling GTPase. *Nat Rev Mol Cell Biol* **2012,** *13* (2), 75-88.

37. Opekarova, M.; Tanner, W., Specific lipid requirements of membrane proteins--a putative bottleneck in heterologous expression. *Biochim Biophys Acta* **2003,** *1610* (1), 11-22.

38. Augusteyn, R. C., alpha-crystallin: a review of its structure and function. *Clin Exp Optom* **2004,** *87* (6), 356-66.

39. Bettelheim, F. A.; Chen, A., Thermodynamic stability of bovine alpha-crystallin in its interactions with other bovine crystallins. *Int J Biol Macromol* **1998,** *22* (3-4), 247-52.

40. Rotter, M.; Aprelev, A.; Adachi, K.; Ferrone, F. A., Molecular crowding limits the role of fetal hemoglobin in therapy for sickle cell disease. *J Mol Biol* **2005,** *347* (5), 1015-23.

41. Di Caprio, G.; Stokes, C.; Higgins, J. M.; Schonbrun, E., Single-cell measurement of red blood cell oxygen affinity. *Proc Natl Acad Sci U S A* **2015,** *112* (32), 9984-9.

42. Longeville, S.; Stingaciu, L. R., Hemoglobin diffusion and the dynamics of oxygen capture by red blood cells. *Sci Rep* **2017,** *7* (1), 10448.

43. Stachowiak, J. C.; Hayden, C. C.; Sasaki, D. Y., Steric confinement of proteins on lipid membranes can drive curvature and tubulation. *Proc Natl Acad Sci U S A* **2010,** *107* (17), 7781-6.

44. Stachowiak, J. C.; Schmid, E. M.; Ryan, C. J.; Ann, H. S.; Sasaki, D. Y.; Sherman, M. B.; Geissler, P. L.; Fletcher, D. A.; Hayden, C. C., Membrane bending by protein-protein crowding. *Nat Cell Biol* **2012,** *14* (9), 944-9.

45. Busch, D. J.; Houser, J. R.; Hayden, C. C.; Sherman, M. B.; Lafer, E. M.; Stachowiak, J. C., Intrinsically disordered proteins drive membrane curvature. *Nat Commun* **2015,** *6*, 7875.

46. Jiang, Z.; de Messieres, M.; Lee, J. C., Membrane remodeling by alpha-synuclein and effects on amyloid formation. *J Am Chem Soc* **2013,** *135* (43), 15970-3.

47. Zeno, W. F.; Thatte, A. S.; Wang, L.; Snead, W. T.; Lafer, E. M.; Stachowiak, J. C., Molecular Mechanisms of Membrane Curvature Sensing by a Disordered Protein. *J Am Chem Soc* **2019,** *141* (26), 10361-10371.

48. Zeno, W. F.; Baul, U.; Snead, W. T.; DeGroot, A. C. M.; Wang, L.; Lafer, E. M.; Thirumalai, D.; Stachowiak, J. C., Synergy between intrinsically disordered domains and structured proteins amplifies membrane curvature sensing. *Nat Commun* **2018,** *9* (1), 4152.

49. Siaw, H. M. H.; Raghunath, G.; Dyer, R. B., Peripheral Protein Unfolding Drives Membrane Bending. *Langmuir* **2018,** *34* (28), 8400-8407.

50. Chen, Z.; Atefi, E.; Baumgart, T., Membrane Shape Instability Induced by Protein Crowding. *Biophys J* **2016,** *111* (9), 1823-1826.

51. de Meyer, F.; Smit, B., Effect of cholesterol on the structure of a phospholipid bilayer. *Proc Natl Acad Sci U S A* **2009,** *106* (10), 3654-8.

Chapter 2

Curvature regulated phase separation in binary lipid mixtures, and its role in membrane bending

2.1 INTRODUCTION

Lipid membranes are complicated two-dimensional structures that exhibit structural heterogeneity at many levels.[1-3] At a bilayer level, the compositional heterogeneity of lipid membranes leads to the formation of lipid rafts, where tightly packed domains of ordered lipids (usually sphingolipids and cholesterol) can laterally diffuse along the bulk of membrane surface, comprised mostly of loosely packed disordered molecules.[4-5] At a cellular level, highly curved membranes envelope organelles such as endoplasmic reticulum (ER), golgi complex (GC), filopodia, etc., generating a curvature gradient along the surface.[6] The interplay between domain formation and the intrinsic curvature of the membranes has been hypothesized to play an important role in regulating cellular processes, especially lipid sorting.[7] For example, sorting endosomes are known for their unique morphology that is characterized by the presence of a vesicular region (low curvature) and a long, narrow tubular region (high-curvature) that are linked to each other.[8-9] It has been observed that the tubular region undergoes budding to deliver cargo to the ER, while the vesicular region matures into the late endosome. The prevalence of long-chain lipids that are found only within the late endosome prompts an important discussion about how lipid sorting can be influenced by the curvature gradient within a single organelle.[10] Therefore, a thorough understanding of the role of chemo-mechanical coupling between the membrane curvature gradient, and the lipid phase behavior is necessary to advance our knowledge pertaining to lipid sorting in biological systems.

To that end, in-vitro experiments have been utilized to demonstrate the importance of membrane curvature in regulating lipid phase segregation as well. For example, several studies have shown that under specific conditions, vesicles formed with binary and

tertiary mixtures of phospholipids such as 1-palmitoyl-2-oleoyl-glycero-3phosphatidylcholine (DOPC), cholesterol (Chol) and lipids with saturated acyl chains (1,2-dipalmitoyl-sn-glycero-3-phosphocholine- DPPC, Sphingomyelin (SM)) exhibit phase segregation.[11] It has been observed that the co-existence of liquid ordered phase (Lo- enriched with SM, DPPC, etc.), and the liquid disordered phase (Ld- enriched with DOPC) within the same vesicle or a patterned solid-supported lipid bilayer (SSLB) system can be severely impacted by the changing the local curvature of the surface.[7] Similar results were observed in dynamic lipid sorting experiments using membrane tubules pulled from giant vesicles. In these experiments, clear de-mixing of the Ld and Lo phases were established by monitoring the movement of Ld-phase selective fluorophores via microscopy.[12] It was found that the Ld phase was enriched at the highly curved tubular regions, as opposed to the vesicle surface (with negligible curvatures) indicating that the sorting of lipid domains was driven by the difference in bending rigidity between the Lo and the Ld domains.

While the idea of membrane curvature acting as a regulatory element in lipid phase separation is not new, very little is known about the role it plays in mediating membrane remodeling by protein association. As established in chapter 1, several protein complexes can sense regions of high membrane curvature, and in turn induce curvature through secondary processes such as lipid clustering, oligomerization, nanoscopic scaffolding and hydrophobic insertion.[13-14] Additionally, given that phase separation can increase local densities of cell-surface receptors such as gangliosides and phosphatidylinositol;[15-16] it is possible that curvature induced lateral segregation can lead to similar effects as well. This opens up the possibility of membrane lipids and their

ligands that do not possess a preference for a particular membrane curvature, might get spatially sorted into specific regions of the surface indirectly by the intrinsic curvature of the membrane.

We sought to address such possibilities utilizing a simple model system. Our design comprised of binary lipid mixtures made with a gel-phase lipid (DPPC) and a Ld favoring nickel-chelating lipid (Ni-NTA-DGS) and Histidine-tagged Dihydrofolate Reductase as its interacting partner. The Ni-NTA-Histidine tag interaction offers a convenient biomimetic platform owing to the reversible nature of binding, commercial availability and specificity of interaction.[17-18] Additionally, membrane bending triggered by protein crowding has recently garnered a lot of attention as an important driver for membrane bending in biological systems.[19-21] The use of these chelator lipids enables us to achieve such high protein densities required for generating membrane curvature using simple, model proteins.

However, quantitative investigation of the coupling between intrinsic membrane curvature, phase separation and the membrane bending capacity is challenging, even with the usage of extremely simple model systems. Particularly, studying membrane deformation at the level of small vesicles (diameter <200nm) has remained a significant problem, as traditional techniques for monitoring tubule formation are based on microscopy, which is inherently restricted by the diffraction limit. Stamou and colleagues were able to mitigate this problem by developing a curvature sensing assay utilizing surface-tethered liposomes.[22-23] While this technique provided valuable insights into the curvature sensing ability of certain protein complexes,[24] their assays do not provide a spectroscopic handle on membrane remodeling carried out by protein

binding. Hence, to study the complex interplay between the intrinsic membrane curvature at a vesicular level, lateral phase separation and the associated protein's membrane bending capacity, we propose a simple spectroscopic approach.
In this study, we provide a quantitative biophysical investigation of membrane deformation of small vesicles using Fluorescence Resonance Energy Transfer (FRET) as the spectroscopic handle. The goals of this chapter can be divided into the following: (1) To develop a simple FRET based assay to observe membrane deformation by protein crowding; (2) to study the effects of vesicle curvature in regulating the phase behavior of a simple binary mixture; and (3) to identify coupling between intrinsic vesicle curvature and the membrane deformation driven by protein crowding.

We developed the FRET assay by utilizing two different lipid-partitioning fluorophores. NBD-PE (donor) and Rhodamine-PE (acceptor) were doped into the unperturbed liposomes, at concentrations where the energy transfer between the donor lipids and the acceptor lipids occurs with maximum efficiency. Upon the addition of proteins at high concentrations, membrane area expansion is triggered, leading to spatial separation of the donor-acceptor pair resulting in significant spectral changes in the relative fluorescence exhibited by the donor-acceptor pair. By testing a wide range of protein concentrations, we were able to accurately determine the amount of protein necessary to drive membrane bending (Critical deformation concentration-CDC) for a given protein to lipid ratio. Interestingly, the CDC decreases with decreasing vesicle radius, indicating that enhancement in intrinsic vesicle curvature can lead to more efficient membrane bending upon protein association. By using a secondary FRET pair consisting of DPH (donor) and TEMPO (acceptor), we show that the DPPC-Ni-NTA-DGS binary mixture

phase separates under the experimental conditions tested. The phase-behavior appears to be strongly dependent on the starting curvature of the liposome, indicating that domain formation is strongly modulated by the packing stress, particularly at low vesicle radius. Taken together, our results indicate a strong coupling between the intrinsic vesicle curvature, and phase behavior of liposomes comprised of binary mixtures. Additionally, this behavior severely impacts the membrane bending capacity of the proteins, a severely under-characterized phenomenon in the current literature. While this study was performed in simplified model systems, we believe that our results have identified novel pathways through which membranes can spatio-temporally regulate the chemical organization of membrane-bound proteins and will pave the way for further mechanistic investigation into membrane bending driven by protein association.

2.2 RESULTS AND DISCUSSION

2.2.1 Design and optimization of donor-acceptor doping levels for the FRET assay.

Our FRET experiments were performed with liposomes by utilizing fluorophore modified phospholipid analogs containing the donor NBD-PE (Ex: 463/Em:532) and the acceptor Rhodamine-PE (Em:582). NBD-Rhodamine lipid analogues have been used in the literature to observe fusion between fluorophore-tagged and un-tagged liposomes.[25-27] Upon fusion, the untagged lipids effectively dilute the tagged lipids, leading to spatial separation of the FRET dyes. As a consequence, the efficiency of energy transfer is greatly diminished- leading to a dequenching of donor-fluorescence. Given that tubule formation in membranes is known to cause membrane area expansion, we reasoned that membrane deformation by protein crowding can be studied

using our FRET probes (Figure 2.1.A). We first wanted to quantify the ideal doping levels of the fluorescent analogs, for our given vesicle composition to account for any artifacts that could arise from the phase-behavior of our lipid mixture.

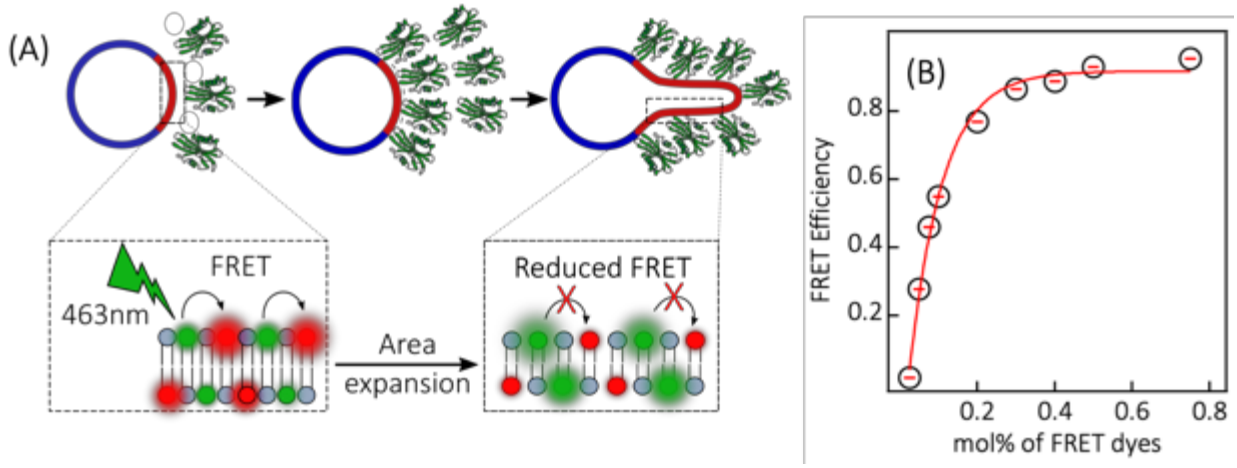

Figure 2.1. Optimization of FRET-pair loading level for detection of membrane deformation (A) A simplified schematic describing membrane deformation assay. Before protein binding, the FRET between the NBD/Rhod pair is efficient. Once deformation is triggered by protein crowding, membrane area expansion should spatially separate the donor-acceptor pair, leading to a decrease in FRET efficiency. (B) Experimentally acquired FRET efficiency data plotted as a function of the doping levels of the dyes. 20 mol% Ni-NTA-DGS alongside DPPC was used for these measurements. The solid line represents an exponential fit. Average of three individual spectral measurements were plotted with the error bars (inside circle) representing the standard deviation.

Using an identical liposome concentration across all measurements (500μM) we prepared our vesicle samples containing 0.02 to 0.8 mol%, each of equimolar concentrations of the FRET dyes. For all the experiments detailed below, the chelator lipid Ni-NTA-DGS (Fluid-phase) loading density was maintained at 20 mol% and the remainder of the lipids were populated by either DPPC (Gel-phase) or DOPC (Fluid-phase). To spare the reader from ambiguity, Gel phase (or Solid Ordered-So lipids) will be referred to as Lo-Phase throughout the chapter. FRET efficiencies were then

measured as a function of the doping level of the dye-pair, resulting in a standard curve, whose midpoint (~0.18 mol%) was utilized for all further experiments. It is worthwhile noting that both the dyes have a propensity to partition into the Ld phase,[28] where tubule formation is likely to be initiated. Regardless of the partitioning preference of these dyes, we expect that the ratiometric measurement of the donor fluorescence and the acceptor fluorescence will act as a sensitive reporter of membrane area expansion.

2.2.2 Spectroscopic observation of membrane area expansion.

Having established the optimal dye-loading conditions, we employed equilibrium fluorescence measurements along with fluorescence lifetime measurements, to quantify the membrane expansion triggered by protein crowding. Liposome solutions (500μM), containing Small Unilamellar Vesicles (SUVs) extruded through 100nm Polycarbonate membranes, were incubated for 30 minutes, with solutions containing different concentrations of *Escherichia coli* DHFR (EcDHFR) ranging from 100nM – 20μM. EcDHFR is an ideal model protein for our studies, as it has a terminal Histidine tag that is useful for purification, and is structurally well characterized. [29-30]The EcDHFR construct used in this study, contains only a single cysteine, which can be kept under reduced conditions by using modest concentrations of a reducing agent (1mM Dithiothreitol).

First, equilibrium fluorescence spectra of membrane deformation were collected using a benchtop fluorometer (Figure 2.2 A). A clear reduction in FRET from the donor to the acceptor can be observed, upon addition of 10 μM EcDHFR indicating spatial separation of the fluorophores as a result of membrane deformation. FLIM analysis was performed on a Nikon-Confocal system with a Time Correlated Single Photon Counting (TCSPC) module. We reasoned that membrane expansion would result in an increase of the

donor's lifetime due to reduced FRET efficiency. As seen in Figure 2.2B, a substantial increase in the donor lifetime could be observed, consistent with our assignment of equilibrium fluorescence data. As an independent probe for membrane area expansion, we performed Dynamic Light Scattering (DLS) on the liposome samples with and without the presence of 10μM DHFR (Figure 2.2B). Careful consideration has to be given when analyzing DLS data on samples that possess non-spherical structures. However, the change in hydrodynamic drag of the liposomes, upon formation of

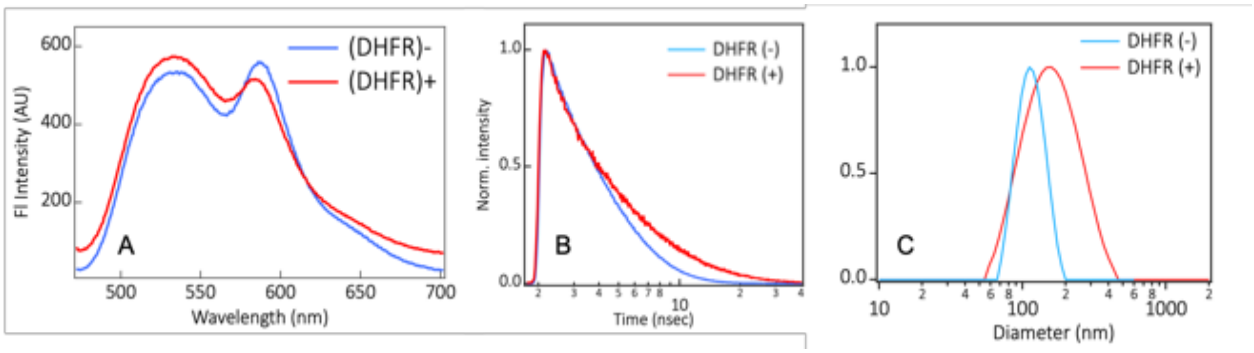

Figure 2.2. Spectroscopic observation of membrane area expansion by protein crowding (A) Representative equilibrium fluorescence spectra of the FRET pairs before and after addition of 10μM DHFR. Excitation was performed at 463nm. The peak centered around 530 represents the donor fluorescence, and the peak at 580 represents the acceptor fluorescence (B) Representative fluorescence lifetime transients of the dye-loaded liposomes before and after the addition of 10μM DHFR. A clear increase in lifetime is observed upon protein addition indicating spatial separation of the fluorophores. (C) Representative dynamic light scattering intensity profiles of liposomes before and after addition of 10μM DHFR.

tubules, will change the diffusion coefficients of the structures enough, to provide a qualitative handle on large scale structural changes such as tubule formation. Hence, the increase in hydrodynamic diameter reported by DLS must be a consequence of morphological changes as a result of protein crowding (Figure 2.2C).[21]

As a negative control, we subjected liposomes made with DOPC (Ld phase) to protein association at same concentrations as described in Figure 2.3. Owing to the unsaturated

nature of its hydrocarbon chains, DOPC and Ni-NTA is known to form uniform vesicles that exhibit no phase-segregation. Hence, we reasoned that a uniform distribution of the chelator lipids across the liposome surface will relieve the steric pressure of protein binding, leading to limited membrane deformation. As expected, we see little to no spectral changes by protein binding to uniform liposomes (Figure 2.3).

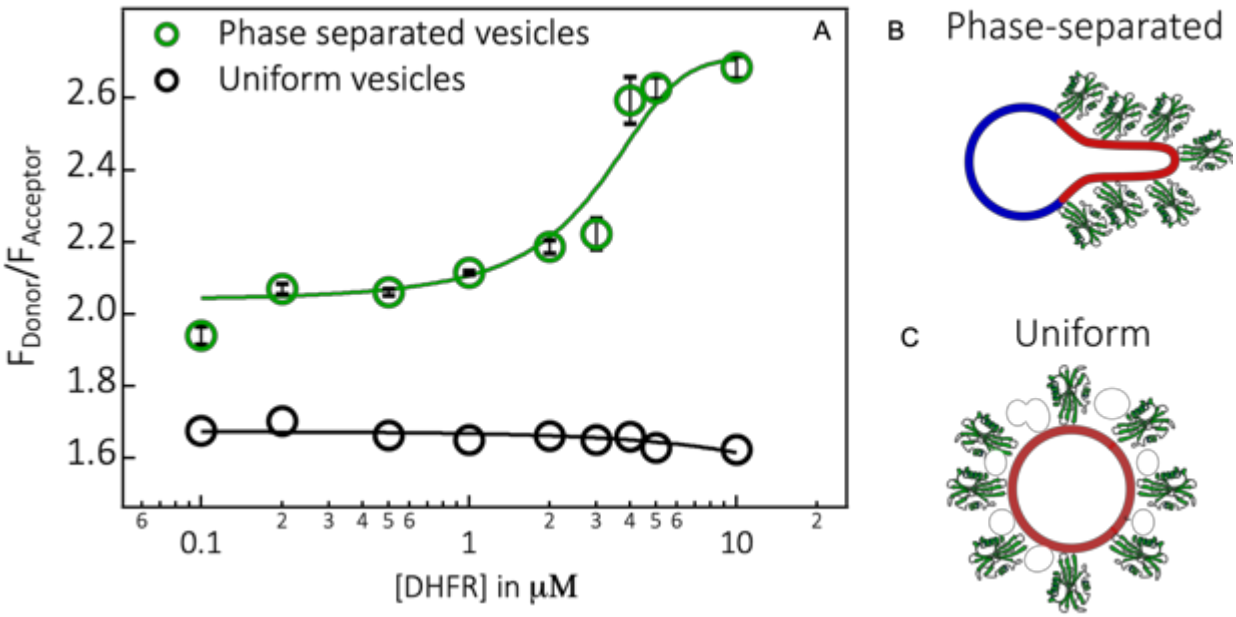

Figure 2.3. Determination of critical deformation concentration (A) Concentration dependent changes in the ratio of donor fluorescence to acceptor fluorescence plotted as a function of protein concentration. Identical concentrations of liposomes (0.5mM) was used across the measurements. The green solid line represents the associated sigmoidal fit, while the black solid line represents a linear fit indicating little to no change in vesicle morphology while using a uniform lipid composition. Error bars for phase-separated vesicles represent standard deviation from triplicate measurements. Uniform vesicles were experimentally tested only once as a control (B) A simplified schematic representing membrane bending by protein crowding in a localized region (red-tubule). (C) A schematic representing the lack of major membrane deformation due to the lack of steric pressure in the case of uniform vesicles.

Concentration dependent changes in the relative fluorescence of the donor and the acceptor was observed using a 96-well plate reader for a high-throughput readout (Figure 2.3A). As seen in Figure 2.3A, a strong concentration dependence in the FRET ratios were observed in the measurement, indicating that a critical protein density has to

be reached at the liposome surface, for spatial separation of the donor-acceptor pair to occur as a result of membrane area expansion (Figure 2.3B). Fitting the fluorescence data to a sigmoidal function leads to the determination of the critical deformation concentration (CDC) of ~ 3.3 μM for the given vesicle composition and concentration.

2.2.3 Vesicle intrinsic curvature modulates critical deformation concentration.

Having established the sensitivity of our FRET assay in quantifying membrane deformation, we wanted to probe if the intrinsic vesicle curvature can influence the membrane bending capacity of the proteins. To accomplish this, we prepared vesicles with varying curvatures by extrusion through polycarbonate membranes with differing pore sizes (30, 50, 100 and 200nm, respectively). All phase separated liposomes were extruded at temperatures above the transition temperature of DPPC (>50°C) and cooled down to room temperature before use. Control experiments were performed by varying the curvatures of vesicles comprised of uniform lipids as well (Figure A2.5). DLS was used to quantify the hydrodynamic diameters of the resulting liposomes (Figure A2.1). The average diameter was found to be 68nm, 88nm, 121nm, 146nm for vesicles extruded through 30, 50, 100 and 200nm PC membranes respectively. This allowed for quantitative investigation of the curvature dependence of the various liposomes, as they cover a wide range of vesicle diameters, inaccessible via giant vesicle imaging techniques as discussed previously in section 2.1.

The comparison of concentration dependent changes in FRET between the donor-acceptor pair incorporated into the membrane follows a sigmoidal trend (Figure 2.4 A & B) irrespective of the vesicle size used. Little to no changes in FRET was observed across the wide protein concentration range used with uniform vesicles, indicating that the

binary mixtures were more likely to deform due to the increased protein density presumably due to phase-separation.

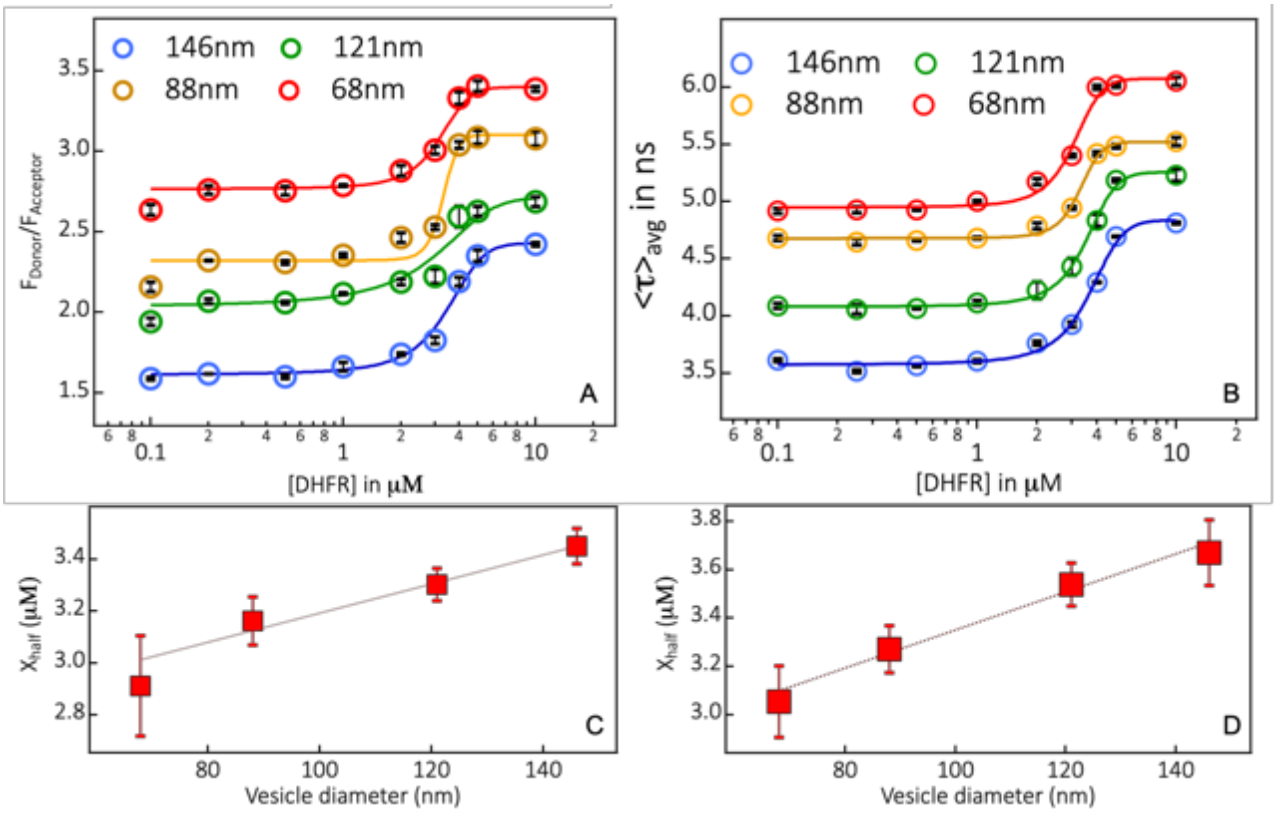

Figure 2.4. Relationship between vesicle size and CDC. Concentration dependent changes in FRET obtained from equilibrium fluorescence (A) and Fluorescence lifetime (average) data (B) plotted as a function of protein concentration. Identical concentrations of phase separated liposomes (0.5mM) were used across the measurements. All traces were offset for clarity. Error bars represent the standard deviation obtained from 3 replicates. The solid lines represent a sigmoidal fit in (C) and (D)- X_{half} values from the sigmoidal fits were plotted as a function of measured vesicle diameter. Values plotted in (C) were obtained via equilibrium fluorescence and those plotted in (D) were obtained via fluorescence lifetime. The linear fits in (C) and (D) are meant to guide the reader. Error bars represent the error from the sigmoidal fits.

Interestingly, the sigmoidal fits from both the fluorescence lifetime and intensity values, reveal a strong correlation between the vesicle size and the CDC for the same lipid composition and concentration. As the vesicle curvature increases (decreasing diameter), the CDC value decreases by almost 15% (Figure 2.4 C & D) when comparing

liposomes with a 68nm average diameter to liposomes with an average diameter of 146nm. This indicates that a lower concentration of protein in bulk is required to drive membrane bending with small vesicles, as opposed to larger vesicles. While this observation was intriguing, careful consideration of several possible mechanistic schemes is necessary to arrive at accurate conclusions about the physical meaning of these results. A number of factors might lead to a lower CDC with decreasing vesicle radius, including: (1) Direct preference of the histidine-tag for highly curved regions on the membrane surface; (2) Curvature dependent changes in lamellarity of the liposomes; (3) Bilayer thickness modulation by changing vesicle radius; (4) Curvature regulated phase-separation of binary lipid mixtures under our experimental conditions. The possibility of the histidine-tagged proteins to prefer highly curved membrane structures can be quickly excluded, as several previous studies have shown that proteins with well-defined structures have very limited curvature sensitivity.[31-32] Hence, to understand the molecular mechanism underlying the curvature dependence of CDC, we tested each of these possible scenarios step by step.

2.2.4 Small Angle X-Ray Scattering reveals that the bilayer thickness and lamellarity is unaffected by vesicle curvature.

First, we sought to investigate if changes to vesicle radius can lead to the formation of multi or pauci-lamellar (<5 bilayer stacks) structures. Second, we wanted to explore if changes to vesicle radius can bring about any major structural changes to the bilayer, particularly its overall thickness. We wanted a thorough investigation of both of these factors, as they could contribute significantly to the ability of proteins to drive membrane bending. For instance, changes in lamellarity of the liposome can lead to artifactual substantial changes in the membrane's physical properties.[33] Notable

changes were observed with the phase-transition behavior of multi-lamellar structures compared to unilamellar liposomes made with the identical lipid composition and concentration.[34] Also, vesicle curvature has been shown to affect the overall bilayer thickness, thereby resulting in changes to bending stiffness of the liposome structures.[33, 35] We reasoned that these perturbations might indirectly affect the curvature generation capacity of our protein complexes. Hence, to address these concerns, a quantitative approach to measure the changes to bilayer lamellarity and thickness was necessary. Small Angle X-Ray Scattering (SAXS) is a versatile technique that allows for monitoring the bilayer structure of freely formed liposome samples. SAXS was an ideal choice for our biophysical investigation due to its sensitivity to the vesicle form factor, lamellarity, size and bilayer thickness. [36] SAXS utilizes scattering that originates from electron densities from the molecules under investigation. An X-ray source of highly collimated, monochromatic beam is shot into the observation chamber, and the forward scattering signal is collected by a 2-D detector. The resulting 2-D scattering pattern is reduced to a one-dimensional scattering function, and important structural information about the samples under observation can thus be acquired. In case of liposomes, SAXS can be used to determine the average thickness of the bilayer by analyzing the scattering patterns that arise from contrast in electron densities between the polar headgroup region (higher relative electron density) and the hydrophobic region (lower relative electron density). The technique is also sensitive to the presence of stacked multilamellar structures due to the presence of Bragg's peaks that arise from close proximity between bilayer structures possessing high electron densities.

As seen in Figure 2.5, a diffraction pattern consistent with the diffuse scattering profile of Unilamellar vesicles was observed. The moderate Q region (0.04-1 $Å^{-1}$) exhibits characteristic dual minima, indicating the electron density at the outer layer of the phospholipid headgroups, and the inner layer of the phospholipid headgroups respectively. Interestingly, we observe little to no shift in these minima across the vesicle sizes tested, indicating that vesicle curvature did not affect the average bilayer thickness to a significant extent (Figure 2.5C).[37] Additionally, the absence of any significant Bragg's peaks in the diffractogram, indicate the absence of multi or pauci-lamellar structures in the sample.[33] These observations effectively eliminate the possibility that the curvature dependent changes in CDC are a consequence of curvature induced changes in bilayer thickness or lamellarity.

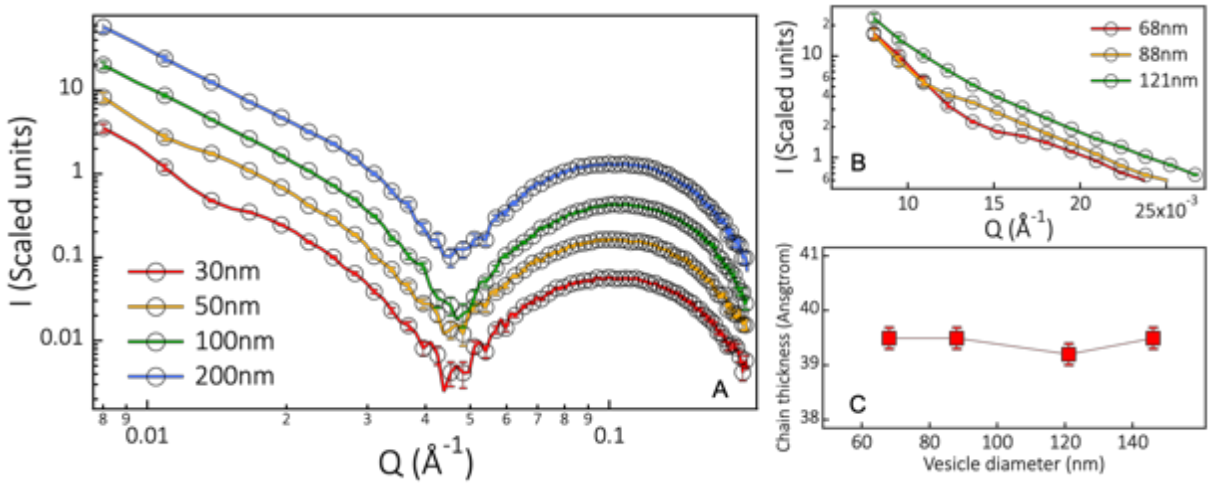

Figure 2.5. (A) SAXS diffractograms of 6.5mM SUVs extruded with different pore sizes. 12 scans were signal averaged, and reference corrected to yield the final diffractogram. Error bars represent the standard deviation. (B) Zoomed in view of the lower-Q range of the diffractogram. The minimum (68nm) centered around 0.015 $Å^{-1}$ indicates a change in the overall form factor of the liposomes and heterogeneity in electron density. (C) Acyl chain thickness plotted as a function of vesicle diameter. Little to no appreciable changes in the overall bilayer thickness is observed, indicating that curvature does not modulate the membrane thickness directly. Lines between markers are meant to guide the reader's eye.

However, at lower vesicle diameters, an unusual feature is observed in the low Q region of the diffractogram (Figure 2.5 B; 0.01 – 0.02 $Å^{-1}$). This region is traditionally thought to be sensitive to large scale structural changes, such as the vesicle shape, polydispersity and aggregation. However, our DLS experiments reveal little to no evidence for liposome aggregation even after overnight incubation, or changes to polydispersity of the liposome samples due to changing vesicle curvatures (Figure A2.1).[37] Hence the deviation from near-linear behavior in this region indicates the presence of in-plane structures along the surface of the lipid bilayer. Interestingly, this observation was found only in liposomes with lower diameters, indicating that these undulations are caused by increasing the mean vesicle curvature. While such features are commonly observed in Small Angle Neutron Scattering (SANS) experiments, a well resolved minimum in the low-Q region with SAXS is relatively uncommon.[38] This is due to the fact that SAXS is sensitive to changes in the electron density, and hence achieving strong contrast between regions of differing electron densities is not trivial. Exploring the origins of such undulations are well beyond the scope of this study. However, we believe that phase separation of Ni-NTA-DGS into domains scattered across the liposome surface, can lead to a large heterogeneity in terms of the electron density leading to changes in low-Q region. This hypothesis can be easily tested by either extracting the metal ion from the headgroup (using EDTA), or by replacing the Ni^{2+} with a more electron dense Cu^{2+}.

2.2.5 Curvature regulated phase-behavior in binary mixtures observed by DPH quenching.

Having eliminated the possibility of curvature induced changes in bilayer lamellarity and thickness, we were interested in exploring if curvature induced packing stress can

regulate the overall phase-behavior of the liposomes. Several instances of curvature modulated phase segregation can be found in the literature. For instance, Parthasarathy et. al show that surfaces containing microfabricated patterns can induce spatial ordering of the different lipid micro-domains on a solid supported lipid bilayer platform.[39] Owing to the varying mechanical properties of the individual lipid phases, it was hypothesized that regions composed of lipids with higher bending rigidity, had less preference for highly curved substrate than its flexible counterpart. Other studies have postulated that sorting of lipid domains with different bending stiffness can be accomplished via changes to vesicle curvature. It has been shown that tubular model membranes can lead to strong curvature-coupled segregation as well.[40] Despite the prevalence of such reports, the relationship between phase-segregation and vesicle size has received limited attention, while dealing with small and large unilamellar liposomes. This is partly due to the experimental limitations imposed by the diffraction limit, which prevents characterization of nano-sized domains present in small and large vesicles composed of binary and ternary mixtures. Hence, to mitigate such limitations, we sought an independent spectroscopic method that allows for quantitative investigation of changes in phase separation as a consequence of changing vesicle radius.

To that end, we utilized the quenching of fluorescence from the fluorescent probe 1,6-diphenyl-1,3,5-hexatriene (DPH) by (2,2,6,6-tetramethylpiperidin-1-yl)oxyl (TEMPO) as a reporter for the formation of nano-domains within our vesicle samples. The rationale behind this assay has been established elsewhere[41] and is represented graphically in figure 2.6A. Briefly, DPH is a well-established fluorophore that is non-fluorescent in aqueous solutions, but becomes fluorescent once it partitions into the lipid bilayer.[42] It has been reported that DPH partitions uniformly to both the liquid ordered and the

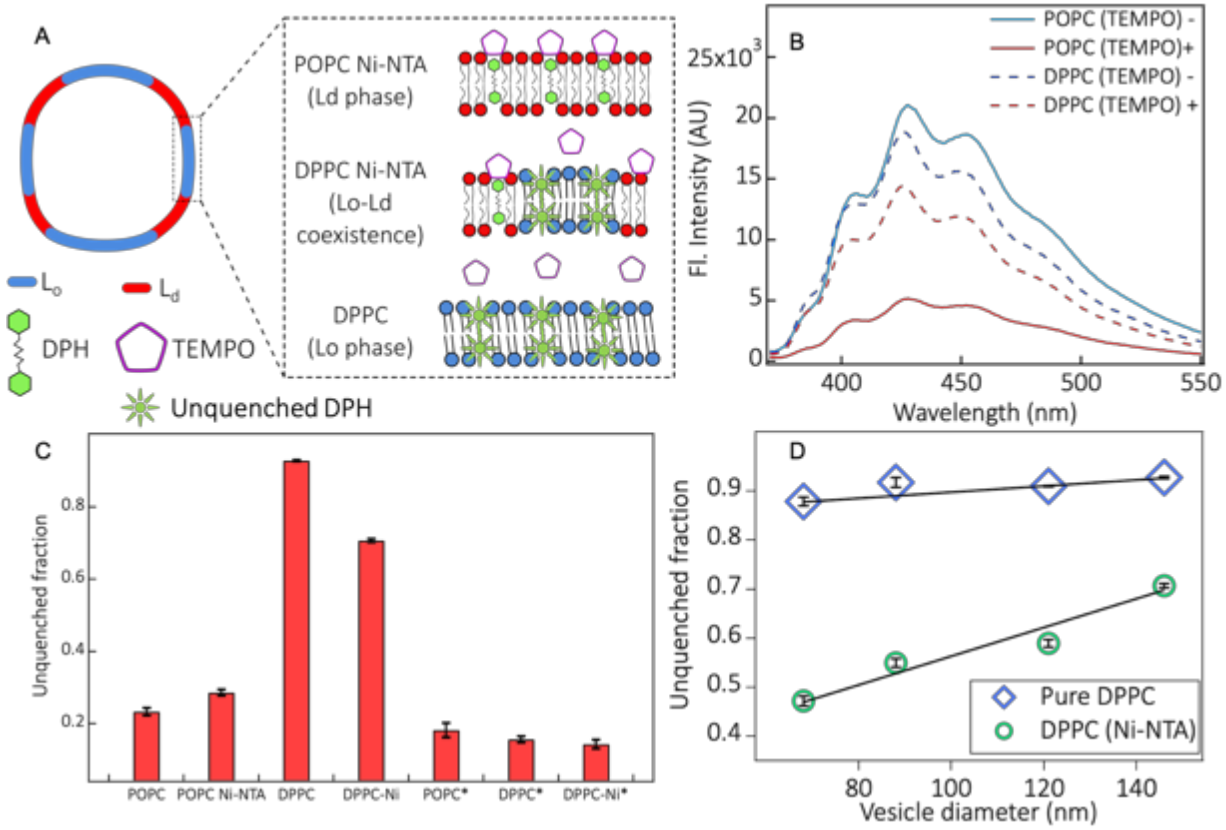

Figure 2.6. Curvature induced phase separation in Ni-NTA-DGS containing binary mixtures (A) A simplified schematic representing the DPH-TEMPO quenching assay. DPH partitions uniformly across both Lo and the Ld phases, whereas TEMPO can quench only the DPH found in Ld phase. (B) Representative fluorescence spectra of quenching of DPH fluorescence by TEMPO. The difference in the degree of quenching reveals the difference in phase structure between liposomes composed of Lo phase (DPPC) and Ld phase (POPC) (C) The unquenched DPH fraction plotted for different lipid compositions. (*) indicates data collected at 60°C, where DPPC containing liposomes will exhibit domain mixing due to phase transition. (D) Curvature dependent changes in the phase-segregation observed in liposomes made with DPPC-Ni-NTA binary mixtures. Increasing the liposome curvature clearly promotes phase de-mixing. All experiments were repeated 3 times and the error bars represent the standard deviation.

liquid disordered domains of the liposomes without any preference for one over the other. [43] [44] The quencher TEMPO, however, partitions purely into the Ld domain and given its small Forster radius (1.2nm), will quench the fluorescence of DPH partitioned into the Ld domain alone. This provides a reliable estimation of the relative fraction of

DPH that remains unquenched by TEMPO, which can be utilized to report on the extent of phase separation as well as the average domain sizes.

We performed equilibrium fluorescence measurements on liposomes composed of binary mixtures (DPPC & Ni-NTA- Ld and Lo) and uniform liposomes made with DPPC (Lo) or POPC-Ni-NTA (Ld) only. As expected, a strong quenching of DPH fluorescence is observed when POPC containing liposomes are used, indicating that TEMPO can access the DPH across the vesicle surface due to its uniform distribution in the Ld Phase (Figure 2.6B- Solid lines). Little to no quenching was observed when liposomes containing only DPPC was used, indicating the inability of TEMPO to partition into the Lo phase (Figure 2.6B- Dotted lines). As an additional control experiment, we also performed these experiments at high temperatures, well (60°C) above the phase transition temperature of DPPC. At these temperatures, the lipid domains must coalesce due to the gel-fluid transition of the Lo phase lipids. We observe that the quenching efficiency increases significantly upon increasing the temperature (Figure 2.6C), indicating that the quenching of DPH fluorescence by TEMPO, was indeed purely due to phase separation.

Additionally, we ensure that partitioning of TEMPO was curvature insensitive, by changing the vesicle radius of pure DPPC liposomes (Figure 2.6D). We find little to no change in the unquenched fraction of DPH, indicating that TEMPO's interaction with the liposomes are intrinsically curvature insensitive. Intriguingly, binary mixtures display a strong curvature dependence of DPH quenching efficiency while using binary mixtures containing both DPPC and Ni-NTA DGS (Figure 2.6D). Decreasing the vesicle diameter from 146nm to 68nm, results in a 21% decrease in the unquenched fraction,

despite using the same lipid composition across the measurements. This observation is extremely important for two major reasons. First it clearly proves that the binary mixture of DPPC and Ni-NTA-DGS exhibit strong phase-separation at room temperature. Second, it confirms our initial hypothesis that the mean curvature of vesicles can significantly modify the phase behavior of the lipid mixture. This indicates a direct coupling between the vesicle intrinsic curvature and the physicochemical state of the liposome.

The physical origins of this observation can be rationalized by considering the packing and the curvature stress experienced by DPPC lipids, particularly at low vesicle diameters. Cryo-EM has revealed that gel-phase liposomes exhibit a non-spherical geometry characterized by the presence of faceted structures that possess significant

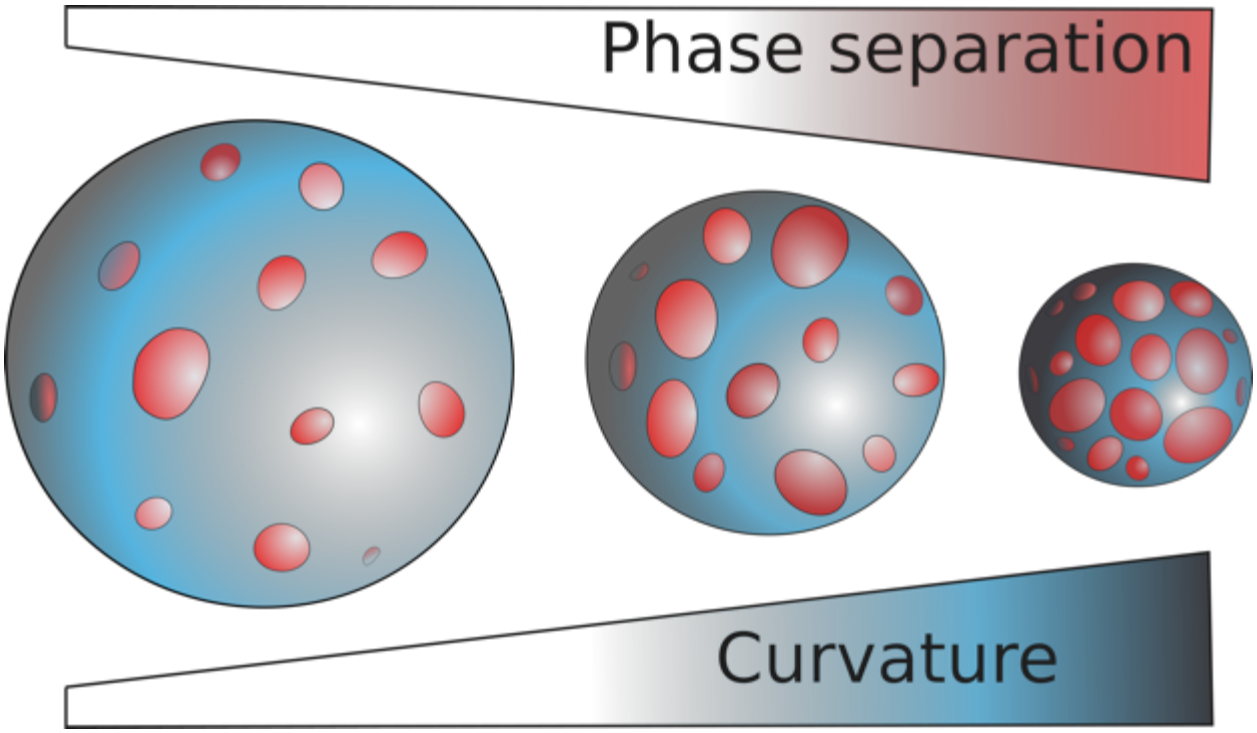

Figure 2.7. A simplified schematic representing curvature regulated modulation of phase segregation in the binary mixtures. As the mean vesicle curvature increases, phase separation becomes more severe.The liposomes are represented as spheres purely for illustrative purposes.

defect sites at the edges.[45] At lower vesicle radius, owing to the curvature stress, defect sites at the ridges joining the facets are believed to be amplified to accommodate the packing stress imposed by the high intrinsic curvature of the liposomes.[46] Hence, it is likely that a small fraction of the gel-phase lipids can exist in fluid phase even below the transition temperature of the lipid mixture.[47] The small, but statistically significant decrease in the unquenched fraction of pure DPPC vesicles as a function of decreasing vesicle diameters (Figure 2.6D) hints at the existence of small fluid-like regions even within vesicles containing only the gel-phase lipid.

We hypothesize that, in binary mixtures the curvature stress induced by the vesicle size can be compensated effectively by populating the Ld lipids to such defect sites. In all of our experiments with binary mixtures, the gel-phase DPPC concentration was significantly higher (80 mol%) than the chelator lipid (20 mol%). Given the unsaturated nature of the acyl chain carrying the Ni-NTA headgroup, it is likely that the bending rigidity of these lipids are significantly lower than the surrounding Lo lipids. Hence, it is probable that partitioning of these fluid domains to regions of high curvature can be greatly enhanced by using liposomes of lower diameters. Similar observations have been made in surface-fabricated supported bilayer systems as well, where spatial arrangement of lipid domains can be directed by the membrane curvature gradient of the underlying patterned substrate.[39] While experimental reports on domain miscibility between Ni-NTA-DGS and DPPC are sparse, a few reports have indicated that, liposomes containing DPPC, DOPC and Cholesterol display an enhancement in lipid de-mixing by decreasing vesicle sizes.[38] Our DPH quenching results are also consistent with conclusions from previously published SANS data, indicating that the relative domain

area of the phase-separated lipids increases with decreasing vesicle diameter (Figure 2.7).

2.2.6 Coupling between membrane bending driven by protein binding and vesicle phase structure.

Given the knowledge that vesicle curvature can regulate the phase behavior of our binary mixture, we wanted to explore the relationship between phase separation and CDC, determined in section 2.2.3. The trend of decreasing CDC with decreasing vesicle radius (and hence, enhanced phase-segregation) can be rationalized via several possible mechanisms. First, it is possible that phase separation of Ni-NTA-DGS from the surrounding DPPC lipids can alter the local density of the chelator lipids at individual domains. Theoretically, increasing the density of Ni-NTA DGS enhances binding affinity of proteins to the membrane surface substantially (Figure A2.2-A2.4). Hence it is entirely possible that the enhanced lipid segregation at lower vesicle radius, will lead to tighter binding of proteins to the liposome surface, even if histidine-tagged proteins do not possess any curvature preference. While our ITC results support the correlation between phase-segregation and protein binding constants (Figure A2.4), it is unclear if the enhancement in phase-separation observed in section 2.2.5 will lead to an increase or decrease in the local chelator lipid density. In other words, it is possible that the Ld domains formed at high vesicle curvatures can be significantly diluted by Lo-preferring lipids that exist in the Ld domain due to packing stress.

Second, the increase in the Ld domain fraction of smaller vesicles might lead to the lowering of the overall bending stiffness of the liposome. It is well known that liquid-disordered domains usually exhibit significantly lower bending rigidity relative to the

liquid ordered domains. Several studies have highlighted the importance of lipid bending rigidity as a major barrier to membrane bending. Hence, this artificial decrease in the average bending rigidity of the liposomes as a consequence of their phase behavior can lead to the lowering of the energy cost associated with membrane bending. Third, the packing and curvature stress experienced by the smaller liposomes, can help to nucleate membrane deformation due to the prevalence of the defect sites across the membrane surface. These defect sites have been proposed to act as nucleation sites for lipid melting in previous lipid melting studies. It is certainly possible that the presence of defect sites that contain regions of extreme curvature can lead lower the energy cost associated with generating tubules and heavily bent membrane structures. All three scenarios are extremely difficult to probe experimentally, and are beyond the scope of this chapter. While the exact physical mechanism underlying the relationship between membrane bending and the phase behavior remains unclear, our results clearly demonstrate a strong co-dependence of various physiochemical parameters in regulating membrane bending.

2.3 Conclusion

In summary, we report a quantitative investigation of the coupling between intrinsic membrane curvature, phase separation and the membrane curvature generation by protein crowding. By using a simple FRET-based assay, we show that the threshold protein concentration required to generate membrane deformation is significantly lower for vesicles of smaller radius relative to the larger ones. Closer inspection of the phase structure of the lipid mixture reveals that the intrinsic vesicle curvature can significantly modulate the domain formation exhibited by the binary mixtures utilized. By eliminating the possibility of curvature induced changes in bilayer thickness and

lamellarity, we find that the enhancement in phase separation as a result of decreasing vesicle radius plays a major role in regulating membrane curvature generation by protein crowding. Our study reveals a complex mechanism by which curvature and packing stress imposed by vesicle can indirectly affect the arrangement of peripherally interacting proteins, which in turn can remodel the membrane structures. These results open up new avenues for exploration of spatio-temporal regulation of macromolecular assemblies on highly curved cellular structures.

2.4 EXPERIMENTAL SECTION

2.4.1 Materials. DPPC, DMPC, DSPC, DLPC, POPC and Ni-NTA-DGS were purchased from Avanti Polar Lipids (Alabaster, AL). NBD-PE and Rhodamine-PE were purchased from ThermoFisher Scientific (Waltham, MA). Deca-His peptide was purchased from New-England Peptide (Gardner, MA). His-tagged EcDHFR was expressed and purified in house from a custom modified plasmid as described later in this section. EDTA, DPH and TEMPO were obtained from Sigma-Aldrich (St. Louis, MO). MOPS, Sodium Chloride, and Amicon Ultra-0.5 mL centrifugal filters (10kDa MWCO) were obtained from EMD Millipore (Billerica, MA).

2.4.2 Protein expression and purification. EcDHFR was expressed and purified following steps as detailed elsewhere.[30] Briefly, protein expression was carried out by using E. coli strain BL21(DE3) with Luria-Bertani (LB) medium containing 100μg/mL ampicillin. A single ampicillin resistant colony that was then inoculated into a 20 mL culture flask containing 5 mL of LB (with ampicillin) medium at 37 °C overnight inside a shaker incubator maintained at 200 rpm. 1 mL of the starter culture was then inoculated into a large conical flask containing 1 L of LB medium with antibiotic and allowed to grow

until the optical density at 600 nm reached 0.6-1.0. Next, inducer was added to a final concentration of 1 mM. Isopropyl β-D-1 thiogalactopyranoside (IPTG) was used as an inducer. The resulting culture was subjected to vigorous shaking in a shaking incubator and allowed to grow for at least 6 hours to overnight. The cells were then harvested by centrifugation and subjected to cell lysis.

The pellets were resuspended in a lysis buffer containing 50 mM Tris, 150 mM NaCl, 5 mM β-Mercaptoethanol, containing protease inhibitor (from tablets of protease inhibitor cocktail). 1 mg/mL of Lysozyme was then added to the mixture, stirred on ice for an hour and sonicated on ice (Sonic Dissemble model 500, Fisher Scientific, Pittsburgh, PA). The lysed cells were then subjected to centrifugation, and the supernatant was filtered and purified using HisPrep affinity column on an AKTA FPLC system (GE Healthcare, Pittsburgh, PA). The proteins were eluted by using an imidazole gradient to competitively unbind the attached proteins to the Ni-NTA column. The eluted protein was subjected to desalting and concentrated using an Amicon concentrator with a 10 kDa molecular weight cutoff. The protein samples were then buffer exchanged to 50 mM MOPS buffer maintained at a pH 7.2. For all DHFR samples, a small concentration of reducing agent (1 mM DTT) was added to prevent the possibility of disulfide formation.

2.4.3 Large unilamellar vesicles preparation. Large unilamellar vesicles (LUVs) were prepared by traditional extrusion method. Briefly, the lipid mixtures were dissolved in chloroform and dried under a stream of Argon gas on the inner wall of a small vial and then placed under vacuum overnight to form stable lipid cakes. The composition of binary mixtures was 79.6 mol% DPPC, 20 mol% Ni-NTA-DGS, 0.2 mol% NBD-PE and 0.2 mol% Rhodamine-PE. For uniform fluid liposomes, POPC was used in the place of DPPC. The

lipid cakes were subsequently rehydrated to a final liposome concentration of 1mM with MOPS buffer (50 mM MOPS, pH 7.2) for 1 hour at room temperature. Every 15 minutes, the rehydrated lipid solution was vortexed thoroughly, and subsequently subjected to at least five freeze thaw cycles. The resulting multi-lamellar vesicle solutions were then extruded through a polycarbonate membrane (pore size 100 nm; Whatman/GE Healthcare) at least 20 times to produce a clear solution of liposomes. For generating vesicles of different curvatures, PC membranes with pore sizes of 30, 50, 100 and 200 nm were used.

2.4.4 Dynamic light scattering measurements. Micromeritics Corporation's NanoPlus, a particle size analyzer was used to perform dynamic light scattering (DLS) to measure the changes in hydrodynamic diameter of the liposomes with and without the presence of protein solution. A final liposome concentration of 0.5 mM was used in all experiments. A micro-volume glass cuvette capable of measuring sample volumes as low as 60 μL was used for all measurements. Optimization of scattering intensity was performed by adjusting the cell-center, and by tuning the laser attenuation. All measurements were performed in room temperature and repeated three times. Cumulant diameter values were reported in the main text and intensity weighted values are reported in the appendix.

2.4.5 Equilibrium fluorescence measurements for CDC determination. Steady state fluorescence measurements were performed on Horiba Fluorometer. A micro-volume cuvette capable of measuring solution volumes as low as 150 μL was used for all measurements. The final bulk concentration of Ni-NTA DGS in the liposome samples were maintained at 100 μM, and the protein solution was added at the reported

concentrations. Determination of CDC, was performed in a high throughput fashion using BioTek Cytation 5 multi-mode microplate reader. Sample excitation was performed at the wavelength of 463 nm. Quantification of critical deformation concentration was performed by fitting the change in $F_{Donor}/F_{Acceptor}$ ratio as a function of protein concentration, to a sigmoidal function. Untreated, clear bottomed flat 96-well plates were used for all experiments. For studying the curvature dependence of CDC, the concentration of the resulting liposomes from extrusion was approximated by the fluorescence emission from the acceptor excitation (560 nm).

2.4.6 Fluorescence lifetime measurements.

Fluorescence lifetime measurements were performed on a Nikon Ti Eclipse Inverted Confocal microscope (C2Si). The confocal system was attached to a Picoquant (Berlin, Germany) Laser Scanning Microscope Time Correlated Single Photon Counting upgrade. For NBD fluorescence, a 485 nm pulsed laser was operated at 20MHz and the donor and the acceptor emission were distinguished by a combination of a dichroic filters (561) and bandpass filters (centered at 520 and 582 nm) respectively. The emitted fluorescence lifetime traces were using SymPhoTime 64 software, utilizing Fast FLIM algorithm. The IRF was collected using heavily quenched samples made of Erythrosine B in a saturated solution of Potassium Iodide. All measurements were repeated for 3 times, and concentration dependent changes of fluorescence lifetimes were acquired by using a clear, untreated 96-well plate.

2.4.7 Isothermal Titration Calorimetry.

All ITC experiments reported in this chapter was performed using a MicroCal VP-ITC in low-feedback mode. A total of 31 injections were performed, resulting in titration of liposomes stock in the titrator syringe into a thoroughly rinsed cell chamber containing

the protein sample. A Ni-NTA DGS concentration of 350 μM (Total liposome concentration of 1.75 mM in case of 20mol% Ni-NTA DGS) was used in all experiments, and the DPPC and POPC concentration was varied to accommodate changing chelator lipid densities. The protein stock solutions were maintained at 9 μM unless otherwise reported. The reference power was maintained at 10 μCal/sec and the cell temperature (20 °C) was equilibrated for at least 30 minutes. The spacing between injections was set 360 seconds and data from the first injection was always discarded due to artifacts from dilution. Data analysis was performed by the MicroCal Analysis software, and the obtained enthalpograms were fit to one (for POPC-Ni-NTA mixtures) or two site model (for binary mixtures).

2.4.8 Observation of domain by DPH quenching.

The quenching of fluorescence from DPH by TEMPO was measured via equilibrium fluorescence spectrometer as described in section 2.4.5. Briefly, liposome suspensions containing a total vesicle concentration of 1mM was mixed vigorously with 0.025 μM DPH for at least 30 minutes. Due to limited aqueous solubility of DPH, stock solutions were formed with Tetrahydrofuran and subsequently diluted with water. For obtaining fluorescence spectra in 2.6B, a relatively higher concentration of DPH was used (25 μM) for improved signal to noise. The 30-minute incubation time leads to spontaneous partitioning of DPH into the bilayer. For quenching experiments, a concentrated 1M stock solution of TEMPO in ethanol was diluted to reach 6mM final concentration for each sample. After incubation for nearly 20 minutes, the fluorescence of DPH was monitored by excitation at 360 nm and emission at 430 nm respectively. The unquenched fraction was calculated by dividing the fluorescence intensities obtained in the presence and absence of TEMPO.

2.4.9 Approximation of domain radius.

The approximation of vesicle curvature dependent domain radius was performed by using the method previously described elsewhere.[41] Briefly, the unquenched fraction (Q) acts as a reporter of the Lo regions inaccessible to TEMPO. Hence, quenching of DPH by TEMPO in the Lo domain is extremely weak. Hence, the factor Q should correlate with the size of the Lo domain. The Förster radii of DPH and TEMPO are 3.6nm and 1.2nm respectively. At the concentrations utilized for our experiments, we expect a large excess of TEMPO that presumably saturates the liposome surface. Given the lipid/DPH ratio was maintained at 40000/1, we expect not more than 1 or 2 DPH molecules to be distributed across the liposome surface. By assuming that the domains are circular in shape, an estimate of relative domain sizes can be computed by using the following equation

$$X = [R_{TEMPO} + R_{DPH}] \left[\frac{Q_{liposome} - Q_{POPC}}{Q_{DPPC} - Q_{POPC}}\right] \qquad (1)$$

Where X is the apparent domain radius. R_{TEMPO} and R_{DPH} represents the Förster radii of TEMPO and DPH respectively. $Q_{liposome}$ is the unquenched fraction of fluorescence from the sample of interest. Q_{DPPC} and Q_{POPC} are the unquenched fluorescence remaining from DPH in DPPC and POPC respectively. For curvature dependent measurements, to account for the slight changes in defect sites found in pure DPPC vesicles, only the Q values from vesicles of similar diameters were considered. The apparent domain sizes were calculated and plotted in Figure A 2.6

2.4.10 Small Angle X-Ray Scattering. The SAXS experiments were performed on a Rigaku BioSAXS-2000 home-source system with a HF007 copper rotating anode with a Pilatus 100K Detector. SAXS data were collected at a fixed sample-to-detector distance

using a silver behenate calibration standard. 6.5mM of extruded SUVs were loaded into the sample using the autosampler attachment. All measurements were performed by subtracting a reference from the sample's scattering signal. At least 12 scans of individual samples were averaged and reduced using Rigaku SAXSlab data collection and processing software. The software - PRIMUS was used for preliminary data analysis. Data fitting, and SLD analysis was performed using our in-house fitting routine described elsewhere.

2.5 References.

1. Huttner, W. B.; Zimmerberg, J., Implications of lipid microdomains for membrane curvature, budding and fission. *Curr Opin Cell Biol* **2001,** *13* (4), 478-84.

2. Gruner, S. M., Intrinsic curvature hypothesis for biomembrane lipid composition: a role for nonbilayer lipids. *Proc Natl Acad Sci U S A* **1985,** *82* (11), 3665-9.

3. Lipowsky, R., Domain-induced budding of fluid membranes. *Biophys J* **1993,** *64* (4), 1133-8.

4. Simons, K.; Toomre, D., Lipid rafts and signal transduction. *Nat Rev Mol Cell Biol* **2000,** *1* (1), 31-9.

5. Edidin, M., Lipids on the frontier: a century of cell-membrane bilayers. *Nat Rev Mol Cell Biol* **2003,** *4* (5), 414-8.

6. Chen, C. S.; Mrksich, M.; Huang, S.; Whitesides, G. M.; Ingber, D. E., Geometric control of cell life and death. *Science* **1997,** *276* (5317), 1425-8.

7. Callan-Jones, A.; Sorre, B.; Bassereau, P., Curvature-driven lipid sorting in biomembranes. *Cold Spring Harb Perspect Biol* **2011,** *3* (2).

8. Carlton, J.; Bujny, M.; Peter, B. J.; Oorschot, V. M.; Rutherford, A.; Mellor, H.; Klumperman, J.; McMahon, H. T.; Cullen, P. J., Sorting nexin-1 mediates tubular endosome-to-TGN transport through coincidence sensing of high- curvature membranes and 3-phosphoinositides. *Curr Biol* **2004,** *14* (20), 1791-800.

9. Bissig, C.; Gruenberg, J., Lipid sorting and multivesicular endosome biogenesis. *Cold Spring Harb Perspect Biol* **2013,** *5* (10), a016816.

10. Obara, K.; Kojima, R.; Kihara, A., Effects on vesicular transport pathways at the late endosome in cells with limited very long-chain fatty acids. *J Lipid Res* **2013,** *54* (3), 831-42.

11. Veatch, S. L.; Keller, S. L., Organization in lipid membranes containing cholesterol. *Phys Rev Lett* **2002,** *89* (26), 268101.

12. Heinrich, M.; Tian, A.; Esposito, C.; Baumgart, T., Dynamic sorting of lipids and proteins in membrane tubes with a moving phase boundary. *Proc Natl Acad Sci U S A* **2010,** *107* (16), 7208-13.

13. Peter, B. J.; Kent, H. M.; Mills, I. G.; Vallis, Y.; Butler, P. J.; Evans, P. R.; McMahon, H. T., BAR domains as sensors of membrane curvature: the amphiphysin BAR structure. *Science* **2004,** *303* (5657), 495-9.

14. Mim, C.; Unger, V. M., Membrane curvature and its generation by BAR proteins. *Trends Biochem Sci* **2012,** *37* (12), 526-33.

15. Sonnino, S.; Mauri, L.; Chigorno, V.; Prinetti, A., Gangliosides as components of lipid membrane domains. *Glycobiology* **2007,** *17* (1), 1R-13R.

16. Heberle, F. A.; Feigenson, G. W., Phase separation in lipid membranes. *Cold Spring Harb Perspect Biol* **2011,** *3* (4).

17. Dietrich, C.; Schmitt, L.; Tampe, R., Molecular organization of histidine-tagged biomolecules at self-assembled lipid interfaces using a novel class of chelator lipids. *Proc Natl Acad Sci U S A* **1995,** *92* (20), 9014-8.

18. Fischer, N. O.; Blanchette, C. D.; Chromy, B. A.; Kuhn, E. A.; Segelke, B. W.; Corzett, M.; Bench, G.; Mason, P. W.; Hoeprich, P. D., Immobilization of His-tagged proteins on nickel-chelating nanolipoprotein particles. *Bioconjug Chem* **2009,** *20* (3), 460-5.

19. Stachowiak, J. C.; Schmid, E. M.; Ryan, C. J.; Ann, H. S.; Sasaki, D. Y.; Sherman, M. B.; Geissler, P. L.; Fletcher, D. A.; Hayden, C. C., Membrane bending by protein-protein crowding. *Nat Cell Biol* **2012,** *14* (9), 944-9.

20. Chen, Z.; Atefi, E.; Baumgart, T., Membrane Shape Instability Induced by Protein Crowding. *Biophys J* **2016,** *111* (9), 1823-1826.

21. Siaw, H. M. H.; Raghunath, G.; Dyer, R. B., Peripheral Protein Unfolding Drives Membrane Bending. *Langmuir* **2018,** *34* (28), 8400-8407.

22. Jensen, M. B.; Bhatia, V. K.; Jao, C. C.; Rasmussen, J. E.; Pedersen, S. L.; Jensen, K. J.; Langen, R.; Stamou, D., Membrane curvature sensing by amphipathic helices: a single liposome study using alpha-synuclein and annexin B12. *J Biol Chem* **2011,** *286* (49), 42603-14.

23. Lohr, C.; Kunding, A. H.; Bhatia, V. K.; Stamou, D., Constructing size distributions of liposomes from single-object fluorescence measurements. *Methods Enzymol* **2009,** *465*, 143-60.

24. Larsen, J. B.; Jensen, M. B.; Bhatia, V. K.; Pedersen, S. L.; Bjornholm, T.; Iversen, L.; Uline, M.; Szleifer, I.; Jensen, K. J.; Hatzakis, N. S.; Stamou, D., Membrane

curvature enables N-Ras lipid anchor sorting to liquid-ordered membrane phases. *Nat Chem Biol* **2015,** *11* (3), 192-4.

25. Chen, I. A.; Szostak, J. W., A kinetic study of the growth of fatty acid vesicles. *Biophys J* **2004,** *87* (2), 988-98.

26. Fung, B. K.; Stryer, L., Surface density determination in membranes by fluorescence energy transfer. *Biochemistry* **1978,** *17* (24), 5241-8.

27. Struck, D. K.; Hoekstra, D.; Pagano, R. E., Use of resonance energy transfer to monitor membrane fusion. *Biochemistry* **1981,** *20* (14), 4093-9.

28. Baumgart, T.; Hunt, G.; Farkas, E. R.; Webb, W. W.; Feigenson, G. W., Fluorescence probe partitioning between Lo/Ld phases in lipid membranes. *Biochim Biophys Acta* **2007,** *1768* (9), 2182-94.

29. Baccanari, D. P.; Averett, D.; Briggs, C.; Burchall, J., Escherichia coli dihydrofolate reductase: isolation and characterization of two isozymes. *Biochemistry* **1977,** *16* (16), 3566-72.

30. Kozlowski, R.; Ragupathi, A.; Dyer, R. B., Characterizing the Surface Coverage of Protein-Gold Nanoparticle Bioconjugates. *Bioconjug Chem* **2018,** *29* (8), 2691-2700.

31. Zeno, W. F.; Baul, U.; Snead, W. T.; DeGroot, A. C. M.; Wang, L.; Lafer, E. M.; Thirumalai, D.; Stachowiak, J. C., Synergy between intrinsically disordered domains and structured proteins amplifies membrane curvature sensing. *Nat Commun* **2018,** *9* (1), 4152.

32. Zeno, W. F.; Thatte, A. S.; Wang, L.; Snead, W. T.; Lafer, E. M.; Stachowiak, J. C., Molecular Mechanisms of Membrane Curvature Sensing by a Disordered Protein. *J Am Chem Soc* **2019,** *141* (26), 10361-10371.

33. Schmiedel, H.; Almasy, L.; Klose, G., Multilamellarity, structure and hydration of extruded POPC vesicles by SANS. *Eur Biophys J* **2006,** *35* (3), 181-9.

34. Fuldner, H. H., Characterization of a third phase transition in multilamellar dipalmitoyllecithin liposomes. *Biochemistry* **1981,** *20* (20), 5707-10.

35. Kiselev, M. A.; Zemlyanaya, E. V.; Aswal, V. K.; Neubert, R. H., What can we learn about the lipid vesicle structure from the small-angle neutron scattering experiment? *Eur Biophys J* **2006,** *35* (6), 477-93.

36. Bouwstra, J. A.; Gooris, G. S.; Bras, W.; Talsma, H., Small angle X-ray scattering: possibilities and limitations in characterization of vesicles. *Chem Phys Lipids* **1993,** *64* (1-3), 83-98.

37. Kucerka, N.; Pencer, J.; Sachs, J. N.; Nagle, J. F.; Katsaras, J., Curvature effect on the structure of phospholipid bilayers. *Langmuir* **2007,** *23* (3), 1292-9.

38. Pencer, J.; Jackson, A.; Kucerka, N.; Nieh, M. P.; Katsaras, J., The influence of curvature on membrane domains. *Eur Biophys J* **2008,** *37* (5), 665-71.

39. Parthasarathy, R.; Yu, C. H.; Groves, J. T., Curvature-modulated phase separation in lipid bilayer membranes. *Langmuir* **2006,** *22* (11), 5095-9.

40. Tian, A.; Capraro, B. R.; Esposito, C.; Baumgart, T., Bending stiffness depends on curvature of ternary lipid mixture tubular membranes. *Biophys J* **2009,** *97* (6), 1636-46.

41. Suga, K.; Umakoshi, H., Detection of nanosized ordered domains in DOPC/DPPC and DOPC/Ch binary lipid mixture systems of large unilamellar vesicles using a TEMPO quenching method. *Langmuir* **2013,** *29* (15), 4830-8.

42. Klausner, R. D.; Kleinfeld, A. M.; Hoover, R. L.; Karnovsky, M. J., Lipid domains in membranes. Evidence derived from structural perturbations induced by free fatty acids and lifetime heterogeneity analysis. *J Biol Chem* **1980,** *255* (4), 1286-95.

43. Pathak, P.; London, E., Measurement of lipid nanodomain (raft) formation and size in sphingomyelin/POPC/cholesterol vesicles shows TX-100 and transmembrane helices increase domain size by coalescing preexisting nanodomains but do not induce domain formation. *Biophys J* **2011,** *101* (10), 2417-25.

44. Ahmed, S. N.; Brown, D. A.; London, E., On the origin of sphingolipid/cholesterol-rich detergent-insoluble cell membranes: physiological concentrations of cholesterol and sphingolipid induce formation of a detergent-insoluble, liquid-ordered lipid phase in model membranes. *Biochemistry* **1997,** *36* (36), 10944-53.

45. Ickenstein, L. M.; Arfvidsson, M. C.; Needham, D.; Mayer, L. D.; Edwards, K., Disc formation in cholesterol-free liposomes during phase transition. *Biochim Biophys Acta* **2003,** *1614* (2), 135-8.

46. Patel, L. A.; Kindt, J. T., Coarse-grained molecular simulations of the melting kinetics of small unilamellar vesicles. *Soft Matter* **2016,** *12* (6), 1765-77.

47. Nagarajan, S.; Schuler, E. E.; Ma, K.; Kindt, J. T.; Dyer, R. B., Dynamics of the gel to fluid phase transformation in unilamellar DPPC vesicles. *J Phys Chem B* **2012,** *116* (46), 13749-56.

Appendix 2: Curvature regulated phase separation in binary lipid mixtures, and its role in membrane bending

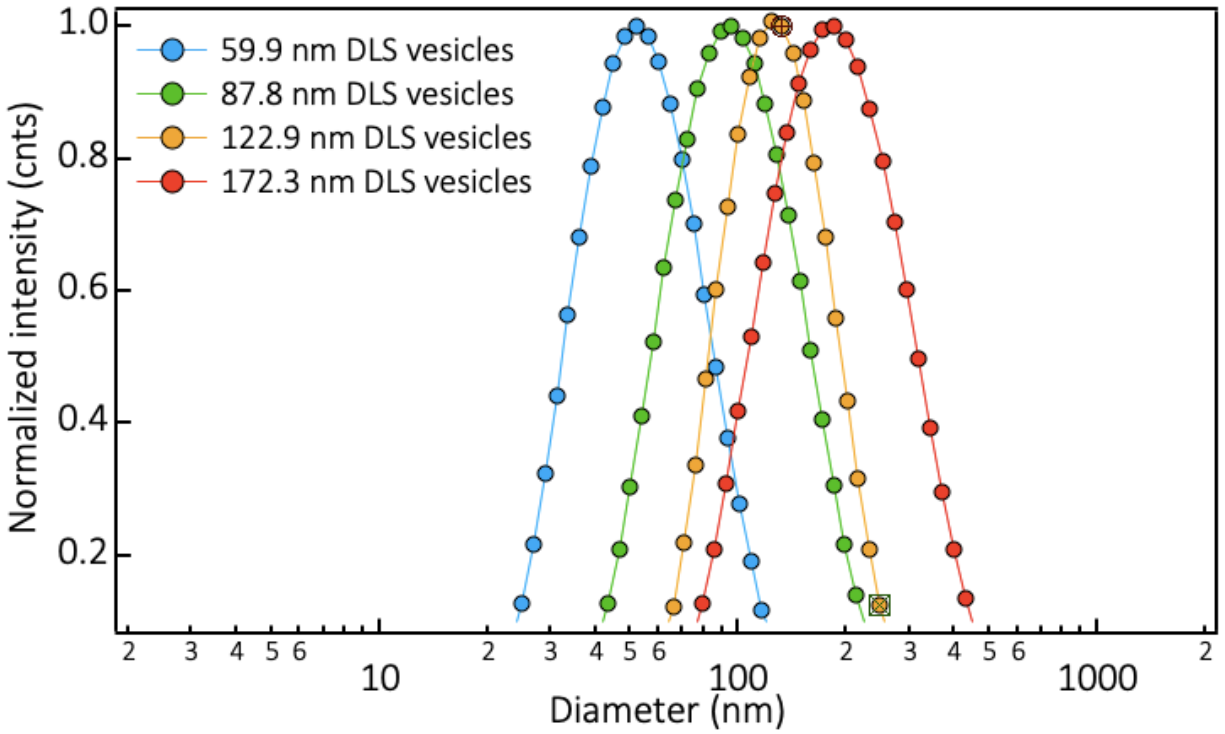

Figure A2.1. Dynamic Light Scattering intensity profiles of vesicles extruded via different pore sized PC membranes. Note that the diameter values in the legend describes the apparent diameters obtained from the intensity distribution. The polydispersity index of all the samples were found to be less than 0.1.

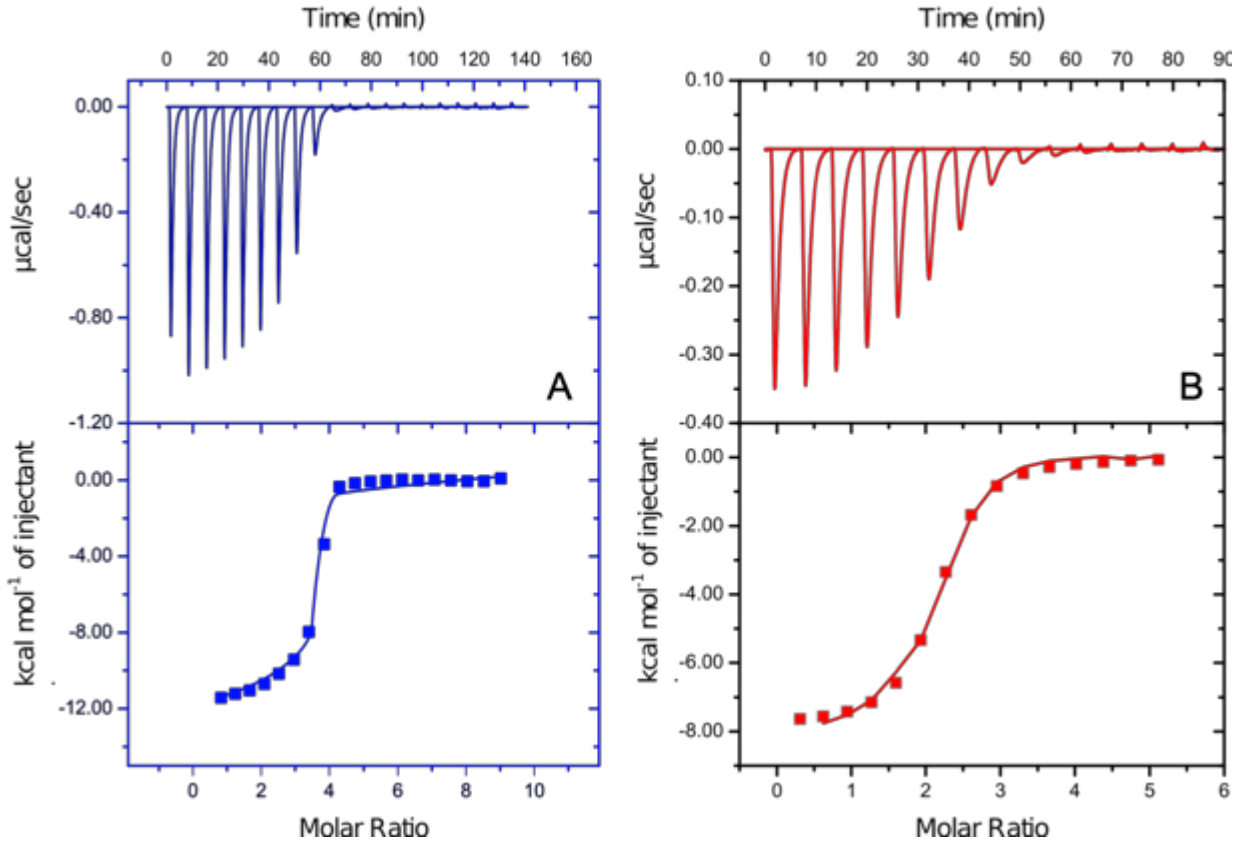

Figure A2.2. Representative ITC thermograms obtained by injecting (A) Binary mixtures containing DPPC and (B) Uniform liposomes containing POPC with the chelator lipid (350 μM Ni-NTA DGS liposomes at a 20 mol% density) into the cell chamber containing 9 μM Deca-His peptide. As seen clearly, the sharper transition in the enthalpograms in binary mixtures indicate a stronger association constant when utilizing binary mixtures.

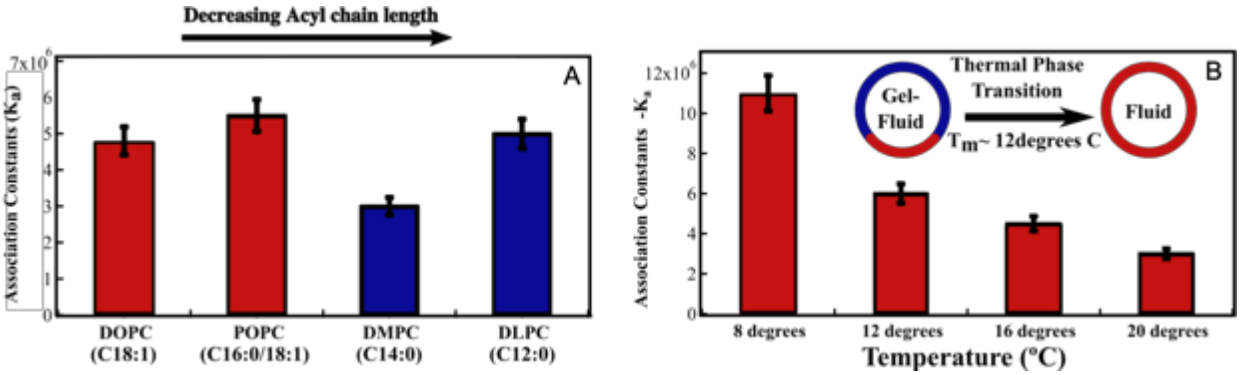

Figure A2.3. Phase separation leads to a strong enhancement of binding affinity by increasing the local chelator lipid density (A) Comparison of Association constants obtained from ITC as a function of decreasing acyl chain lengths. Red bars indicate unsaturated hydrocarbon lipids and blue bars indicate saturated hydrocarbon chain lipids above transition temperature. (B) DMPC-Ni-NTA DGS containing liposomes exhibit a decrease in association constants upon thermal phase transition, indicating that phase-separation is critical for regulating binding affinity of proteins to the liposome surface. Insets show a schematic of phase separation purely for illustrative purposes.

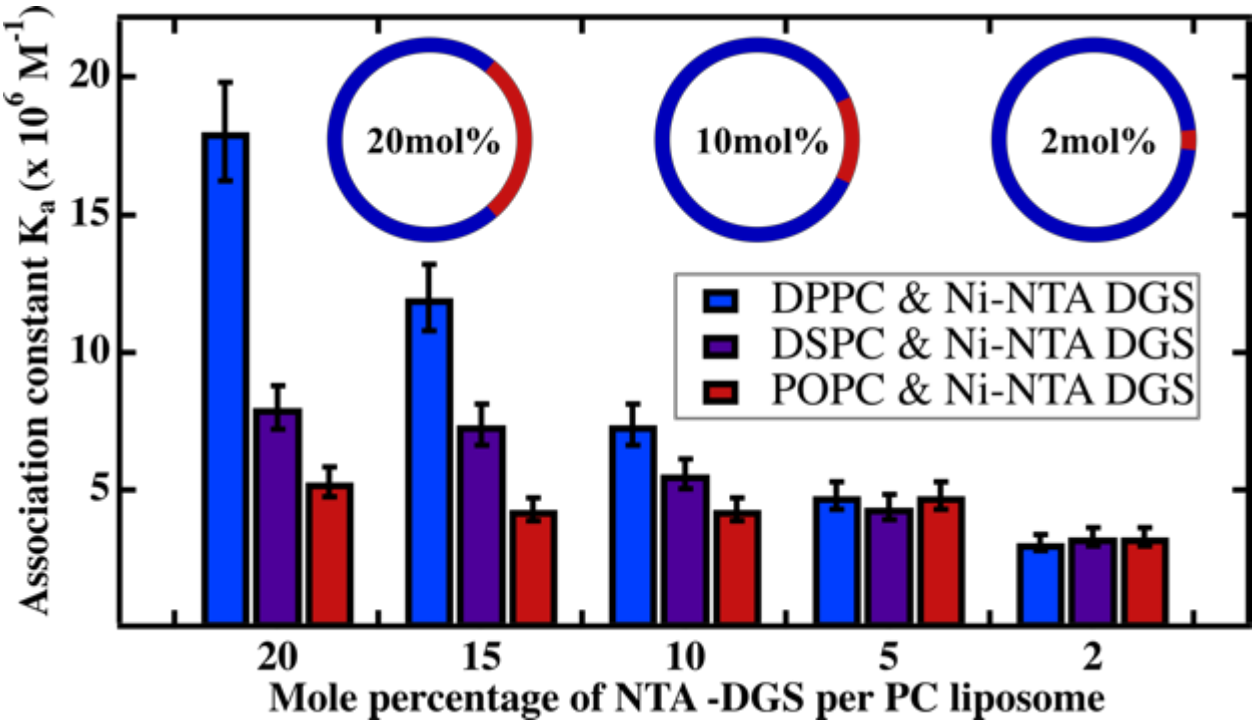

Figure A2.4. Correlation between Ni-NTA doping level and association constants. Decreasing the overall concentration of the chelator lipid leads to a significant decrease in binding constants in case of binary mixture of liposomes. With POPC containing vesicles, the change in Ka with differing chelator lipid density is extremely small.

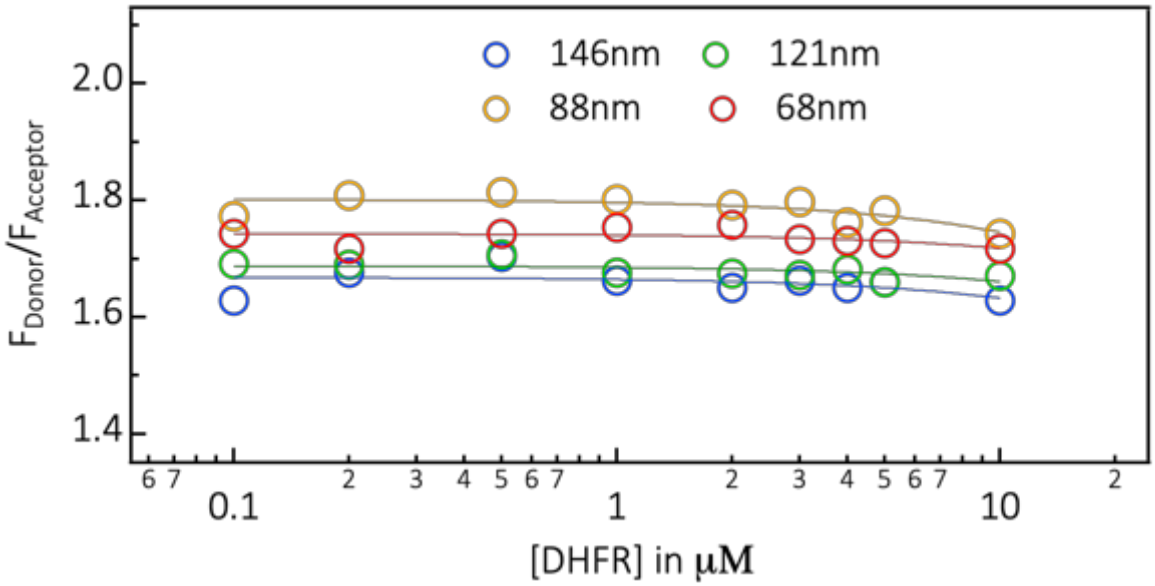

Figure A2.5. Curvature dependence of changes in NBD-Rhod FRET using POPC-Ni-NTA liposomes. No change in FRET signal is observed across the protein concentration range, indicating that membrane deformation does not occur in fluid liposomes due to the availability of liposome surface area.

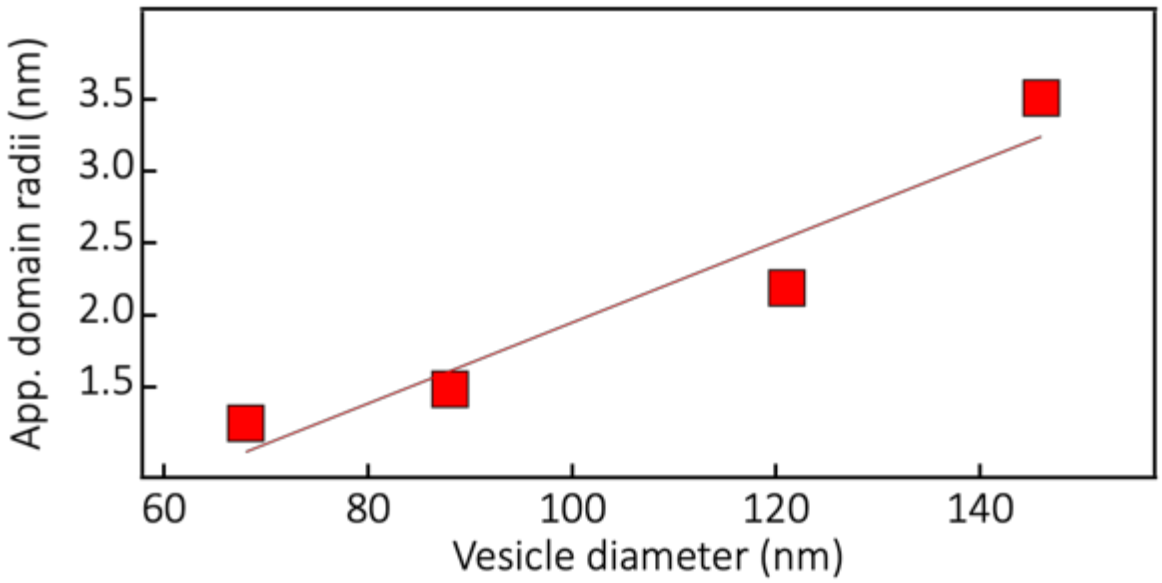

Figure A2.6. Calculation of apparent domain sizes by TEMPO quenching of DPH fluorescence. The data clearly shows that the relative size of the gel-phase domains increases with increasing vesicle diameter. The linear fit between data points is meant to guide the reader.

Chapter 3

Kinetics of histidine tagged protein association to nickel-decorated liposome surfaces

3.1 INTRODUCTION

Regulation of peripheral protein association with the membrane surface plays an indispensable role in cell signaling, recognition, division, and several other important physiological processes. [1-2] At a molecular level, peripheral membrane protein attachment is capable of manipulating the membrane structure, and reciprocally, membrane surfaces can control the protein conformation, orientation and oligomerization.[3-4] A complex relationship between protein binding and the structure of membrane surfaces has been observed in a number of biological systems.[5-6] For instance, cytochrome c was found to induce non-bilayer structures in cardiolipin containing liposomes. Conversely, spontaneous curvature of cardiolipin doped vesicles was found to modulate the conformational state of the protein, thereby influencing its redox potential.[7] Hence, understanding the mechanism underlying this complex interplay between peripherally bound proteins and membrane surfaces has recently garnered tremendous interest.[8-9] Studying the dynamical nature of such interactions, however, has remained a challenge due to the complexity of the interface. Particularly, fundamental details regarding the kinetics of protein attachment to membrane surfaces remains elusive, as variables such as lipid packing, membrane lateral fluidity and the hydrodynamics of the protein structure account for only a few among the many critical factors that affect the binding mechanism and lateral organization of the bound proteins.[10-11] Hence, there exists a persistent demand for model systems that enable quantitative investigation of the kinetics of transient membrane-protein interactions.

A key requirement for such model systems is a conjugation method that emulates the transient nature of peripheral protein interaction with membrane surfaces. Nickel-chelating lipids offer a facile solution to this problem due to the reversibility of the

interaction and their widespread availability.[12] Additionally, given the ubiquity of recombinantly engineered Histidine tags in molecular biology, the nickel-nitrilotriacetic acid (Ni-NTA)-6x-His conjugation has been utilized for several applications including but not restricted to electrochemistry, 2-D protein crystallization and drug delivery.[13-15] Recently, several investigators have employed nickel containing liposomes to study membrane bending triggered by protein crowding[16]. Vesicle deformation and fission were observed at high protein densities using simple model proteins such as a 6xHis-green-fluorescent protein (GFP), purely through a non-specific colligative mechanism, indicating the importance of macromolecular crowding at a protein-membrane interface.[17-18]

For the above mentioned reasons, several groups have taken interest in characterizing protein interactions with Ni-containing liposome surfaces.[19-20] A recent study by Wasserberg *et al*, has shown that it is possible to control the orientation of fluorogenic proteins relative to a Ni-NTA containing monolayer surface by modifying the positions of histidine tags on the protein structure.[21] Through MD simulations, they show that peripheral electrostatic interactions with the monolayer can influence the orientational preference of the bound-protein structures. Despite such comprehensive studies, specific details regarding the kinetics of protein association to Ni-NTA containing surfaces remain sparse, thus limiting the mechanistic understanding of interfacial binding. One consequence has been inconsistent conclusions regarding optimal conditions for stable protein immobilization Some groups report a stable protein-lipid interaction at a supported lipid bilayer (SLB) interface,[22] whereas others report rapid unbinding of the protein layer upon mild perturbations.[23] Even the studies that have explored the

timescales of protein desorption do not provide quantitative rate constants for association due to the limited time resolution of their techniques.[20]

Additionally, most studies are performed by using a Ni-NTA decorated SLB surface, which does not adequately represent the complexity of a protein-liposome interface, where membrane structural changes are a common occurrence in biology as a direct consequence of transient protein association.[24-25] The dearth of mechanistic knowledge pertaining to such complex systems greatly inhibit our understanding of physiologically relevant processes such as membrane bending triggered by protein crowding. Protein hydrodynamics and association to a crowded liposome interface has been identified to be important for generating membrane curvature in a number of studies.[26] Intrinsically disordered proteins were found to induce membrane curvature with greater efficiency than compact globular proteins.[27] α-synuclein, for instance has been proposed to induce membrane curvature through a concerted mechanism involving both membrane penetration and crowding.[28] For these reasons, a quantitative approach to understanding the association kinetics is necessary to further our mechanistic knowledge about the nature of his-tagged protein- liposome interaction.

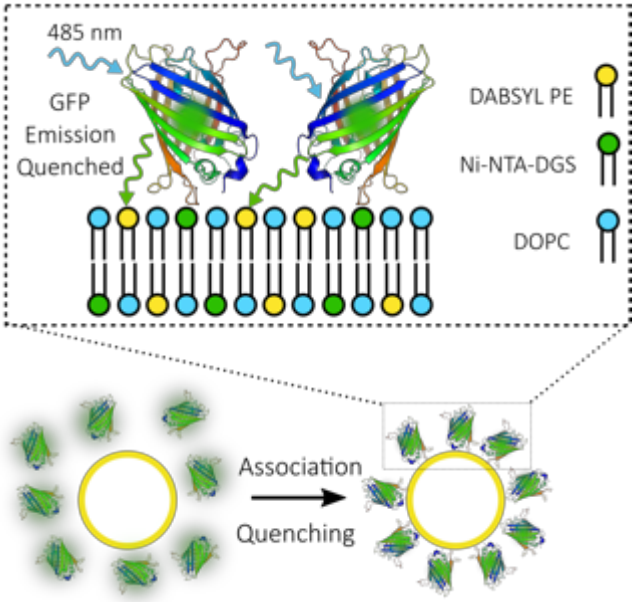

Figure 3.1. A schematic of SfGFP fluorescence quenching by Dabsyl-PE. Both the chelator lipid and the surrounding lipid DOPC contain unsaturated hydrocarbon tail, resulting in liposomes that exist purely in the fluid phase.

In this chapter, we systematically investigate the association kinetics of a histidine-tagged protein to a Ni-NTA decorated liposome, utilizing SfGFP as a model system. We utilized the intrinsic fluorescence from histidine-tagged SfGFP as a spectroscopic probe for our experiments. SfGFP was the ideal candidate for investigation due to its structural stability and the buried nature of the intrinsic GFP chromophore.[29] For the quencher, we employed the non-fluorescent dark quencher DABSYL-PE,[30] incorporated to the vesicles at 5 mol% of the total vesicle concentration. The quenching of SfGFP fluorescence upon binding to the vesicle surfaces containing the chelator lipid (Ni-NTA-DGS) could then be observed both in steady state and time-resolved stopped flow measurements.

This simple, yet sensitive methodology enabled us to explore a number of experimental variables, including membrane composition, lateral fluidity, chelator lipid density, protein concentration and protein surface charge and their effects on the protein-liposome association. We show that the association kinetics is multi-phasic with a fast phase preceding slow phases across the wide concentration range investigated. At lower concentrations, we find that the fast phase follows a behavior similar to bimolecular association with an increase in protein concentrations resulting in an enhancement of binding rates. Interestingly, we observe a break in that behavior for the slower phase rate constants. While the rate constants do initially increase with increasing protein concentrations, they start decreasing once a threshold is reached. Careful investigation of the binding kinetics from different experimental conditions, coupled with fluorescence anisotropy data leads us to conclude that the protein association to the membrane surface occurs through multiple independent, interconvertible conformations with varying

protein packing densities. Our studies have yielded novel mechanistic insights into the nature of interaction between histidine-tagged proteins and nickel-chelator lipids, and emphasizes the importance of considering protein conformation and hydrodynamics while designing bioconjugates that utilize similar immobilization strategies.

3.2 RESULTS AND DISCUSSION

3.2.1 Equilibrium characterization of liposome-SfGFP interaction. We optimized the experimental conditions for association kinetics measurements by characterizing the equilibrium association of SfGFP with liposomes. First, using dynamic light scattering (DLS) we found a concentration range for which the liposome morphology

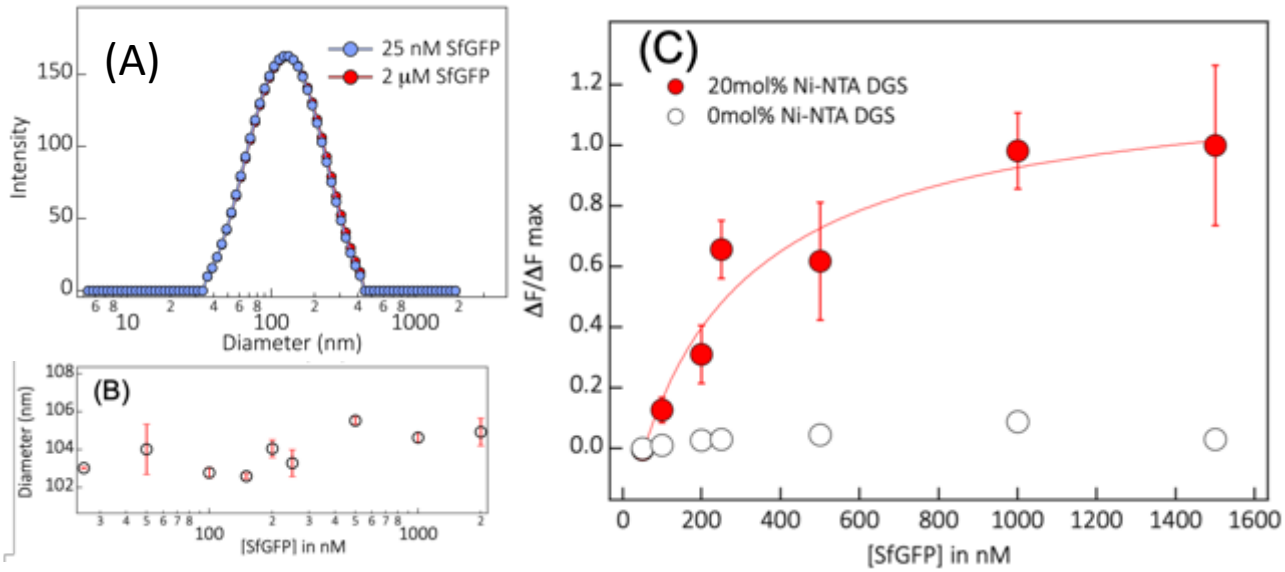

Figure 3.2. Steady state characterization of the liposome-SfGFP interaction. (A) Representative DLS intensity distribution and (B) calculated diameters of vesicles containing 20 mol% Ni-NTA DGS after incubation with protein samples of varying concentrations. Practically no change in vesicle diameter was observed, indicating that the membrane structural integrity is maintained. The average of three measurements were plotted as open circles and the error bars represent the standard deviation(C) Concentration dependent changes in steady state SfGFP fluorescence intensity. ΔF/ΔFmax was calculated by dividing the decrease in fluorescence at the given concentration by the maximal decrease in fluorescence. The data were fit to the Hill equation and coefficients are reported in (Table A3.2). Error bars represent the standard deviations from triplicate measurements.

remains (Fig. 3.2). Identification of the ideal concentration regime was important due to recent observations from several groups about the possibility of membrane deformation under high-concentrations of histidine-tagged proteins and Ni-NTA-DGS containing liposomes.

Using an identical liposome concentration (1 mM) across all measurements (with and without the presence of chelator lipids), we observe no change in hydrodynamic diameter from DLS measurements. This indicates that the structural integrity of the liposomes was preserved, even at higher concentrations of the protein (2μM SfGFP). Once optimal conditions were identified, we verified the sensitivity of the SfGFP-Dabsyl fluorophore-quencher pair by performing equilibrium fluorescence characterization using a fluorescence plate reader. Keeping the liposome concentration identical across the wells in a 96-well plate, we varied the protein concentration to monitor the concentration dependence of the measured fluorescence in a high-throughput fashion. With liposomes containing Ni-NTA DGS we observed a strong concentration dependence of the change in fluorescence with wells containing the chelator lipids (Fig. 3.2C). To verify the specificity of the Ni-NTA and His-tag interaction, we performed control experiments either with liposomes void of Ni-NTA DGS or incubation of the bioconjugates with EDTA, a chelator known to sequester metal ions from NTA headgroups. Little to no change in fluorescence was observed in these control experiments. An apparent dissociation constant (K_d) of 247.3nM (+/- 45.3) was determined from these steady-state fluorescence measurements using the Hill-Waud model.[31] This value is smaller than expected for traditional histidine-tag and Ni-NTA interactions.[32-33] However, it is consistent with studies that have utilized chelator lipids at high densities[34] and our own isothermal titration calorimetry (ITC) measurements (Figure S3)

3.2.2 Stopped-Flow fluorescence reveals a complex, multi-phasic binding kinetics.

We employed stopped-flow fluorescence to measure the kinetics of interaction between the protein and the liposome surface. The starting concentration of the liposomes was maintained at 1 mM (DOPC with 20 mol% Ni-NTA DGS and 5mol% Dabsyl PE) and the protein concentration was varied from 50 nM to 4 μM. Under these conditions, the net concentration of Ni-NTA DGS was consistently maintained at a considerable excess relative to the total protein concentration. We observed a time-dependent quenching of the fluorescence intensity from the GFP fluorophore upon initiation of the reaction (Fig. 3.3A), consistent with our observations in the steady state fluorescence measurements.

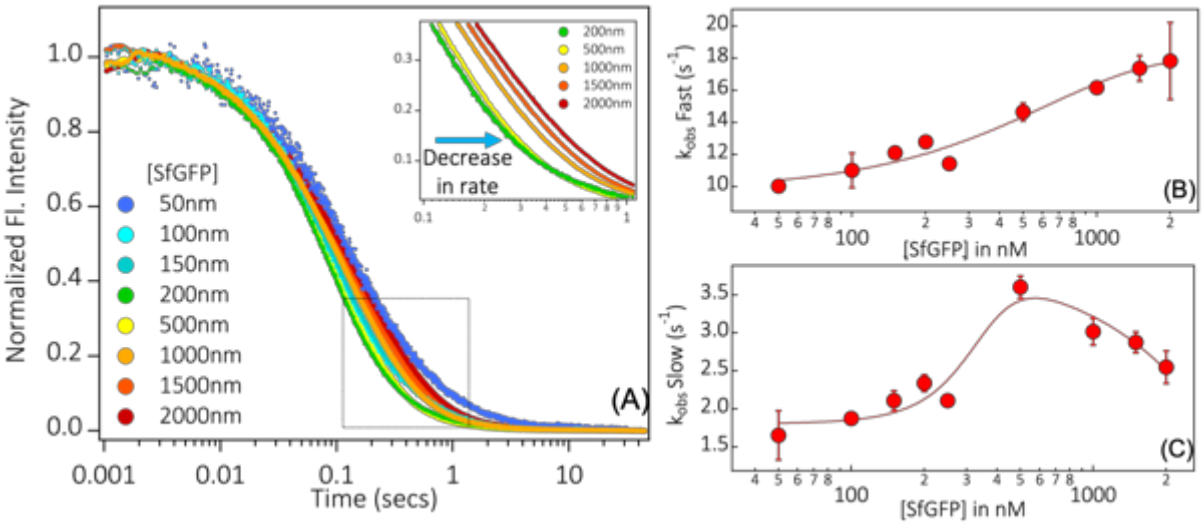

Figure 3.3. Stopped flow fluorescence transients of SfGFP fluorescence quenching by Ni-NTA DGS and Dabsyl containing liposomes. (A) Normalized fluorescence intensity of stopped flow transients and associated bi-exponential fits plotted as a function of time. Inset highlights the slowing down of quenching rates at higher SfGFP concentrations. (B) Fast phase rate constants plotted as a function of protein concentration. (C) Slow phase rate constants plotted as a function of protein concentration. Error bars represent standard deviation from three independent measurements. Solid lines are fits meant to guide the reader's eye.

We saw little to no quenching from control experiments performed with stock solutions comprising of liposomes void of the chelator lipid (Fig. A3.3). This observation confirms that fluorescence quenching is a consequence of protein binding to the liposome through a specific interaction between the histidine-tag of the protein and the Ni-NTA headgroups on the liposome surface. We observed that the stopped flow transients exhibit nonexponential fluorescence decay, requiring a bi-exponential function to adequately fit the data. Across the concentration range that was sampled, we found that the association behavior was characterized by the presence of a fast phase (k_1 = 10-20 s^{-1}) and a slower phase (k_2 = 1–4 s^{-1}). At lower protein concentrations (50 nM – 250 nM), the concentration dependence of both the fast and the slow phase rate constants exhibits a bi-molecular behavior, with increasing concentrations resulting in an increase in both the fast and the slow-phase rate constants. However, we observed that the concentration dependent increase in the fast phase rate constants plateaus once a critical concentration (~250 nM) is reached (Fig. 3.3B). Surprisingly, at the higher concentration range (500 nM – 2 μM), we notice a decrease in the slow-phase rate constants with increasing protein concentrations (Fig. 3.3C).

This observation was puzzling for a number of reasons. First, a decrease in rate constants upon increasing reactant concentrations has very little precedent in the literature. A notable exception is bacteriophage T7 RNA polymerase, which is believed to undergo extensive conformational changes upon interaction with the promoter DNA resulting in decreasing rate constants for DNA binding at higher DNA concentrations.[35] This scenario is unlikely in our experiments as the stability of our super folder construct makes it highly unlikely for any major protein structural changes as a result of binding to a liposome surface.[29] Second, the relative amplitudes obtained from the bi-exponential fits in Figure

3.3 indicate that the relative contribution to the fluorescence quenching from the slow-phase species increases with protein concentration. Interestingly, the relative amplitudes from the fast phase decreases simultaneously, with increasing protein concentration (Figure A5). This observation implies that despite a decrease in binding rate, the slower-phase represents the dominant species, particularly at higher protein concentrations. Third, the concentration of Ni-NTA-DGS (100 μM) was maintained throughout these experiments at a considerable excess relative to the protein concentration (50 nM – 2 μM) indicating that the origin of this decrease in rate constants is not a consequence of stoichiometric saturation of the available Ni-NTA sites. It is entirely possible that the charged nature of the chelator and the quencher lipid headgroups used in this study, could lead to additional electrostatic interactions between the periphery of the protein and the lipid surface. Wasserberg *et al*, have found that despite the net negative charge carried by fluorogenic proteins such as RFP, the positively charged amino acids on the protein surface, can interact with the monolayer. [21] To disrupt such interactions, a high surface density of protein at the interface was required. All these factors led us to suspect that the possibility that protein crowding at the membrane surface influences the fast and the slow binding rates.

We hypothesized that the anomalous decrease in the protein association rate with increasing protein concentration shown in Fig. 3.3C is due to the depletion of *accessible* Ni binding sites on the membrane surface. A number of factors might contribute to the accessibility of Ni binding sites and thus to the apparent slowing of the association rate, including: (1) exclusion of membrane surface area; (2) His-tag binding to multiple lipid-Ni-NTA sites (multi-valent binding); (3) protein oligomerization and (4) heterogeneity of

the protein orientation relative to the membrane surface. We tested each of these possible contributions by varying the chelator lipid density, the lateral mobility of the lipids, the protein charge and the protein orientation, to elucidate the molecular origin of the concentration dependent decrease in kinetics of protein association to the liposome surface.

3.2.3 The role of chelator lipid density on association kinetics.

First, we tested whether the unusual concentration dependence of the slow rate is a consequence of an area exclusion effect of the protein's footprint at the liposome surface.[36] We expect the surface area available for stable immobilization of the protein to decrease with higher surface density, since the concentration of the liposomes was maintained constant as the protein concentration was increased. Therefore, we postulated that the decrease in observed binding rate with increasing protein concentration is a consequence of the reduced surface area available for binding. We tested this hypothesis by changing the density of the chelator lipid on the liposome surface as a means of controlling the protein-surface occupancy and the availability of binding surface area for the histidine-tagged protein. A positive correlation between chelator-lipid loading and protein surface coverage is well established in the literature.[37] Hence, for a given lipid composition that does not exhibit phase separation, the total liposome surface area available for the protein to bind should increase with decreasing chelator lipid density.

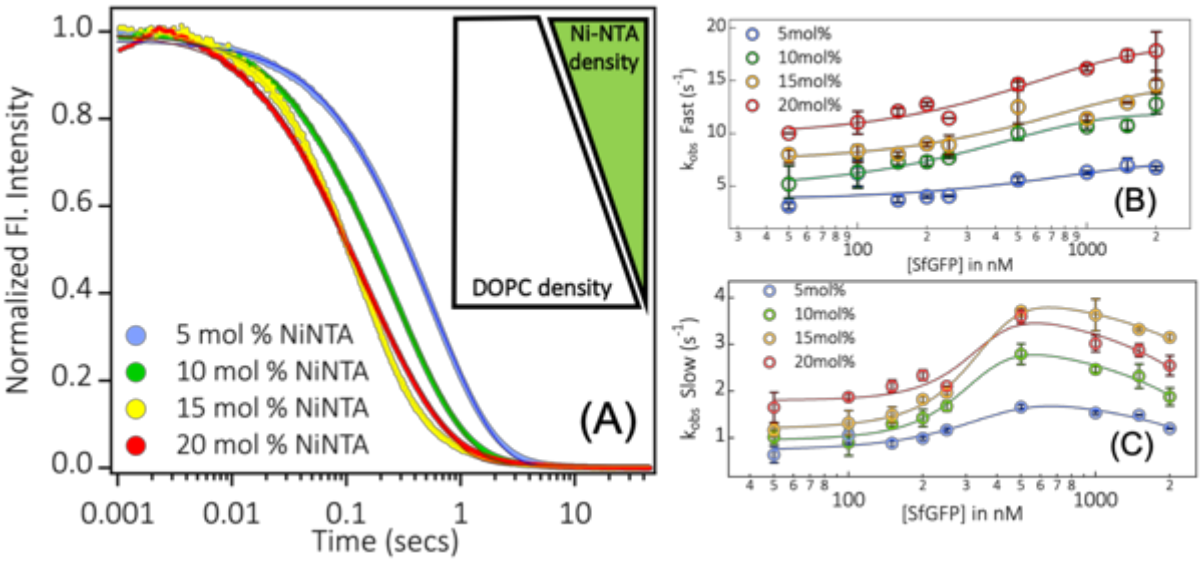

Figure 3.4 Effects of chelator lipid density on protein binding kinetics (A) Representative stopped flow transients and associated bi-exponential fits plotted as a function of time. Inset represents how the bulk concentration of Ni-NTA-DGS was maintained constant, by changing the DOPC concentration. (B) Fast phase rate constants plotted as a function of protein concentration. (C) Slow phase rate constants plotted as a function of protein concentration. Error bars represent standard deviation from three independent measurements. Solid lines are fits meant to guide the reader's eye.

To generate different densities of the chelator lipid in the liposomes, we maintained a constant bulk concentration of the Ni-NTA-DGS (200 μM) and instead varied the amount of DOPC (non-chelating lipid) and the DABSYL-PE quencher incorporated in the lipid cakes, before hydration and vesicle formation (see Experimental Section). It was critical to maintain a constant concentration of the chelator lipids to allow direct comparison of the kinetics of protein binding across a range of protein concentrations. Stopped flow kinetics were measured for four different chelator lipid densities ranging from 5 mol% Ni-NTA-DGS to 20 mol% Ni-NTA-DGS as a function of SfGFP concentration (Fig. 3.4). Analysis of the stopped flow transients revealed that changing the density of the chelator lipids, significantly affects the overall rates of protein association (Figure 3.4A). Both the

slow and the fast phase rate constants were found to increase as a function of increasing chelator lipid densities across the range of protein concentration sampled (Figure 3.4B & 4C). We attributed this increase in observed rates to the slowing down of the dissociation rates as a consequence of stronger interaction with the Ni-NTA headgroups due to increased chelator density,[37] and possible electrostatic interactions between the positively charged amino acids present on the surface of the protein, and the negatively charged bilayer surface.[21] The enhancement in binding affinity by increasing Ni-NTA density has been previously observed in the literature[20, 37] and subsequently corroborated by our ITC measurements (Figure A3.3).

The unusual trend of decreasing rate constants with increasing protein concentration persisted over the full range of chelator lipid doping levels examined (Figure 3.4C). At higher protein concentrations (>500 nM), we found that the rate of the slow phase decreased linearly, irrespective of the Ni-NTA density. The rate of decrease (k_{fall}) was obtained by a linear fit of the the slow-phase rate constants at concentrations >500 nM (Figure A3.6). Interestingly, the absolute values for kfall increases as the Ni-NTA density is increased, indicating that chelator lipid accessibility and depletion of available membrane surface area upon the initial protein binding event might be responsible for the unusual slowing of the association kinetics.

Nye et al reached a similar conclusion from protein desorption studies performed on a supported bilayer.[20] According to their model, the initial protein binding step is followed by the recruitment of multiple chelator lipids, resulting in a stable polyvalent species resistant to quick desorption. Hence, at very high protein concentrations, the initial binding step can saturate the available binding sites, thereby inhibiting the formation of a stable multivalent species, leading to a kinetic trap. Given the lateral fluidity of the lipid

membranes containing the chelator lipids, it is possible that the long-range diffusion and the ability of the His-tagged protein to recruit multiple chelator lipids might be responsible for the unusual concentration dependence of the kinetics.

3.2.4 Understanding the effects of lipid lateral mobility on association kinetics.

To assess whether the multi-valent nature of the His-tag and Ni-NTA interaction was responsible for the unusual kinetics, we measured the dependence of the kinetics on the lateral mobility of the lipids in the bilayer. The Nye model postulates His-tag binding of multiple lipid-Ni-NTA groups to form a stable poly-valent interaction. This process involves an initial monovalent association of the protein to the surface followed by recruitment of additional chelator lipids; the second step depends on the lateral mobility of lipids within the supported lipid bilayer.[22, 38] Therefore, if the unusual association kinetics is indeed a consequence of equilibration of the transient monovalent population to a stable, multi-valent complex, we reasoned that restricting the lateral mobility of the liposome surface should alter the binding kinetics. We used cholesterol to modulate systematically the lateral mobility of the liposome surface. The effects of cholesterol incorporation in fluid membranes have been studied extensively.[39] Incorporation of cholesterol into uniform DOPC membranes results in as much as a 50% decrease in the lipid lateral diffusion coefficient, relative to the pure DOPC membranes.[40]

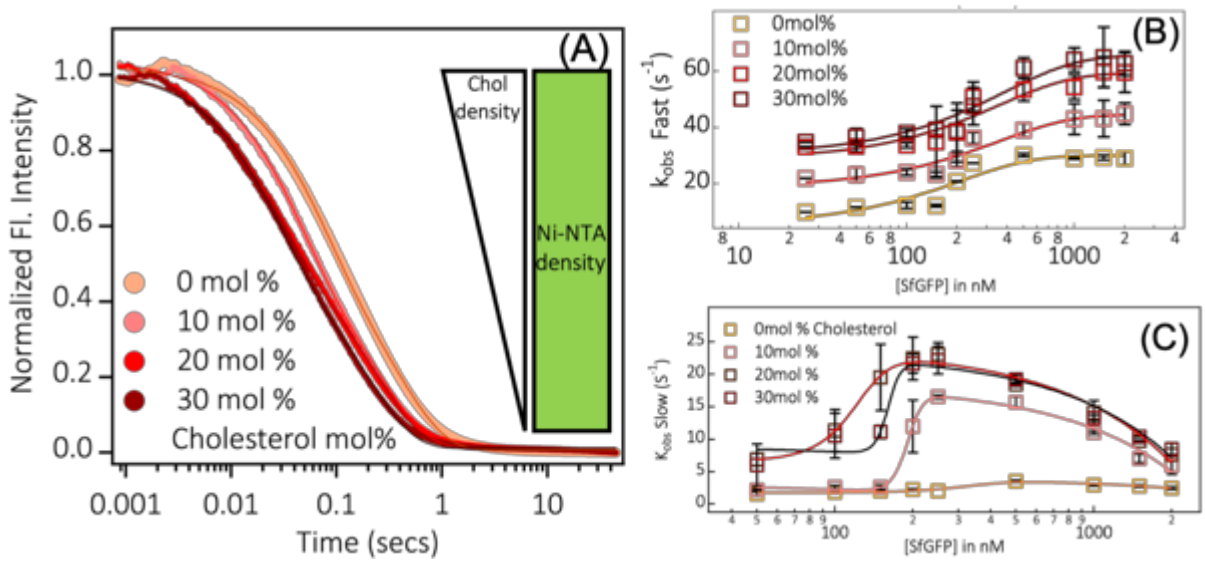

Figure 3.5. Effects of modulating lateral lipid mobility by changing cholesterol doping levels (A) Representative stopped flow transients and associated tri-exponential fits plotted as a function of time. Inset represents how the bulk concentration of Ni-NTA-DGS was maintained constant, with changes occurring only with regards to cholesterol density. (B) Fast phase rate constants plotted as a function of protein concentrations. (C) Slow phase rate constants plotted as a function of protein concentration. Error bars represent standard deviation from three independent measurements. Solid lines are fits meant to guide the reader's eye.

To quantify the change in long-range lateral diffusion coefficients upon cholesterol incorporation, we performed fluorescence recovery after photobleaching (FRAP) on supported lipid bilayers made with cholesterol doping levels ranging from 0 mol% to 30 mol% containing identical amounts of Ni-NTA-DGS and a fluorescent probe, Rhodamine-PE (Figure A7). We observed a sharp decrease in the fluorescence recovery times as the cholesterol doping level increased, indicating that incorporation of cholesterol in the lipid composition results in severe restriction of lateral membrane mobility, as expected.

Stopped flow transients were acquired with identical protein and liposome concentrations as described in previous sections (Figs. 3.3 and 3.4), but with varying

cholesterol doping levels (Fig. 3.5). Surprisingly, a significant enhancement (4-fold increase at 30 mol% cholesterol doping level) in overall binding rates was observed across the concentration range of the protein. The Nye model predicts that restriction of the lateral mobility of chelator lipids should produce a decrease in association rate, due to the decrease in the overall binding affinity, whereas we observe the opposite trend. To test the effect of incorporation of cholesterol in the membrane on the binding affinity of the protein, we performed ITC measurements (Figure A3.8). ITC data indicated an increase in binding affinity of His-tagged protein to the Ni-NTA surface with increasing cholesterol doping levels. This increase is likely due to the ability for cholesterol to alter the thickness and the orientation of PC headgroups on a liposome surface.[38] Cholesterol is known to induce strong re-orientation of surrounding lipids in a bilayer surface apart from enhancing the diffusion of surface waters around the bilayer interface.[41-42]Additionally, Blanchette *et al.* have speculated that the rotational mobility of nitrilotriacetic acid moieties can also play a role in increasing the effective density of the chelator lipids.[37] Therefore, it is plausible that cholesterol induced changes in the orientation of the Ni-NTA, can alter the accessibility of the Ni-chelating headgroups, thereby leading to enhanced binding affinity.

Regardless of the mechanistic origins of the enhanced binding rates from cholesterol incorporation, the concentration dependence of slow-phase rate constants continues to show a negative trend at high protein concentrations (Fig. 3.5C). The parameter k_{fall} obtained by a linear fit to the slow-phase rate constants as a function of concentration, provided a measure of the magnitude of this phenomenon (Figure A3.9B). We found that the absolute value of k_{fall} increases at higher cholesterol doping levels indicating that the

depletion of available protein binding surface area was accelerated by incorporation of cholesterol in the vesicle samples.

Since cholesterol can both increase the effective chelator lipid density, as well as modulate the long-range mobility of the Ni-functionalized lipids, careful consideration of both possible contributions is critical for drawing physically meaningful conclusions. If the slow-phase rate constants were a result of chelator lipid recruitment by the monovalent bound species of the protein, we would expect such an effect to manifest even at low protein concentrations. At low protein concentrations (<250 nM) however, the local protein density is very low and the availability of Ni-NTA sites (and overall membrane surface area) is abundant. Hence, decreasing the lateral mobility of the lipids by using cholesterol should significantly slow down the recruitment of the chelator lipids, but no such decrease in association rate was observed at low protein concentrations. Instead, both the fast and slow phases exhibit normal biomolecular association kinetics at low protein concentrations (Figure A3.9A). Fitting the linear increase in rate constants as a function of protein concentration yielded apparent bimolecular association constants (k_{assoc}) that were comparable irrespective of the cholesterol doping levels for both the fast and the slow phases (Figure A3.9A). This observation almost certainly excludes the possibility of long-range receptor recruitment as a plausible explanation for the slowing down of the association rates at higher protein densities. Therefore, the trend of decreasing association rates at high protein densities must be a consequence of steric occlusion of Ni-NTA binding sites from the initial protein binding step.

To validate this steric occlusion hypothesis, we modified the divalent cation bound to the chelator lipid headgroup. By utilizing Cu (II) instead of Ni (II) as the divalent cation in the chelate complex, we were able to enhance the binding affinity[43] of His-tag interaction with the liposome, without changing the lateral mobility of the surface. Stopped flow kinetics with the Cu-NTA doped liposomes revealed an enhancement in overall binding rates, with rate constants exceeding those observed with Ni-NTA containing liposome samples. However, the slow-phase rate constants decreased at higher protein densities (Figure A3.11). This observation further supports our argument that the unusual concentration dependence of slow-phase rate constants is a result of decreasing chelator lipid accessibility from the initial protein binding step, and not a result of long-range chelator lipid recruitment.

3.2.5 Protein surface charge does not significantly modify the association kinetics at high protein densities.

Another possible mechanism for the anomalous association kinetics is protein oligomerization at high densities, given the literature precedent for protein oligomerization at a crowded membrane interface.[44] To test for this possibility we designed control experiments using a super charged variant of SfGFP (-30 GFP, with a net charge of -30), which was reported in the literature to have extremely low propensity for forming higher-order oligomers or aggregates.[45] The -30 GFP was an ideal choice for this experiment, as the supercharged variants have identical structural, and fluorogenic properties as the SfGFP (net charge -7) with changes only in the overall charge at the protein surface. Hence, the electrostatic repulsion at the crowded protein interface should inhibit formation of any higher order oligomers. We acquired stopped flow transients for -30 SfGFP binding using the same liposome concentration as previously described, while

observing the protein binding timescales at higher protein concentrations (>500 nM). While the overall time scales of association were found to be different when -30 GFP was used instead of SfGFP, the stopped flow transients revealed no major change with regards to the trend of decreasing rate constants at high protein densities (Figure A3.12). This observation clearly indicates that induced protein oligomerization at very high concentrations is not responsible for the unusual association kinetics at high protein densities.

3.2.6 Protein binding to the liposome surface can occur via multiple conformations.

Having eliminated multiple scenarios that could help explain the anomalous binding kinetics, we explored the possibility of orientational heterogeneity in protein binding as an explanation for the observed behavior. While the relationship between protein orientation and protein footprint has received little attention in the literature, it is an important factor to consider for proteins that possess non-spherical tertiary folds. In the case of SfGFP, analysis of its crystal structure reveals that the beta barrel fold of the protein is likely to possess varying footprints on the membrane surface depending on the orientation of the structures relative to the membrane surface (Fig. 3.6A).[21] Theoretical prediction of the available membrane surface area upon protein binding is shown in Figure 6A. Assuming a stokes radius of 2.57nm for the end-on conformation, and 3.82nm for the side-on conformation, we estimate that protein binding leads to a strong depletion of the available membrane surface area under our experimental conditions. Hypothetically, if all protein molecules bound to the surface in a side-on mode; we expect the saturation of the membrane surface to occur at much lower concentrations owing to the higher footprint (Figure 4.6A-Inset). Interestingly, Nye *et al.* have estimated that the

packing density of GFP can vary to a large extent (between 80,000 to 200,000 molecules/μm^2) based on the orientation of the protein relative to the membrane surface.[20] Protein orientational heterogeneity was also observed in other peripherally bound systems such as streptavidin conjugates and their binding interaction with membrane surfaces.[46] Additionally, experimental exploration of globular proteins on monolayer surfaces has revealed that maximal surface density is attained only upon reorganization of globular proteins by formation of quasi-crystalline arrays on the surface.[47] Theoretical studies performed on non-specific adsorbates on planar surfaces have suggested that protein binding on a surface can occur via multiple modes – through a higher-affinity side-on conformation that leads to higher area exclusion (with lower packing capacity) or through a lower affinity end-on conformations that leads to decreased area exclusion (with better packing capacity).[48-49] The kinetic data from these models also reveal that the side-on conformation binds to the surface faster than the end-on.

However, as the protein density increases, the adsorbate flipping rate decreases presumably due to restriction of the protein's conformational freedom. Hence, despite the thermodynamic instability of the population (at high surface coverage) present in the side-on conformation, the overall protein binding timescales were slower as the adsorbate interconversion between orientations would be the rate-limiting step due to the high footprint exhibited by the side-on population (Figure 3.6A).[48]

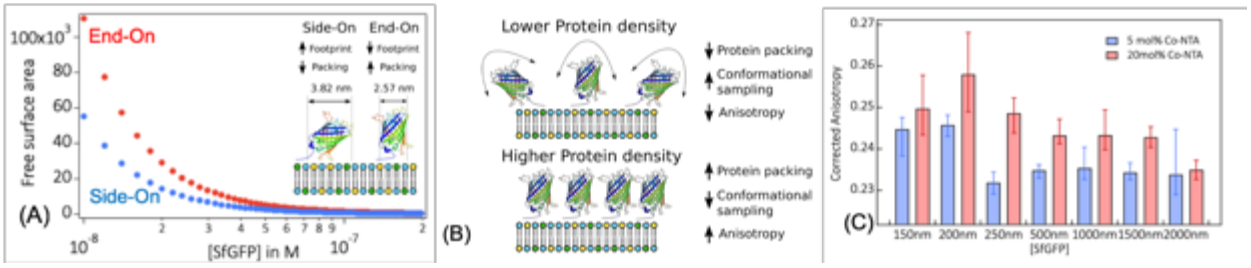

Figure 3.6. Protein footprint from alternative conformations can lead to differential surface saturation (A) Theoretical estimation of the total available liposome surface area upon SfGFP binding in different conformations. The apparent protein footprint from both structures were obtained from crystal structures explained in the Experimental section (PDB ID 2B3P). (B) Schematic representing the restricted conformational sampling as the local density of the proteins increase on the membrane surface. We hypothesized that fluorescence anisotropy should decrease further upon increasing protein packing, which in turn will decrease the degrees of conformational freedom available for the SfGFP to sample. (C) Fluorescence anisotropy describing SfGFP binding to lipid membrane surface. Correction for the scrambling of polarized light was performed using Teale. Et al's method (Figure A13).

While this model qualitatively explains a number of our experimental observations, it is worthwhile noting that a quantitative application of the model to our experiments was challenging for a number of reasons. First, the theoretical analysis by Minton et.al[48] was performed assuming that the adsorbate and the surface interacted through a non-specific mechanism. In our case, we have already proven the specificity of His-tag binding to the liposome surface via several control experiments (Fig. 3.2A). Second, the assumption

from Minton *et al's* previously published work one conformation can bind to the surface with a higher binding affinity was based on the binding potential of the interacting species. This assumption does not hold true in our experimental conditions, due to the specific nature of the protein interaction with the surface. Third, direct measurements of the changes in binding affinities between the two interconvertible protein conformations, even if existent, is extremely difficult due to experimental constraints. As a result, quantification of protein binding kinetics to distinguish the two different orientations was not feasible. To mitigate such limitations, we sought a simple, qualitative method to measure the change in the protein's ability to sample multiple conformations upon severe area exclusion at high protein densities.

Fluorescence anisotropy offers a convenient approach to measure changes in fluorophore emission transition moment relative to the excitation transition moment.[50] The technique, by virtue of its sensitivity to changes in the orientation of the fluorophore's excited state owing to molecular rotation and tumbling, has been employed in the numerous studies involving protein folding,[51-52] protein insertion into lipid membranes,[48] peripheral membrane interactions and many more.[53] If protein binding to membrane surfaces occurred with different possible binding orientations as predicted by the model of Minton *et al.*, the heterogeneity of binding and thus the fluorescence anisotropy should be sensitive to the surface packing density (Fig. 3.6B). The rotation of the 100 nm liposomes is slow on the timescale of the fluorescence lifetime and therefore does not contribute to any observed reduction of the anisotropy. At low packing densities, the protein should be able to adopt multiple side-on conformations. Increasing the packing density (by increasing the protein concentration) should produce a more highly constrained protein, predominantly in the end-on conformation and hence a larger

fluorescence anisotropy. Therefore, it should be possible to employ fluorescence anisotropy to detect changes in the average protein orientation on the liposome surface caused by a change in surface density.

Fluorescence anisotropy experiments on proteins bound to liposomes are challenging for several reasons. First, protein binding to the membrane surface has a much bigger effect on the anisotropy than the subtle difference that arises due to changes in protein orientation.[48] Second, due to the transient nature of the Ni-NTA – Histidine interaction, it is difficult to eliminate the contribution to fluorescence from the bulk, unbound protein. Third, light scattering by the liposomes will cause intrinsic depolarization of the excitation and the emitted light as reported by Teale. et al.[54] We addressed these concerns by careful experimental design. We eliminated the contribution to fluorescence emission from the bulk, unbound SfGFP, by employing a different divalent metal cation as a chelate complex. We first bound the His-tagged SfGFP to chelator lipids containing Co (II) instead of Ni (II). The oxidation of Co (II) to Co (III) provides near covalent immobilization of histidine tagged proteins as reported in the literature.[55] After size exclusion, we were able to perform measurements with conjugates only containing the liposome-protein complex and eliminate any contribution from the unbound protein in solution. We were then able to perform a calibration measurement accounting for the changes in anisotropy due to turbidity in the medium, resulting in a correction factor that enabled accurate investigation of changes in fluorescence anisotropy.[54]

We performed fluorescence anisotropy on the conjugates by comparing liposomes containing lower density of chelator lipid (5 mol% Co-NTA) against higher density of chelator lipid (20 mol% Co-NTA). We spanned a wide concentration range of the protein from 150 nM to 2 μM (Fig. 3.6C). At higher protein densities, we observed a decrease in anisotropy in both the high and the low chelator lipid densities. We attributed this decrease to homo-FRET, a well-established phenomenon observed in numerous fluorophores, particularly in the case of SfGFP.[56] Several studies have utilized this effect to study GFP clustering in cells and for quantifying the size of lipid membrane microdomains.[57] Despite artifacts from homo-FRET, it is evident that, irrespective of the concentration of the protein used, there was a subtle, yet consistent decrease in fluorescence anisotropy when liposomes containing lower density of the chelator lipid was used. This greater fluorescence depolarization clearly demonstrates that when steric crowding is relieved (at lower protein densities), the surface bound proteins are able to sample multiple conformations through local fluctuations of the GFP orientation on the timescale of the fluorescence lifetime. Thus,

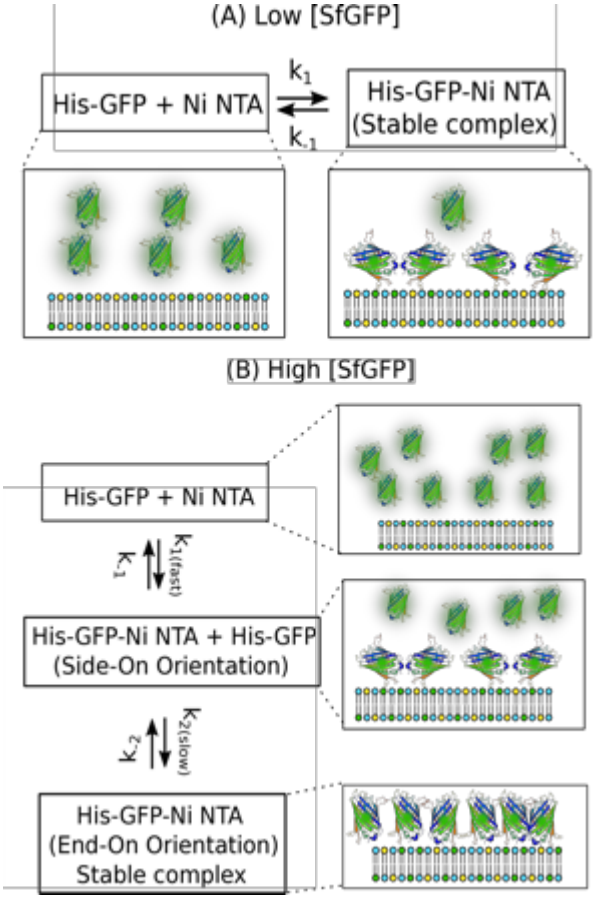

Figure 3.7. Proposed schematic for protein association to lipid surface. (A) At low concentrations, SfGFP binding to Ni-NTA containing surfaces follow mono-exponential binding kinetics due to availability of excess membrane surface area. (B) At high concentrations, SfGFP binding to lipid surfaces follow bi-exponential binding kinetics due to depletion of available binding surface area.

the fluorescence anisotropy data provides direct evidence for the idea that protein binding to vesicle surface with limited available surface area can occur via multiple orientations. As suggested by Minton et al., such orientational heterogeneity might play an important role in the relative surface area occupied by the protein structures and can thus affect the association kinetics to a great extent (Figure 3.7). The non-specific nature of multi-modal binding suggested in the literature is very different from our experimental design and hence, warrants discussion. In particular, careful consideration of the timescales of protein re-orientation and conformational fluctuations is required for drawing meaningful mechanistic conclusions. We anticipate the protein re-orientation to occur at much faster timescales (ns-μs) than the slowing of binding rates observed in our stopped flow results in the millisecond-second regime. This indicates that the bound-protein complexes have to overcome additional kinetic barriers to achieve equilibrium in longer timescales. We propose that side-on conformation of the protein complexes can be stabilized by electrostatic contacts between the protein surface and the charged bilayer of the liposome surface. Despite the net negative charge of the protein sequence (-7 for SfGFP), GFP variants are capable of establishing electrostatic contacts with the negatively charged membrane surface independent from the histidine-tag interaction. [21] The stabilization of the side-on orientation by such electrostatic contacts can not only saturate the membrane surface better than the end-on, but also restricts the accessibility of Ni-NTA from forming co-ordinate complexes with additional histidine tagged proteins in the bulk solution. Hence, at higher protein concentrations, these stabilizing interactions have to be broken to accommodate the additional binding of proteins in a conformationally constrained end-on conformation.

Based on our experimental observations, we conclude that protein binding to a vesicle surface occurs multimodally. At lower protein concentrations (Figure 4.7A), the availability of free membrane surface area allows for better conformational sampling of the membrane-bound protein structures. This leads to bimolecular association kinetics as observed in our stopped flow data. However, as the membrane surface begins to saturate with increasing protein concentration (Figure 4.7B), the conformational freedom of the surface-bound proteins is heavily restricted. Therefore, the flipping of proteins from a side-on conformation to a restrictive end-on conformation represents a major kinetic bottleneck to complete protein association, leading to the slowing of overall binding rates.

3.3 CONCLUSIONS

In this work, we provide a thorough and quantitative investigation of the kinetics of histidine tagged proteins binding to Ni-NTA surfaces utilizing an array of biophysical techniques. Utilizing SfGFP as a model system, we illustrate that the protein binding occurs via a complicated multi-step mechanism characterized by a poly-exponential fluorescence quenching behavior as observed via stopped flow. Subsequent mechanistic investigation reveals that protein binding occurs multimodally with at least two independent binding conformations that exhibit different protein footprint at the membrane surface. Our results demonstrate that protein association to a liposome surface does not always exhibit a simple bimolecular behavior. Instead, careful consideration of the available surface area, membrane composition and protein footprint are necessary for efficient immobilization of such biomolecular conjugates. This study is

valuable for the improvement of conjugation strategies and will pave the way for further investigation of mechanisms underlying complex protein-lipid interfaces.

3.4 EXPERIMENTAL SECTION

3.4.1 Materials. DOPC, Cholesterol, Dabsyl-PE, NTA-DGS and Ni-NTA-DGS were purchased from Avanti Polar Lipids (Alabaster, AL). FITC (5/6 fluorescein isothiocyanate) and Rhodamine-PE was purchased from ThermoFisher Scientific (Waltham, MA). His-tagged SfGFP was expressed and purified in house from the plasmid SfGFP-pBAD. [29] SfGFP-pBAD was a gift from Michael Davidson & Geoffrey Waldo (Addgene plasmid #54519; http://n2t.net/addgene:54519; RRID: Addgene_54519). -30 GFP was expressed and purified from the plasmid- pET-6xHis-(-30) GFP was a gift from David Liu (Addgene plasmid # 62936; http://n2t.net/addgene:62936; RRID: Addgene_62936). [45] EDTA, Cobalt (II) chloride, and Copper (II) chloride was obtained from Sigma-Aldrich (St. Louis, MO). MOPS, Sodium Chloride, and Amicon Ultra-0.5 mL centrifugal filters (10kDa MWCO) were obtained from EMD Millipore (Billerica, MA).

3.4.2 Large unilamellar vesicles preparation. Large unilamellar vesicles (LUVs) were prepared by extrusion. Lipid mixtures were dissolved in chloroform and dried under a stream of Argon gas on the inner wall of a small vial and then placed under vacuum overnight to form stable lipid cakes. For measurements involving different chelator lipid densities, we changed the amount of DOPC in the lipid mixtures dissolved in chloroform, by keeping the Ni-NTA DGS content the same. For instance, 5mol% Ni-NTA DGS samples were made by mixing 200μM Ni-NTA DGS with 4mM DOPC whereas 20mol% Ni-NTA DGS samples were made with 200μM Ni-NTA DGS with 800μM DOPC. 5mol% Dabsyl PE (in chloroform) was incorporated into the lipid cakes before drying. Lipid cakes were

then rehydrated to a final liposome concentration of 1mM with MOPS buffer (50 mM MOPS, pH 7.2) for 1 hour at room temperature. Every 15 minutes, the rehydrated lipid solution was vortexed thoroughly, and subsequently subjected to five freeze thaw cycles. The resulting multi-lamellar vesicle solutions were then extruded through a polycarbonate membrane (pore size 100nm; Whatman/GE Healthcare) 20 times to produce a clear solution of liposomes.

3.4.3 Dynamic light scattering measurements. Micromeritics Corporation's NanoPlus, a particle size analyzer was used to perform dynamic light scattering (DLS) to measure the hydrodynamic diameter of the liposomes with and without the presence of protein. A final liposome concentration of 500 μM was used in all experiments. A micro-volume glass cuvette capable of measuring sample volumes as low as 60μL was used for all measurements. Optimization of scattering intensity was performed by adjusting the cell-center, and by tuning the laser attenuation.

3.4.4 Steady state fluorescence measurements. Steady state fluorescence measurements were performed by using BioTek Cytation 5 multi-mode microplate reader. Untreated, clear bottomed flat 96-well plates were used for all experiments. The final bulk concentration of Ni-NTA DGS in the liposome samples were maintained at 100uM, and protein concentrations were changed across the plate by using MOPS buffer to dilute a concentrated protein stock solution. Sample excitation was performed at the wavelength of 485nm. Quantification of apparent dissociation constants (Figure A2 & supplemental table 1) and details of fluorescence anisotropy measurements are described in the APPENDIX.

3.4.5 Stopped flow fluorescence measurements. The association kinetics of protein binding to liposomes were quantified by using SX20 stopped flow apparatus (Applied Photophysics, UK). The starting concentration of the liposomes was maintained at 1mM (DOPC with 20mol% Ni-NTA DGS) and the protein concentration was varied from 50nM to 4μM. Upon initiation of the stopped-flow, the two solutions were mixed in an observation chamber a short deadtime (~ms) and the fluorescence was monitored by a Photomultiplier tube (PMT) with a 495nm Long-Pass filter to eliminate any scattering of the excitation light (485nm) from reaching the detector. All measurements were performed at room temperature and curve fitting was performed using Igor Pro (Wavemetrics, Portland, OR) detailed in APPENDIX (Figure A4).

3.4.6 Theoretical estimation of protein footprint on membrane surfaces. To estimate the orientation dependence of the protein footprint on membrane surfaces, we considered the morphology of the liposomes. Assuming the liposomes to be spherical, we calculated the overall available surface area exhibited by the liposome samples by computing the number of lipid molecules per liposome using the following equation

$$N = \frac{\left[4\pi\left(\frac{D}{2}\right)^2 + 4\pi\left(\frac{D}{2} - h\right)^2\right]}{a} \qquad (1)$$

Where D denotes the diameter of the liposome, h denotes the bilayer thickness, and a denotes the average molecular headgroup area of the lipid. Assuming a headgroup area of 0.71 nm^2 for phosphatidylcholine lipids,[58] we were able to calculate the surface area per liposome, and subsequently, the total available membrane surface area.

Given that our experimental design involved modulation of the Ni-NTA density, we needed to account for the difference in binding affinities of protein binding to the

membrane surface as a function of changing chelator lipid densities. Changing the binding constants of the complexes will affect the fraction of protein bound to the surface, in turn, affecting the fraction coverage. We utilized the binding constants acquired from our steady state fluorescence and ITC measurements (Figure A2 & A3) to estimate the bound protein fraction. The fraction of proteins bound to the surface was estimated as described in the literature briefly summarized as follows.

$$\boldsymbol{\theta} = \frac{[\boldsymbol{SfGFP}]}{[\boldsymbol{SfGFP}]+\boldsymbol{K_d}} \qquad (2)$$

Here, the parameter θ represents the fraction of proteins bound to the surface. [SfGFP] denotes the concentration of the protein solution and K_d represents the binding affinity of His-SfGFP construct to the Ni-NTA DGS decorated liposome surfaces. The parameter θ, thus enabled for a theoretical estimation of the protein footprint at the membrane surface by assuming a stokes radius of 2.5 nm for the protein binding to the surface with an end-on conformation and a radius of 3.7 nm for the side-on conformation. The assumptions were based on the literature reported values of surface coverage by controlled orientation of the RFP β-barrel and from analysis of crystal structures using PyMol.[29]

3.4.7 Protein expression and purification. All proteins used for the study- SfGFP, -30 GFP and EcDHFR were expressed and purified following steps as detailed elsewhere. Briefly, all genes were expressed by using E. coli strain BL21(DE3) with Luria-Bertani (LB) medium containing 100 μg/mL ampicillin. Care was taken to pick a single ampicillin resistant colony that was then inoculated into a 20 mL culture flask containing 5 mL of LB (with ampicillin) medium at 37 °C overnight inside a shaker incubator maintained at 200 rpm. 1 mL of the starter culture was then inoculated into a large conical flask

containing 1 L of LB medium with antibiotic and allowed to grow until the optical density at 600 nm reached 0.6-1.0. Next, inducer was added to a final concentration of 1 mM. Either IPTG or L-Arabinose was used as an inducer depending on the construct of interest. The resulting culture was subjected to vigorous shaking in a shaking incubator and allowed to grow for at least 6 hours to overnight. The cells were then harvested by centrifugation and subjected to cell lysis.

The pellets were resuspended in a lysis buffer containing 50 mM Tris, 150 mM NaCl, 5 mM β-Mercaptoethanol, containing protease inhibitor (from tablets of protease inhibitor cocktail). 1 mg/mL of Lysozyme was then added to the mixture, stirred on ice for an hour and sonicated on ice (Sonic Dissemble model 500, Fisher Scientific, Pittsburgh, PA). The lysed cells were then subjected to centrifugation, and the supernatant was filtered and purified using HisPrep affinity column on an AKTA FPLC system (GE Healthcare, Pittsburgh, PA). The proteins were eluted by using an imidazole gradient to competitively unbind the attached proteins to the Ni-NTA column. The eluted protein was subjected to desalting and concentrated using an Amicon concentrator with a 10 kDa molecular weight cutoff. The protein samples were then buffer exchanged to 50 mM MOPS buffer maintained at a pH 7.2. For EcDHFR samples, a small concentration of reducing agent (1 mM DTT) was added to prevent the possibility of disulfide formation.

3.4.8 Isothermal Titration Calorimetry. All ITC experiments reported in the chapter was performed using a MicroCal VP-ITC in low-feedback mode. A total of 31 injections were performed, resulting in titration of liposomes stock in the titrator syringe into a thoroughly rinsed cell chamber containing the protein sample. A Ni-NTA DGS concentration of 350 μM (Total liposome concentration of 1.75 mM in case of 20mol% Ni-

NTA DGS) was used in all experiments, and the DOPC concentration was varied to accommodate changing chelator lipid densities. The protein stock solutions were maintained at 9 μM unless otherwise reported. The reference power was maintained at 10 μCal/sec and the cell temperature (20 °C) was equilibrated for at least 30 minutes. The spacing between injections were set 360 seconds and data from the first injection was always discarded due to artifacts from dilution. Data analysis was performed by the MicroCal Analysis software, and the obtained enthalpograms were fit to one set of sites (for sample void of cholesterol) or two set of sites model (for samples containing cholesterol) and the coefficients are reported in Table A2.

3.4.9 Analysis of steady state fluorescence data. Steady state fluorescence quenching from SfGFP-liposome interaction was analyzed based on traditional fluorometric assays of protein binding to liposomes. Given the complex nature of the binding process, we employed the use of the Hill equation as described previously. A constant ligand (Ni-NTA DGS) concentration was chosen to eliminate changes to light scattering due to increasing liposome presence and the vesicle samples were incubated with different protein concentrations.

$$\frac{\Delta F}{\Delta F_{max}} = \frac{[P]_b}{[P]_o} = \frac{1}{1+(K_d/[P]_0)^h} \qquad \text{(S1)}$$

Where $[P]_b$, $[P]_o$ represents the bound protein concentration and total protein concentrations respectively. K_d here represents the apparent dissociation constant and h represents the Hill coefficient. ΔF and ΔF_{max} indicate the fluorescence intensity decrease at a given protein concentration, and the maximal intensity decrease, respectively. Given that the amount of protein bound must correlate with the decrease in fluorescence, we were then able to fit the individual binding isotherms to the Hill equation (Figure A2) to

yield apparent dissociation constants that correlate well with the data acquired via ITC. The fit coefficients are summarized in Table A1.

3.4.10 Fluorescence recovery after photobleaching. Lipid lateral mobility changes upon addition of Cholesterol was assessed by using Nikon C2 inverted confocal microscope using an excitation laser centered at 561 nm and emission captured using a lower energy bandpass filter placed in front of a 3-channel standard Photomultiplier tube detector system. 0.02 mol% of Rhodamine PE was doped in to the lipid cakes for FRAP experiments. The lipid cakes were hydrated, extruded and ultimately supported lipid bilayers were formed by spontaneous fusion on plasma cleaned glass surfaces as described elsewhere. Time-lapse images were acquired over 420 seconds after photobleaching a circular spot of diameters ranging from 10-25 μm. The fluorescence recovery transients were subsequently fit to exponential function, enabling us to estimate the lipid lateral mobility and the changes in diffusivity upon changing cholesterol concentration.

3.4.11 Preparation of Cu and Co containing liposomes. To change the divalent cations bound to the chelator lipid headgroup, we followed protocols described elsewhere. Briefly, we doped Ni-free NTA-DGS into DOPC containing lipid cakes at 20 mol% density. After liposome extrusion, we incubated the liposome solution in a buffer stock containing 2-fold molar excess of $CuCl_2$ or $CoCl_2$ and the excess divalent cations were removed from solution through several rounds of centrifugal filtration. All liposome samples were subjected to dynamic light scattering measurements and we did not observe any significant changes in the morphology of the liposomes (data not shown), indicating that the addition of divalent cations did not affect the liposomes hydrodynamic diameter.

For Co(II) oxidation experiments, we first incubated the Co(II) NTA doped vesicles with SfGFP at varying concentrations for at least 2 hours in room temperature to reach equilibrium. Once the incubation time was complete, we added 10mM Hydrogen Peroxide to all the samples. After an hour, we removed the unbound SfGFP from the samples by subjecting them to centrifugal filtration utilizing a 50kDa molecular weight cutoff filter. After 3 rounds of filtration, we observed little to no presence of SfGFP in the filtrate indicating the successful oxidation of Co(II) to Co(III) and subsequently, immobilization of proteins to the surface (data not shown).

3.4.12 Analysis of stopped flow transients. To obtain the rate constants associated with stopped flow transients, we fit the fluorescence decay globally to either bi or tri exponential functions. We noticed that, in presence of cholesterol, protein binding to liposomes exhibited a tri-exponential behavior with no clear concentration dependent trend. While a thorough exploration of these rate constants was beyond the scope of this chapter, it is certainly possible that long-range structural effects due to protein binding to cholesterol containing liposomes might cause extensive re-arrangement leading to such behavior. Regardless, we report the rate constants of the slower phase in supplementary Figure A10 for reference.

To fit the concentration dependence of slow phase rate constants, we fit the rate constants to a modified sigmoidal fit as shown in equation S2. The fits were performed purely to guide the readers eye, and not to imply any direct physical meaning.

$$y = base + \left(\frac{max}{1+ e^{(xhalf-x)/rate}}\right) + (a\,.x) + b \qquad \text{(S2)}$$

Where base is the baseline, max represents the maximum value, xhalf represents the midpoint of the sigmoidal fit, rate represents the rising rate, a represents the slope of the line (negative slope at higher SfGFP concentrations) and *b* represents the fitting constant.

3.4.13 Anisotropy correction. To account for the artificial depolarization in anisotropy by light scattering in a turbid medium, we performed a correction, by accounting for the optical density of the solution in the 96-well plate. We slightly modified the protocol followed by Lentz et al. Briefly, to account for the turbidity of the medium, we utilized liposomes void of the chelator lipid. Given that the change in chelator lipid density was accomplished by varying the total DOPC content, we established a standard curve measurement by keeping the SfGFP concentration the same, and by changing the liposome concentration across a wide range. This changes the optical density of the medium significantly (data not shown). By sampling a wide range of liposome concentration, we were able to obtain a correction factor by fitting the anisotropy depolarization as a function of increasing concentrations to a linear function by using equation (S3)

$$r_{obs} = r' - (r'.K.[DOPC]) \qquad \text{(S3)}$$

Where r_{obs} is the observed anisotropy, r' is the extrapolated anisotropy at zero optical density and K is the proportionality constant. This correction was used to account for scattering induced depolarization of the polarized light for all data presented in Figure 6C.

3.5 REFERENCES

1. Lee, A. G., Lipid-protein interactions in biological membranes: a structural perspective. *Biochim Biophys Acta* **2003,** *1612* (1), 1-40.

2. Escriba, P. V.; Gonzalez-Ros, J. M.; Goni, F. M.; Kinnunen, P. K.; Vigh, L.; Sanchez-Magraner, L.; Fernandez, A. M.; Busquets, X.; Horvath, I.; Barcelo-Coblijn, G., Membranes: a meeting point for lipids, proteins and therapies. *J Cell Mol Med* **2008,** *12* (3), 829-75.

3. Sonntag, Y.; Musgaard, M.; Olesen, C.; Schiott, B.; Moller, J. V.; Nissen, P.; Thogersen, L., Mutual adaptation of a membrane protein and its lipid bilayer during conformational changes. *Nat Commun* **2011,** *2*, 304.

4. Marsh, D., Protein modulation of lipids, and vice-versa, in membranes. *Biochim Biophys Acta* **2008,** *1778* (7-8), 1545-75.

5. Kirchhausen, T.; Owen, D.; Harrison, S. C., Molecular structure, function, and dynamics of clathrin-mediated membrane traffic. *Cold Spring Harb Perspect Biol* **2014,** *6* (5), a016725.

6. Lee, M. T.; Mishra, A.; Lambright, D. G., Structural mechanisms for regulation of membrane traffic by rab GTPases. *Traffic* **2009,** *10* (10), 1377-89.

7. de Kruijff, B.; Cullis, P. R., Cytochrome c specifically induces non-bilayer structures in cardiolipin-containing model membranes. *Biochim Biophys Acta* **1980,** *602* (3), 477-90.

8. Duncan, A. L.; Reddy, T.; Koldso, H.; Helie, J.; Fowler, P. W.; Chavent, M.; Sansom, M. S. P., Protein crowding and lipid complexity influence the nanoscale dynamic organization of ion channels in cell membranes. *Sci Rep* **2017,** *7* (1), 16647.

9. Chavent, M.; Duncan, A. L.; Rassam, P.; Birkholz, O.; Helie, J.; Reddy, T.; Beliaev, D.; Hambly, B.; Piehler, J.; Kleanthous, C.; Sansom, M. S. P., How nanoscale protein interactions determine the mesoscale dynamic organisation of bacterial outer membrane proteins. *Nat Commun* **2018,** *9* (1), 2846.

10. De Franceschi, N.; Alqabandi, M.; Miguet, N.; Caillat, C.; Mangenot, S.; Weissenhorn, W.; Bassereau, P., The ESCRT protein CHMP2B acts as a diffusion barrier on reconstituted membrane necks. *J Cell Sci* **2018,** *132* (4).

11. Arumugam, S.; Bassereau, P., Membrane nanodomains: contribution of curvature and interaction with proteins and cytoskeleton. *Essays Biochem* **2015,** *57*, 109-19.

12. Dietrich, C.; Schmitt, L.; Tampe, R., Molecular organization of histidine-tagged biomolecules at self-assembled lipid interfaces using a novel class of chelator lipids. *Proc Natl Acad Sci U S A* **1995,** *92* (20), 9014-8.

13. Watson, D. S.; Platt, V. M.; Cao, L.; Venditto, V. J.; Szoka, F. C., Jr., Antibody response to polyhistidine-tagged peptide and protein antigens attached to liposomes via lipid-linked nitrilotriacetic acid in mice. *Clin Vaccine Immunol* **2011,** *18* (2), 289-97.

14. Tanaka, M.; Hermann, J.; Haase, I.; Fischer, M.; Boxer, S. G., Frictional drag and electrical manipulation of recombinant proteins in polymer-supported membranes. *Langmuir* **2007,** *23* (10), 5638-44.

15. Celia, H.; Wilson-Kubalek, E.; Milligan, R. A.; Teyton, L., Structure and function of a membrane-bound murine MHC class I molecule. *Proc Natl Acad Sci U S A* **1999,** *96* (10), 5634-9.

16. Stachowiak, J. C.; Schmid, E. M.; Ryan, C. J.; Ann, H. S.; Sasaki, D. Y.; Sherman, M. B.; Geissler, P. L.; Fletcher, D. A.; Hayden, C. C., Membrane bending by protein-protein crowding. *Nat Cell Biol* **2012,** *14* (9), 944-9.

17. Snead, W. T.; Hayden, C. C.; Gadok, A. K.; Zhao, C.; Lafer, E. M.; Rangamani, P.; Stachowiak, J. C., Membrane fission by protein crowding. *Proc Natl Acad Sci U S A* **2017,** *114* (16), E3258-E3267.

18. Snead, W. T.; Stachowiak, J. C., Structure Versus Stochasticity-The Role of Molecular Crowding and Intrinsic Disorder in Membrane Fission. *J Mol Biol* **2018,** *430* (16), 2293-2308.

19. Chen, Z.; Moon, J. J.; Cheng, W., Quantitation and Stability of Protein Conjugation on Liposomes for Controlled Density of Surface Epitopes. *Bioconjug Chem* **2018,** *29* (4), 1251-1260.

20. Nye, J. A.; Groves, J. T., Kinetic control of histidine-tagged protein surface density on supported lipid bilayers. *Langmuir* **2008,** *24* (8), 4145-9.

21. Wasserberg, D.; Cabanas-Danes, J.; Prangsma, J.; O'Mahony, S.; Cazade, P. A.; Tromp, E.; Blum, C.; Thompson, D.; Huskens, J.; Subramaniam, V.; Jonkheijm, P., Controlling Protein Surface Orientation by Strategic Placement of Oligo-Histidine Tags. *ACS Nano* **2017,** *11* (9), 9068-9083.

22. Krogsgaard, M.; Li, Q. J.; Sumen, C.; Huppa, J. B.; Huse, M.; Davis, M. M., Agonist/endogenous peptide-MHC heterodimers drive T cell activation and sensitivity. *Nature* **2005,** *434* (7030), 238-43.

23. Sigal, G. B.; Bamdad, C.; Barberis, A.; Strominger, J.; Whitesides, G. M., A self-assembled monolayer for the binding and study of histidine-tagged proteins by surface plasmon resonance. *Anal Chem* **1996,** *68* (3), 490-7.

24. Kirchhausen, T., Bending membranes. *Nat Cell Biol* **2012,** *14* (9), 906-8.

25. Cocucci, E.; Aguet, F.; Boulant, S.; Kirchhausen, T., The first five seconds in the life of a clathrin-coated pit. *Cell* **2012,** *150* (3), 495-507.

26. Siaw, H. M. H.; Raghunath, G.; Dyer, R. B., Peripheral Protein Unfolding Drives Membrane Bending. *Langmuir* **2018,** *34* (28), 8400-8407.

27. Busch, D. J.; Houser, J. R.; Hayden, C. C.; Sherman, M. B.; Lafer, E. M.; Stachowiak, J. C., Intrinsically disordered proteins drive membrane curvature. *Nat Commun* **2015,** *6*, 7875.

28. Fakhree, M. A. A.; Engelbertink, S. A. J.; van Leijenhorst-Groener, K. A.; Blum, C.; Claessens, M., Cooperation of Helix Insertion and Lateral Pressure to Remodel Membranes. *Biomacromolecules* **2019,** *20* (3), 1217-1223.

29. Pedelacq, J. D.; Cabantous, S.; Tran, T.; Terwilliger, T. C.; Waldo, G. S., Engineering and characterization of a superfolder green fluorescent protein. *Nat Biotechnol* **2006,** *24* (1), 79-88.

30. Kim, H.; Afsari, H. S.; Cho, W., High-throughput fluorescence assay for membrane-protein interaction. *J Lipid Res* **2013,** *54* (12), 3531-8.

31. Cho, W.; Bittova, L.; Stahelin, R. V., Membrane binding assays for peripheral proteins. *Anal Biochem* **2001,** *296* (2), 153-61.

32. Khan, F.; He, M.; Taussig, M. J., Double-hexahistidine tag with high-affinity binding for protein immobilization, purification, and detection on ni-nitrilotriacetic acid surfaces. *Anal Chem* **2006,** *78* (9), 3072-9.

33. Huang, Z.; Hwang, P.; Watson, D. S.; Cao, L.; Szoka, F. C., Jr., Tris-nitrilotriacetic acids of subnanomolar affinity toward hexahistidine tagged molecules. *Bioconjug Chem* **2009,** *20* (8), 1667-72.

34. Chen, Z.; Atefi, E.; Baumgart, T., Membrane Shape Instability Induced by Protein Crowding. *Biophys J* **2016,** *111* (9), 1823-1826.

35. Jia, Y.; Kumar, A.; Patel, S. S., Equilibrium and stopped-flow kinetic studies of interaction between T7 RNA polymerase and its promoters measured by protein and 2-aminopurine fluorescence changes. *J Biol Chem* **1996,** *271* (48), 30451-8.

36. Hlavacek, W. S.; Posner, R. G.; Perelson, A. S., Steric effects on multivalent ligand-receptor binding: exclusion of ligand sites by bound cell surface receptors. *Biophys J* **1999,** *76* (6), 3031-43.

37. Blanchette, C. D.; Fischer, N. O.; Corzett, M.; Bench, G.; Hoeprich, P. D., Kinetic analysis of his-tagged protein binding to nickel-chelating nanolipoprotein particles. *Bioconjug Chem* **2010,** *21* (7), 1321-30.

38. de Meyer, F.; Smit, B., Effect of cholesterol on the structure of a phospholipid bilayer. *Proc Natl Acad Sci U S A* **2009,** *106* (10), 3654-8.

39. Goluszko, P.; Nowicki, B., Membrane cholesterol: a crucial molecule affecting interactions of microbial pathogens with mammalian cells. *Infect Immun* **2005,** *73* (12), 7791-6.

40. Filippov, A.; Oradd, G.; Lindblom, G., The effect of cholesterol on the lateral diffusion of phospholipids in oriented bilayers. *Biophys J* **2003,** *84* (5), 3079-86.

41. Cheng, C. Y.; Olijve, L. L.; Kausik, R.; Han, S., Cholesterol enhances surface water diffusion of phospholipid bilayers. *J Chem Phys* **2014,** *141* (22), 22D513.

42. Radhakrishnan, A.; McConnell, H., Condensed complexes in vesicles containing cholesterol and phospholipids. *Proc Natl Acad Sci U S A* **2005,** *102* (36), 12662-6.

43. Porath, J.; Carlsson, J.; Olsson, I.; Belfrage, G., Metal chelate affinity chromatography, a new approach to protein fractionation. *Nature* **1975,** *258* (5536), 598-9.

44. Pfefferkorn, C. M.; Jiang, Z.; Lee, J. C., Biophysics of alpha-synuclein membrane interactions. *Biochim Biophys Acta* **2012,** *1818* (2), 162-71.

45. Lawrence, M. S.; Phillips, K. J.; Liu, D. R., Supercharging proteins can impart unusual resilience. *J Am Chem Soc* **2007,** *129* (33), 10110-2.

46. Dubacheva, G. V.; Araya-Callis, C.; Geert Volbeda, A.; Fairhead, M.; Codee, J.; Howarth, M.; Richter, R. P., Controlling Multivalent Binding through Surface Chemistry: Model Study on Streptavidin. *J Am Chem Soc* **2017,** *139* (11), 4157-4167.

47. Ramsden, J. J.; Bachmanova, G. I.; Archakov, A. I., Kinetic evidence for protein clustering at a surface. *Phys Rev E Stat Phys Plasmas Fluids Relat Interdiscip Topics* **1994,** *50* (6), 5072-5076.

48. Minton, A. P., Adsorption of globular proteins on locally planar surfaces. II. Models for the effect of multiple adsorbate conformations on adsorption equilibria and kinetics. *Biophys J* **1999,** *76* (1 Pt 1), 176-87.

49. Chatelier, R. C.; Minton, A. P., Adsorption of globular proteins on locally planar surfaces: models for the effect of excluded surface area and aggregation of adsorbed protein on adsorption equilibria. *Biophys J* **1996,** *71* (5), 2367-74.

50. Mattheyses, A. L.; Kampmann, M.; Atkinson, C. E.; Simon, S. M., Fluorescence anisotropy reveals order and disorder of protein domains in the nuclear pore complex. *Biophys J* **2010,** *99* (6), 1706-17.

51. Canet, D.; Doering, K.; Dobson, C. M.; Dupont, Y., High-sensitivity fluorescence anisotropy detection of protein-folding events: application to alpha-lactalbumin. *Biophys J* **2001,** *80* (4), 1996-2003.

52. Neves, P.; Lopes, S. C.; Sousa, I.; Garcia, S.; Eaton, P.; Gameiro, P., Characterization of membrane protein reconstitution in LUVs of different lipid composition by fluorescence anisotropy. *J Pharm Biomed Anal* **2009,** *49* (2), 276-81.

53. Erdelyi, M.; Simon, J.; Barnard, E. A.; Kaminski, C. F., Analyzing receptor assemblies in the cell membrane using fluorescence anisotropy imaging with TIRF microscopy. *PLoS One* **2014,** *9* (6), e100526.

54. Teale, F. W., Fluorescence depolarization by light-scattering in turbid solutions. *Photochem Photobiol* **1969,** *10* (6), 363-74.

55. Wegner, S. V.; Spatz, J. P., Cobalt(III) as a stable and inert mediator ion between NTA and His6-tagged proteins. *Angew Chem Int Ed Engl* **2013,** *52* (29), 7593-6.

56. Gautier, I.; Tramier, M.; Durieux, C.; Coppey, J.; Pansu, R. B.; Nicolas, J. C.; Kemnitz, K.; Coppey-Moisan, M., Homo-FRET microscopy in living cells to measure monomer-dimer transition of GFP-tagged proteins. *Biophys J* **2001,** *80* (6), 3000-8.

57. Bader, A. N.; Hofman, E. G.; Voortman, J.; en Henegouwen, P. M.; Gerritsen, H. C., Homo-FRET imaging enables quantification of protein cluster sizes with subcellular resolution. *Biophys J* **2009,** *97* (9), 2613-22.

58. Nagle, J. F., Area/lipid of bilayers from NMR. *Biophys J* **1993,** *64* (5), 1476-81.

Appendix 3: Kinetics of histidine tagged protein association to nickel-decorated liposome surfaces.

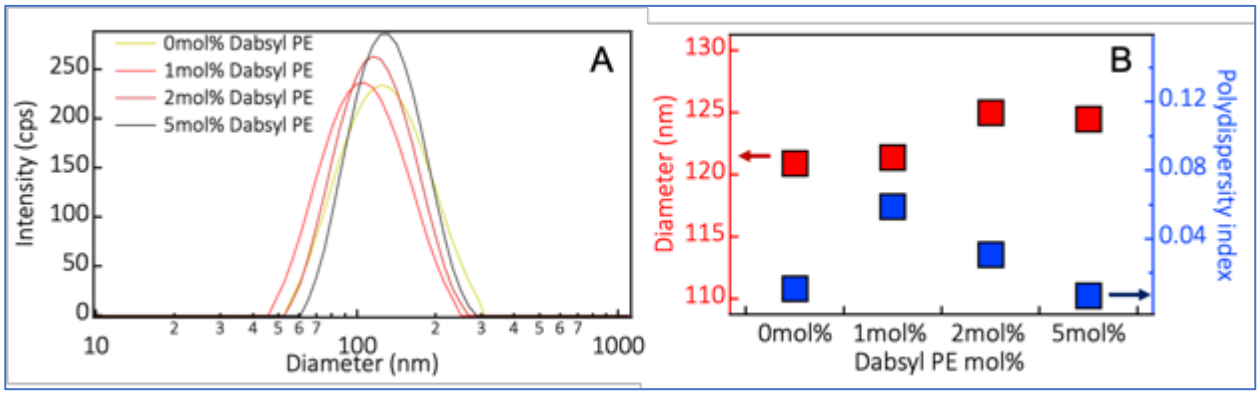

Figure A3.1. Ensuring proper formation of liposomes with increasing concentrations of Dabsyl PE. (A) Dynamic Light Scattering intensity profile of 1 mM DOPC liposomes containing 0, 1, 2, 5 mol% Dabsyl PE. (B) Average diameters (Red squares- reported on the axis on the left) and polydispersity index of the liposomes (Blue squares- reported on the axis on the right) of the vesicle samples with increasing Dabsyl PE loading levels. The vesicles were extruded through a 100 nm polycarbonate membrane as described in the experimental section, leading to a highly monodisperse population.

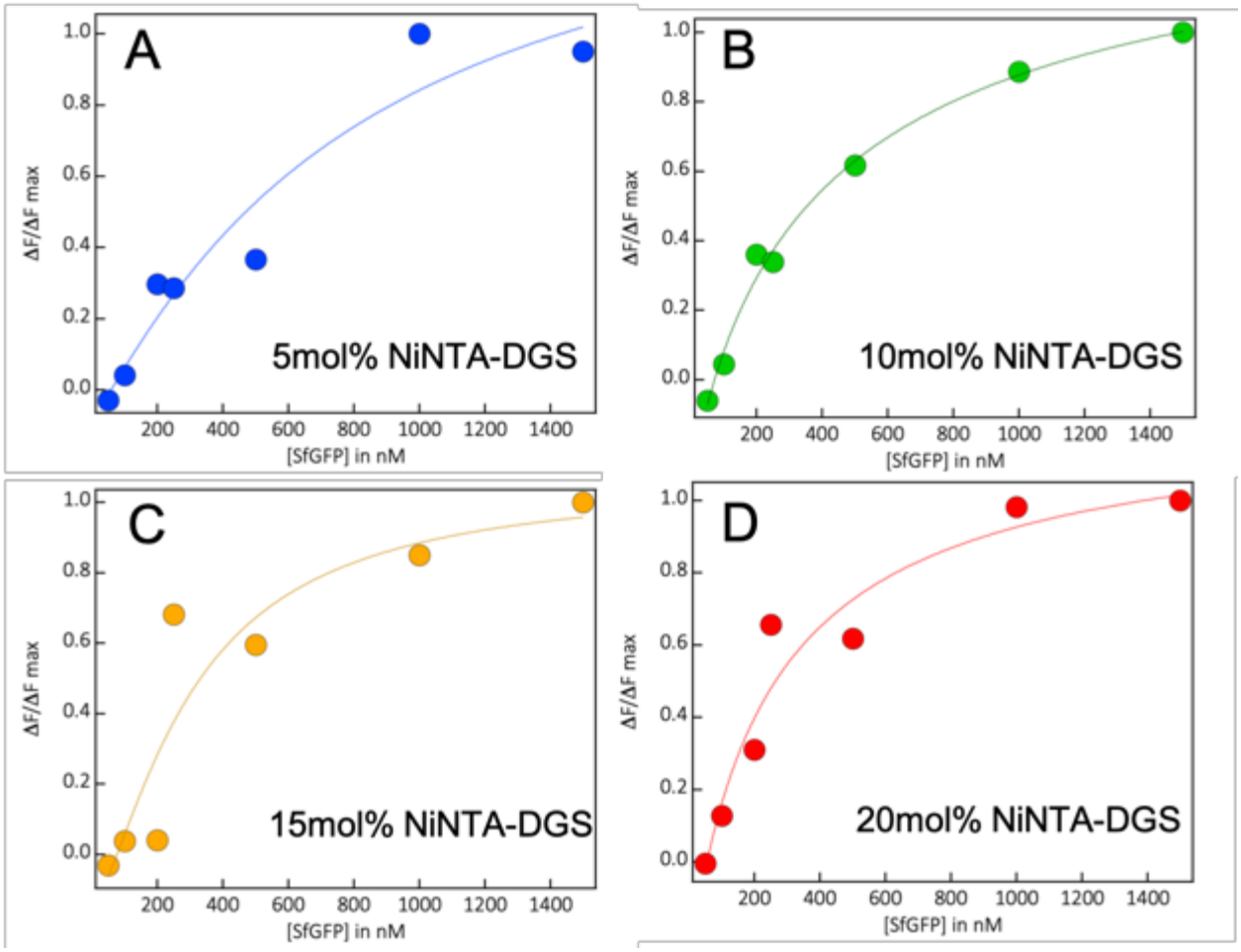

Figure A3.2. Steady state fluorescence binding isotherms. Change in steady state fluorescence intensity as a function of increasing SfGFP concentration and associated fits to the Hill equation. Increasing the chelator lipid density enhances the apparent dissociation constants as reported in Table S1. (A), (B), (C), (D) represent data acquired on liposomes containing 5, 10, 15 and 20 mol% Ni-NTA DGS respectively.

Table A3.1. Coefficients from fits in Figure S2.

Chelator density	5mol%	10mol%	15mol%	20mol%
Apparent Dissociation constant Kd(in nM)	812.04	418.69	302.96	247.29
Hill coefficient (h)	1.117	0.851	1.22	0.94

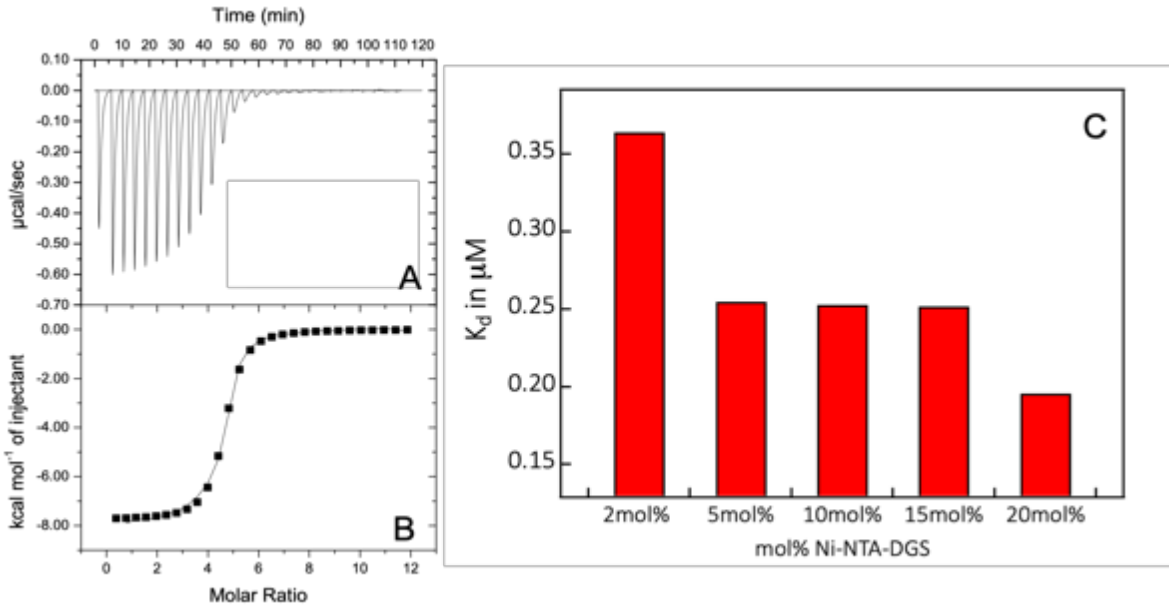

Figure A3.3. Isothermal titration calorimetry of SfGFP binding to Ni-NTA DGS containing liposomes. (A) Representative ITC thermograms obtained by injecting (350 μM Ni-NTA DGS liposomes at a 20 mol% density) into the cell chamber containing 9 μM SfGFP. (B) Enthalpograms obtained under the same conditions. The solid line represents the associated fit to a single set of sites model. (C) Dissociation constants obtained via ITC as a function of increasing chelator lipid densities.

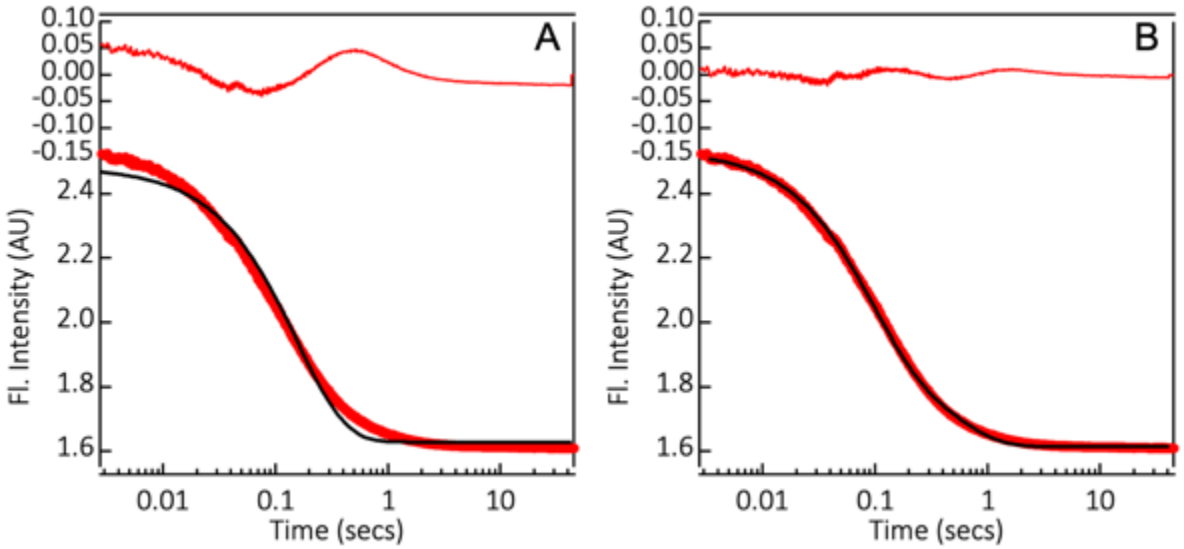

Figure A3.4. Stopped flow transients and their associated fits Representative stopped flow fluorescence plotting the decrease in fluorescence intensity as a function of time. 200 μM Ni-NTA DGS and 1 μM SfGFP stock solutions were mixed in an observation chamber. (A) Stopped flow transient and the associated mono-exponential fit. The residuals reported at the top clearly shows that a single exponential is not adequate to describe the fluorescence quenching. (B) Stopped flow transient and associated bi-exponential fit. The residuals reported at the top show that a bi-exponential fit is appropriate for analysis.

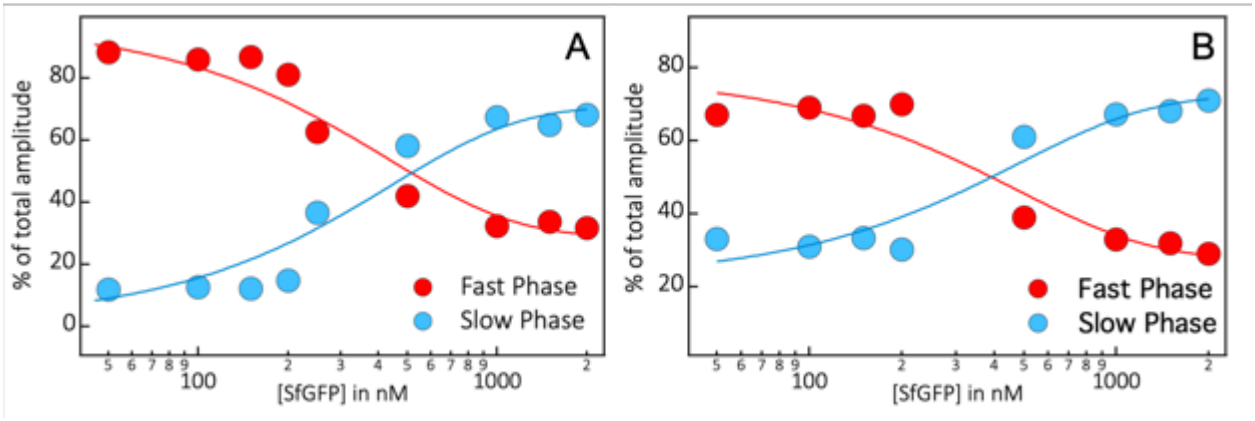

Figure A3.5. Relative amplitudes of the two exponential phases obtained from stopped flow experiments. (A) represents the relative amplitudes of the fast and the slow phases, for liposomes containing 5 mol% Ni-NTA DGS and (B) represents the relative amplitudes of the fast and the slow phases for liposomes containing 20 mol% Ni-NTA DGS. As evidenced from the opposing trends, the slow phase amplitudes clearly have a bigger contribution to the overall fluorescence decay relative to the fast phase, particularly at higher protein concentrations. The fast and the slow phase amplitudes were fit to an exponential function to lead the reader's eye and not to imply any direct physical meaning.

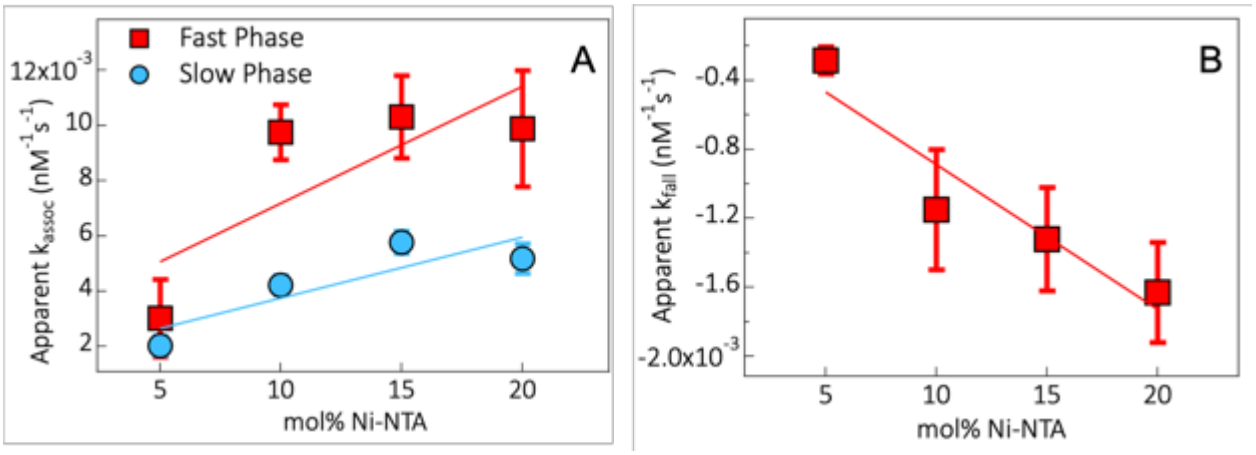

Figure A3.6. Calculation of apparent association constants. (A) Calculation of apparent association constants from stopped flow fluorescence data. Bi-exponential rate constants (k_{fast} and k_{slow}) at low concentration (<500 nM) data from SfGFP binding to liposomes were fit to a linear function to obtain apparent k_{assoc} ($nM^{-1}s^{-1}$). The apparent association constants were found to increase as a function of increasing chelator lipid density, indicating a bimolecular behavior for protein binding to liposomes under non-crowding conditions. (B) The slow-phase rates undergo a break in bimolecular behavior to exhibit a negative concentration dependence ([SfGFP] > 500 nM). The magnitude of this effect was reported by the use of k_{fall}, a parameter obtained by fitting the rate constant data for the slow-phases at higher SfGFP concentrations, to a linear function. The negative rates are meant to be a qualitative guide and do not imply any direct physical meaning.

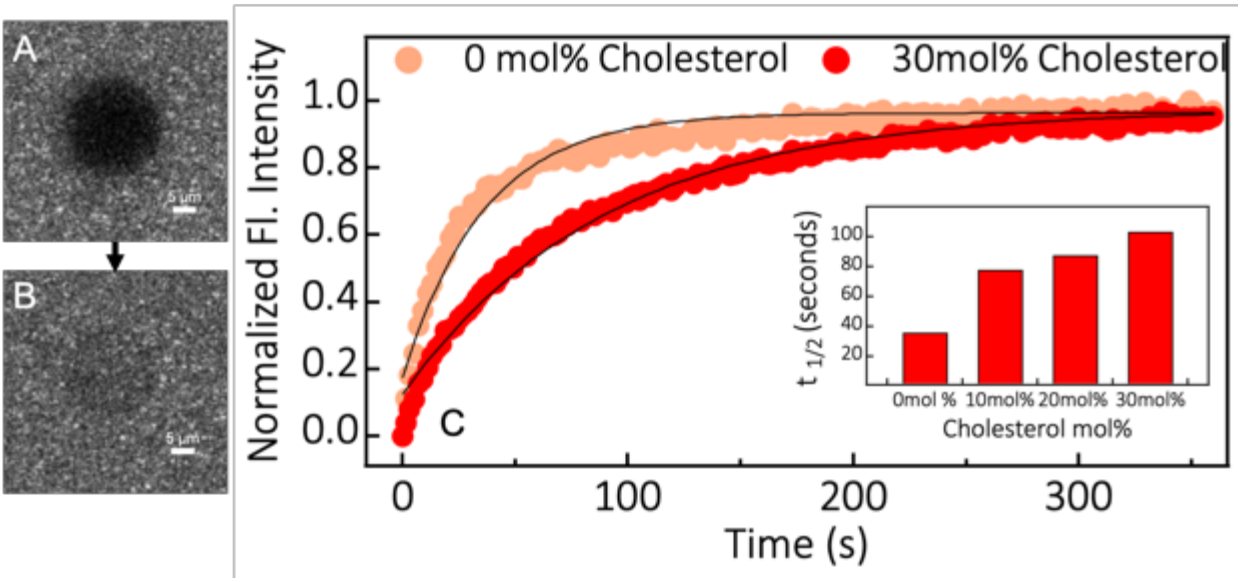

Figure A3.7. Fluorescence recovery after photobleaching. (A) Representative confocal time-lapse image at t = 0, after photobleaching a spot at high laser powers. (B) Representative confocal image at t = 300 after recovery of the photobleached sample under observation conditions. Both images were captured by excitation at 561 nm wavelength, and observation via a bandpass filter centered at 582 nm. 0.02mol% of Rhodamine PE was doped into the vesicle composition, and used as a fluorescent reporter. (C) Normalized fluorescence intensity plotted as a function of time representing the recovery of fluorescence after photobleaching. Clearly, increasing cholesterol concentration decreases the lateral mobility of the lipids involved in the formation of the Supported lipid bilayer, indicating the restriction of lateral mobility by cholesterol loading. The recovery kinetics were fit to a single exponential leading to the calculation of a $t_{1/2}$(secs) and reported in the inset.

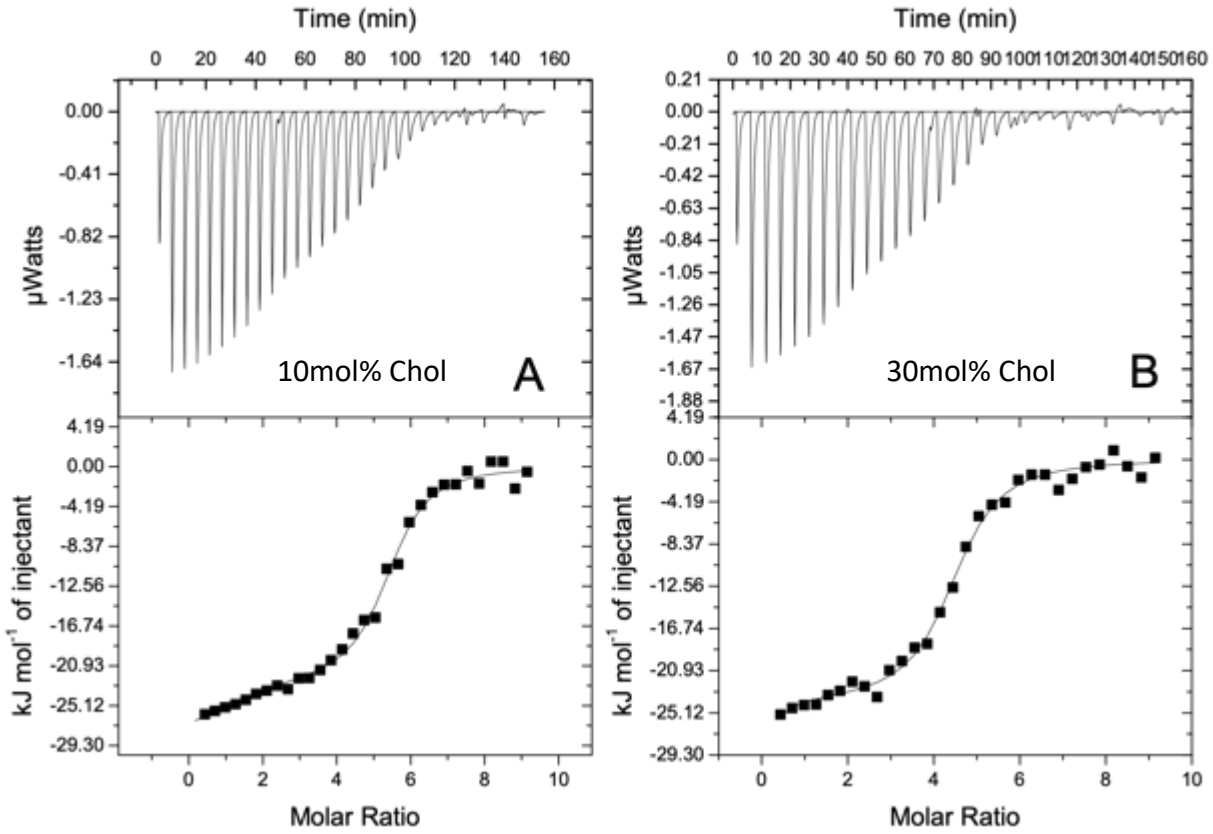

Figure A3.8. Isothermal titration calorimetry of SfGFP binding to Ni-NTA DGS containing liposomes with varying Cholesterol doping levels. (A) Representative ITC thermograms obtained by injecting 350 μM Ni-NTA DGS decorated liposomes (10 mol% Cholesterol along with 20 mol% Ni-NTA DGS) into the cell chamber containing 9 μM SfGFP. Enthalpogram obtained under the same conditions is reported in the lower half of the graph. (B) Representative ITC thermograms obtained by injecting 350 μM Ni-NTA DGS decorated liposomes (30 mol% Cholesterol along with 20 mol% Ni-NTA DGS) into the cell chamber containing 9 μM SfGFP. Enthalpogram obtained under the same conditions are reported in the lower half of the graph. Both enthalpograms were fit to a two-set of binding sites model and the dissociation constants and stoichiometries are listed in Table S2 below.

Table A3.2. Dissociation constants and stoichiometries obtained from fits in Figure S8.

Cholesterol density	10 mol%	20 mol%	30 mol%
K_{d1} in (nM)	100 nM	71.32 nM	63.29 nM
K_{d2} in (nM)	740 nM	628 nM	591 nM
Stoichiometry (n_1)	1.22	1.30	1.24
Stoichiometry (n_2)	4.40	4.04	4.24

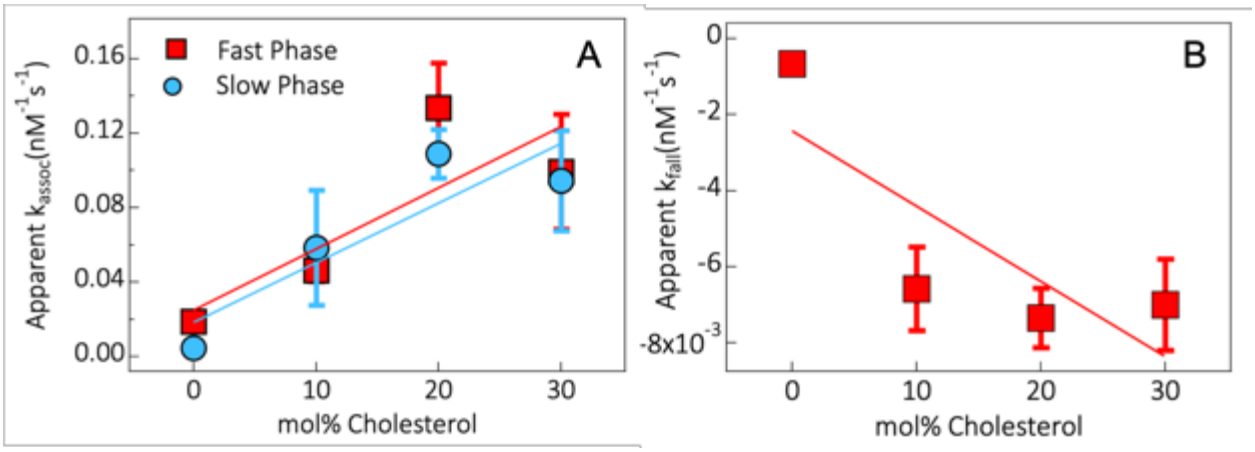

Figure A3.9. Calculation of apparent association constants. (A) Calculation of apparent association constants from stopped flow fluorescence data. Rate constants from poly exponential fits (k_{fast} and k_{slow}) at low concentration (<500 nM) data from SfGFP binding to liposomes were fit to a linear function to obtain apparent k_{assoc} ($nM^{-1}s^{-1}$). (B) The slow-phase rates undergo a break in bimolecular behavior to exhibit a negative concentration dependence ([SfGFP] > 500 nM). The magnitude of this effect was reported by the use of k_{fall}, a parameter obtained by fitting the rate constant data for the slow-phases at higher SfGFP concentrations, to a linear function. The negative rates are meant to be a qualitative guide and do not imply any direct physical meaning.

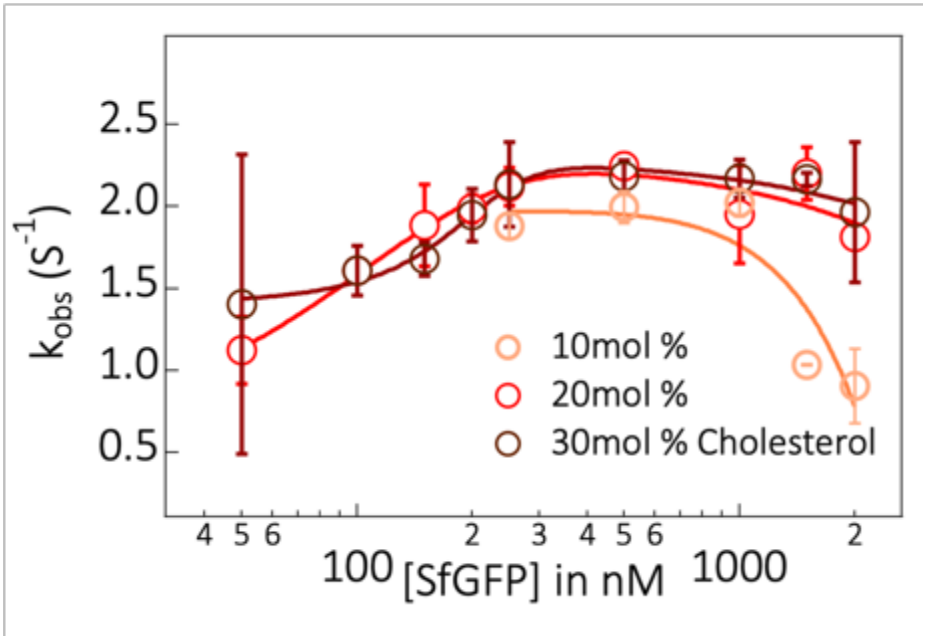

Figure A3.10. Third phase rate constants observed in stopped flow transients with liposomes containing cholesterol. Concentration dependence of the slower, third phase rates obtained from stopped flow transients and their tri-exponential fits. At 10 mol% cholesterol doping levels, we didn't observe a tri-exponential at SfGFP concentrations below 250 nM. However, a tri-exponential fitting function was necessary to describe the fluorescence decay at higher cholesterol loading levels.

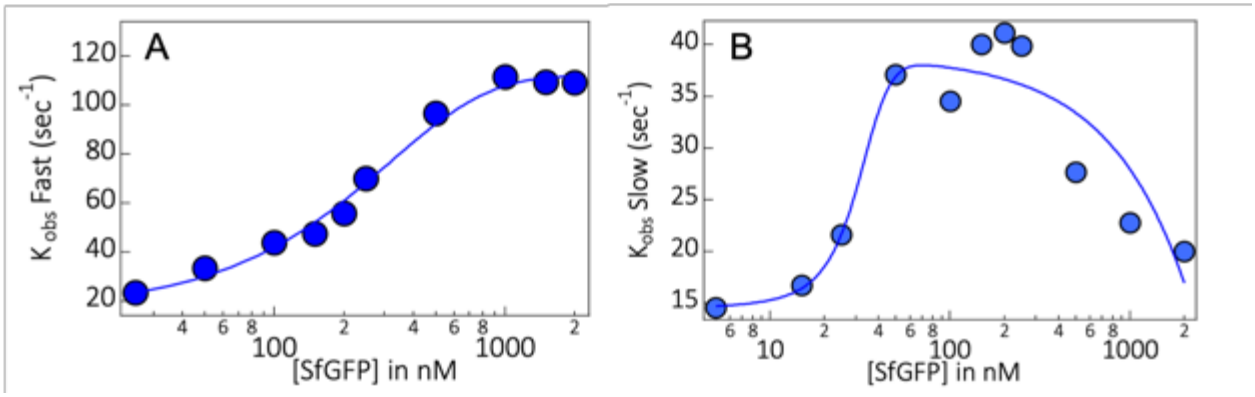

Figure A3.11. Effects of changing divalent cations on the chelator lipid headgroup. Rate constants from bi-exponential fits to the stopped flow transients. Upon replacing the divalent cation from Ni^{2+} to Cu^{2+}, we observe a large enhancement in binding rates for both the fast and the slow phases. (A) Fast phase rate constants plotted as a function of SfGFP concentration and (B) Slow Phase rate constants plotted as a function of SfGFP concentration. Despite enhancement in overall binding rates, we continued to observe the trend of decreasing rate constants in the slow phase.

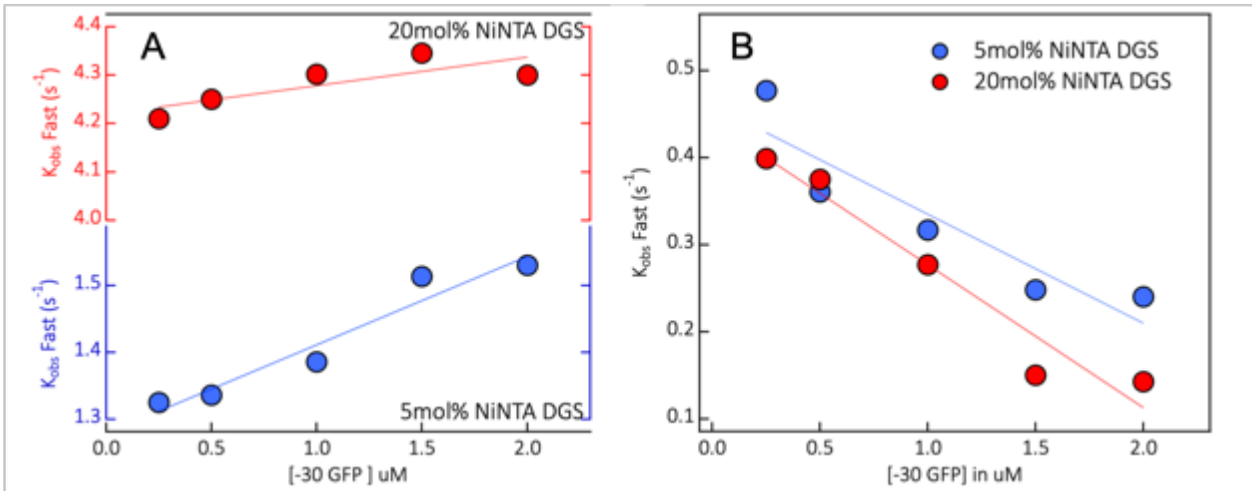

Figure A3.12. Effects of changing protein surface charge on binding kinetics. Observed rate constants from bi-exponential fits at high protein concentrations (>250 nM) by using -30GFP. (A) Fast phase rate constants at 5 mol% Ni-NTA DGS (bottom) and 20 mol% Ni-NTA DGS (top) and (B) Slow phase rate constants at 5 mol% Ni-NTA DGS (bottom) and 20 mol% Ni-NTA DGS (top). Despite changes in overall binding rates, we observed a clear trend of decreasing slow phase rate constants.

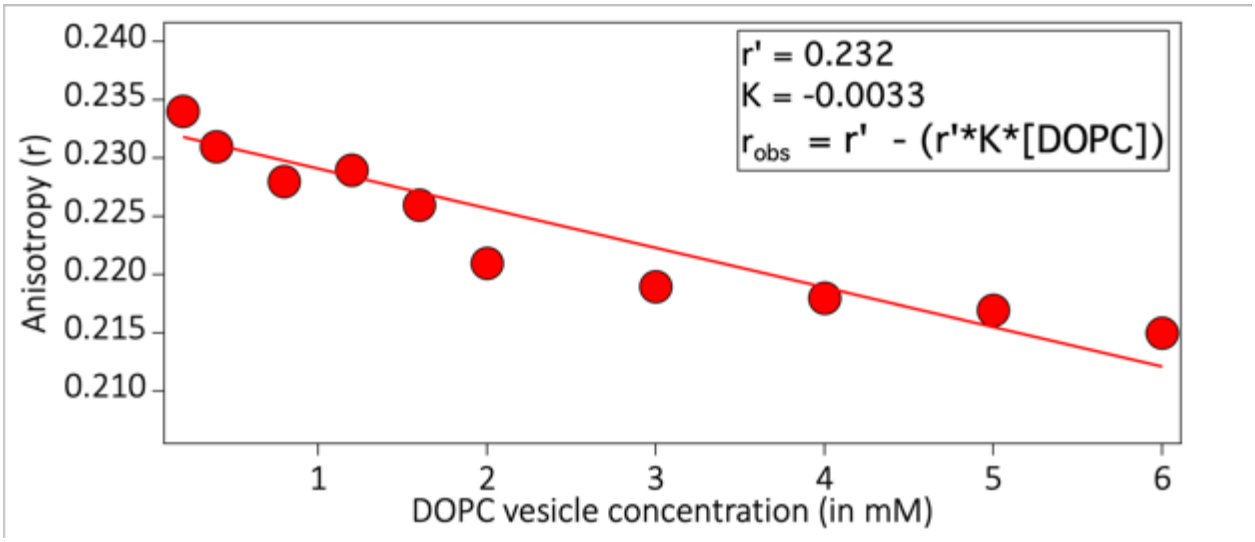

Figure A3.13. Anisotropy correction for turbid media. Anisotropy (r) of SfGFP fluorescence in presence of liposomes void of chelator lipid. By using Ni-free liposomes, we were able to account for the increase in turbidity of the optical medium without any major changes to the physical environment of the fluorophore. Figure legend denotes the parameters used for anisotropy correction. K is the proportionality constant, r' is the extrapolated anisotropy at zero optical density and r_{obs} is the observed anisotropy.

Chapter 4

Membrane thinning precedes membrane bending by protein crowding

4.1 Introduction:

As established in the previous chapters, membrane structural changes driven by protein crowding is implicated in a number of critical biological processes.[1-2] However, molecular understanding of the mechanisms that underlie the bending process remains rudimentary.[3] For example, speculations have been made about how incorporation of Ni-NTA-DGS in model membranes can cause artifactual increase in local membrane curvature due to its steric bulk. However, the experimental evidence supporting such claims are sparse.[4] Additionally, we have little to no structural information about what protein crowding does to the bilayer integrity apart from causing large-scale deformations. For instance, several groups have reported that membrane deformations triggered via asymmetric protein partitioning into the outer leaflet of a vesicle surface can lead to generation of regions of tight curvature that in turn promote deformation and vesicle fission.[5] In the case of α-Synuclein, independent reports have observed that binding, and subsequent aggregation of the protein on the surface of the lipids can lead to lipid displacement, resulting in an overall decrease in the bilayer thickness.[6] This membrane thinning event, upon insertion of α-Synuclein to the membrane surface is also speculated to decrease the bending rigidity of the membranes culminating in the formation of tubular structures.[7] Despite such studies, several fundamental questions still remain. How does protein binding influence the lipid bilayer structure at a molecular level? How does protein association overcome the large barrier to membrane deformation posed by the bending rigidity of a normal phospholipid bilayer? Does the transition from normal vesicles to tubular structures happen in a two-state fashion, or, is the transition characterized by the presence of previously unresolved intermediates?

Conventionally, to study tubule formation triggered by protein binding, imaging-based techniques, such as Giant Vesicle tubulation assay, and micropipette aspiration are used.[8-9] While these techniques are convenient in reporting on the large-scale morphological changes in vesicle structure, phase separation, protein density, and surface coverage. they often lack molecular and the temporal resolution required to address the issues discussed previously. The lack of methodology presents an implicit experimental challenge for analysis of membrane remodeling events, where structural data alongside temporal information is needed for the constructing a thorough mechanistic picture. The equilibrium FRET assay developed in Chapter 2 provided us with a quantitative handle on the membrane deformation process. However, they were not utilized completely for performing kinetic studies. We hypothesized that stopped flow fluorescence can be used to quantify the membrane bending timescales, by utilizing the FRET probes developed in chapter 2. For information about membrane thickness and molecular level structural detail, we turned to Small Angle X-Ray Scattering (SAXS). Additionally, to account for the uniform distribution of the fluorophores across the bilayer leaflet, we employed asymmetric vesicles. Stopped flow analysis of asymmetric vesicles enabled for delineating the relative contribution to fluorescence changes from the individual leaflets.

We utilized *Escherichia coli* DHFR (EcDHFR) as a model protein for studying membrane expansion upon protein binding. Unlike in Chapter 3, utilizing His-SfGFP for the membrane expansion assay will severely complicate the analysis of fluorescence signals due to the overlap between the excitation and emission profiles of the membrane-associated fluorescent donor (NBD-PE) and the intrinsic GFP fluorophore.

EcDHFR offered a convenient alternative, due to its solubility, stability and the presence of histidine-tag.[10-11] While EcDHFR has a similar stokes radius to SfGFP, it does not have any intrinsic chromophores or fluorophores, making it ideal for our FRET assay. Stopped flow fluorescence reveals that the membrane expansion process is multi-phasic. While a positive phase ($k_{expansion}$ ~0.6-1.4 sec^{-1}) occurs in the longer time regime indicative of the membrane expansion process, we also observe an initial phase exhibiting negative amplitude, indicating a previously unresolved process. We speculated that the initial phase might be a consequence of enhancement in cross bilayer FRET due to the uniform distribution of the donor and the acceptor across the bilayer leaflet. SAXS results clearly show that, at protein concentrations above the critical deformation concentration (CDC- refer Chapter 2), substantial membrane thinning (~3-7% change in thickness) occurs upon protein binding. Interestingly, membrane thinning was also found to be strongly dependent on the bulk protein concentration. Preparation of Asymmetric Small Unilamellar Vesicles (aSUV) allowed us to temporally separate the two processes, leading us to conclude that protein binding leads to an initial thinning of the bilayer, subsequently resulting in deformation.

4.2 Results and Discussion

4.2.1 Equilibrium characterization of liposome deformation driven by protein crowding.

We first sought to identify and optimize the experimental conditions for triggering membrane bending by first performing equilibrium fluorescence measurements. We have previously established the experimental conditions for triggering membrane remodeling in Chapter 2. Briefly, a steady concentration (0.5 mM) of Small Unilamellar

Vesicles (SUVs) extruded through 100nm Polycarbonate membranes, were incubated for 30 minutes, in solutions containing different concentrations of EcDHFR ranging from 100nM – 20μM. The composition of the lipids under steady state conditions were maintained at 80 mol% DPPC and 20 mol% Ni-NTA-DGS (the chelator lipid) unless otherwise mentioned. The loading levels of the fluorophores (NBD-PE and Rhod-PE) were both maintained at 0.2mol%.

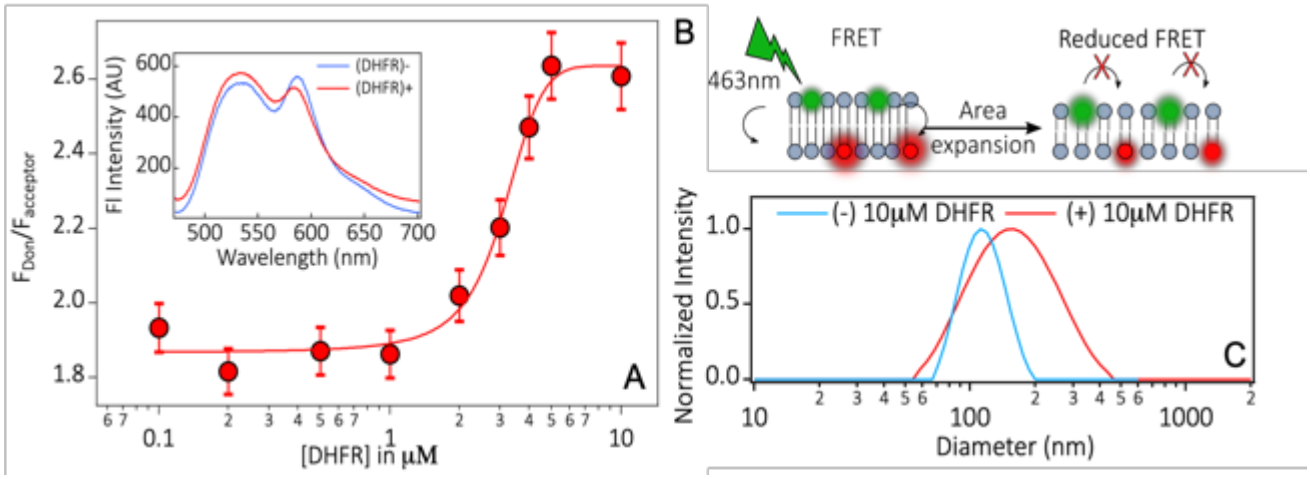

Figure 4.1. Equilibrium characterization of membrane deformation by protein crowding. (A) Ratio of donor fluorescence to acceptor fluorescence plotted as a function of protein concentration. Solid line is a sigmoidal fit with a midpoint of ~3.3 μM. Error bars represent the errors to the fit. Inset shows representative fluorescence spectra (Excitation at 463 nm) of the liposomes before and after addition of 10μM DHFR. NBD emission max (533 nm) increases relative to Rhodamine emission (582 nm) upon addition of the protein solution indicating substantial dequenching due to membrane area expansion. (B) A schematic describing the dequenching of NBD fluorescence upon membrane area expansion (C) Representative DLS intensity profile showing substantial morphological changes upon protein binding.

Concentration dependence of $F_{donor}/F_{acceptor}$ data was collected using a 96-well plate reader for a high-throughput readout (Figure 4.1A). Spectral data were collected with a steady state fluorometer under identical conditions (Figure 4.1A-inset). As seen in Figure

4.1A, a strong concentration dependence in relative fluorescence ($F_{Donor}/F_{Acceptor}$) was observed in the measurement, indicating that a critical protein density has to be reached at the liposome surface, for fluorescence de-quenching to occur as a result of vesicle expansion (Figure 4.2B). Fitting the fluorescence data to a sigmoidal function leads to the determination of the critical deformation concentration (CDC) of ~ 3.3 μM.

As an independent probe for membrane deformation, we performed Dynamic Light Scattering (DLS) on the liposome samples with and without the presence of 10μM DHFR (Figure 4.1C). As discussed in Chapter 2, careful consideration has to be given when analyzing DLS data on samples that possess non-spherical structures. However, we reasoned that the change in hydrodynamic drag of the liposomes, upon formation of tubules, will change the diffusion coefficients of the structures enough, to provide a qualitative handle on large scale structural changes. Using similar concentrations to the fluorescence measurements, we observe a large increase in the observed hydrodynamic radii of the vesicles, indicating that protein binding above the CDC causes significant membrane deformation.

4.2.2 Stopped flow transients reveal an unresolved intermediate that precedes membrane deformation.

We employed stopped-flow fluorescence to measure the kinetics of membrane deformation by protein crowding. The total concentration of lipids was maintained at 1 mM (DPPC with 20 mol% Ni-NTA DGS and 0.2mol% of NBD PE and Rhodamine-PE) and the protein concentration was varied from 5 to 20μM. Under these conditions, the bulk concentration of Ni-NTA DGS was maintained at a moderate excess relative to the

total protein concentration. However, due to the limited surface area at the vesicle surface and phase separation, significant steric crowding is expected.

We observed a strong time-dependent increase of the F_{Donor} to $F_{Acceptor}$ ratio from protein binding upon initiation of the stopped flow (Fig. 4.2A). We observed no major changes in control experiments performed with fluid liposome composition, (POPC with Ni-NTA-DGS) indicating that phase separation between DPPC (gel-phase lipid) and Ni-NTA-DGS (fluid-phase lipid) is important for generating steric pressure adequate to trigger membrane deformation.

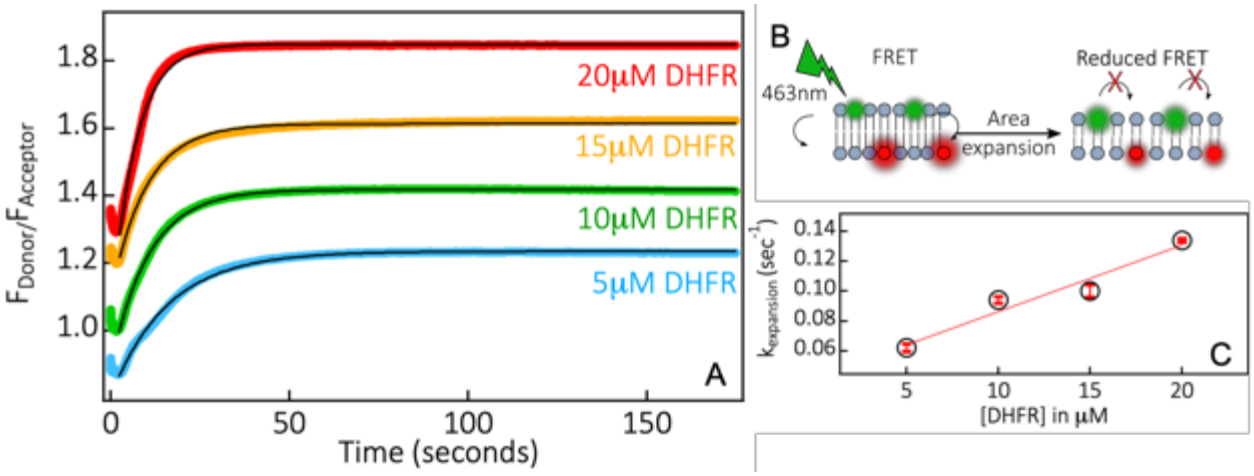

Figure 4.2. Stopped flow fluorescence transients of membrane expansion driven by protein crowding. (A) Ratio of donor fluorescence to acceptor fluorescence plotted as a function of time. A reproducible negative feature is observed in the early timescale indicating the presence of an intermediate. The solid lines represent single exponential fits from t=2 seconds. The traces are offset for clarity (B) A schematic of the dequenching of NBD fluorescence upon membrane area expansion (C) Rate constants obtained from single exponential fits plotted as a function of DHFR concentration. Error bars represent standard deviation from three independent measurements. The linear fit is meant to guide the reader's eye.

Interestingly, we observed that the stopped flow transients exhibited a complex behavior with the faster phase exhibiting a decrease in the $F_{Donor}/F_{Acceptor}$ ratio, initially (<2

seconds) before it starts increasing at slower timescales ($k_{expansion}$ ~0.6-1.4 sec^{-1}). The increase in the relative fluorescence can be attributed to the time it takes for the bilayer to stretch, leading to dequenching of the fluorophores. The slow phase rate constants obtained from single exponential fits, increased linearly as a function of increasing protein concentration (Figure 4.2C). It is worthwhile noting that the timescales of vesicle expansion (7-16 seconds) is more than an order of magnitude slower than the expected timescales of protein binding (250-700 milliseconds for the slow-phase of protein binding) observed in chapter 3. This shows that protein binding itself is not a rate determining step. However, we do expect the protein conformational heterogeneity at the interface to modulate the amount of steric pressure generated in a concentration dependent fashion. Therefore, the increase in the slow-phase rate constants as a function of protein concentration can be attributed to the increase in steric pressure due to increasing protein density at the membrane surface.

While a clear trend was established with the slow phase rate constants, we found it challenging to interpret the decrease in relative fluorescence in the earlier timescale (t<2 seconds). Upon closer examination of the R_o of our FRET pair (~5 nm),[12-13] we speculated that fluctuations in the lipid bilayer structure might lead to an enhancement in cross-bilayer FRET. Given that the average thickness of a DPPC bilayer (~4.8 nm) [14] is very similar to the R_o of our FRET pair, we suspected that even minor changes to membrane thickness upon protein association would lead to a considerable change in $F_{Donor}/F_{Acceptor}$ ratio.

However, to test this hypothesis, a number of factors have to be considered. First, the precedence for peripheral protein induced membrane thinning is limited in the literature. Many anti-microbial peptides such as Mastoparan,[15] Aurein,[16] Magainin 2, etc.,[17-18] have

been found to induce membrane thinning upon binding to model liposomes. α-Synuclein has also been found to induce membrane thinning by an aggregation driven lipid displacement mechanism.[6] However, both α-Synuclein and the anti-microbial peptides usually insert into the membranes directly, to cause extreme perturbations to the bilayer structure. In our experimental setup, our model proteins bind to the liposome surface transiently, and peripherally via the Ni-NTA-His tag interaction.[19]

Second, synthetic liposomes prepared via extrusion, sonication and electro formation, pose an intrinsic limitation in terms of controlling the symmetry of lipid distribution across the bilayer leaflet. This is due to the fact that the self-assembly of the lipid bilayers upon hydration of lipid cakes (multi-lamellar structures) is spontaneous, and the distribution cannot be controlled experimentally.[20-21] Finally, temporally separating the membrane thinning and membrane bending is extremely difficult due to the severe lack of experimental methodologies that allow us to probe these processes simultaneously.

4.2.3 Synthesis and characterization of Asymmetric vesicles.

Asymmetric vesicles (aSUV) offer a facile solution to a number of the aforementioned issues. We hypothesized that by gaining control over the distribution of lipids on either side of the bilayer leaflet, we can specifically target the FRET pairs to individual leaflets. This enables for the deconvolution of the complex stopped flow transients, that is not possible in liposomes containing uniform bilayers with equal distribution.

To synthesize asymmetric vesicles, we chose the catalyzed lipid-exchange method. This method relies on methyl-β-cyclodextrin (mβCD) to act as a lipid carrier.[22] mβCD is a water-soluble oligosaccharide that is characterized by a hydrophilic exterior and a hydrophobic core, whose pocket is large enough to adequately fit a lipid chain[23-24] (Figure

4.3A). By modulating the concentration of mβCD in solution, it has been discovered that a reversible mβCD-lipid complex can be formed. This phenomenon, can be manipulated to facilitate the exchange of lipids, and target them to a specific leaflet in the bilayer. We utilized this method to synthesize and purify asymmetric vesicles containing identical lipid compositions as described in section 4.2.1 and 4.2.2 (Experimental section).

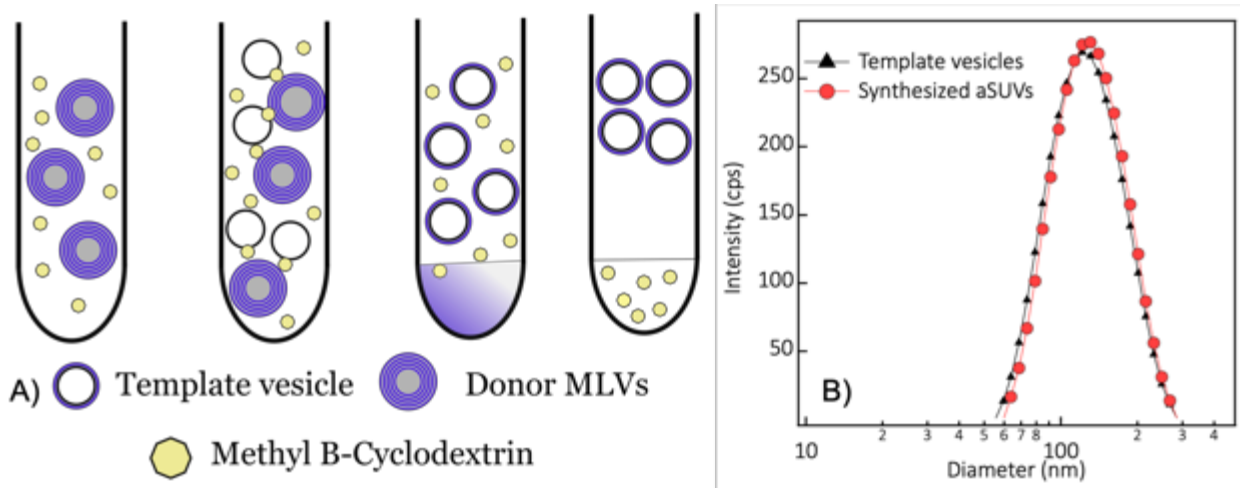

Figure 4.3. Synthesis and characterization of asymmetric vesicles. Heavy-donor strategy used in this study. The donor MLVs containing sucrose inside the vesicle core enabling easy sedimentation upon centrifugation. A brief overview of the protocol followed here can be found in the experimental section. The illustration in A) is adapted from Doktorova *et al.*[22] B) DLS intensity profile comparing the hydrodynamic radii of template vesicles and final synthesized asymmetric vesicles.

We characterized the integrity of the purified aSUVs by DLS. Careful measurements of DLS were necessary, due to the possible loss in yield upon chemical modifications of acceptor lipids due to mβCD treatment and centrifugation. Hence, we devised an approach to utilize DLS, to not just report on the changes in hydrodynamic radii of the acceptor vesicles upon preparation, but also, to report on the concentration of the vesicles once purification is complete (See Experimental Section). Under all conditions tested, we

noticed that the hydrodynamic diameter shifts by a modest amount (ranging from 2-5%) relative to the original size of the acceptor vesicles. This subtle change in the average vesicle size, indicates that no major aggregates are found due to donor lipid contamination.[22]

Once we verified that the purity and the overall integrity of the vesicles are intact, we

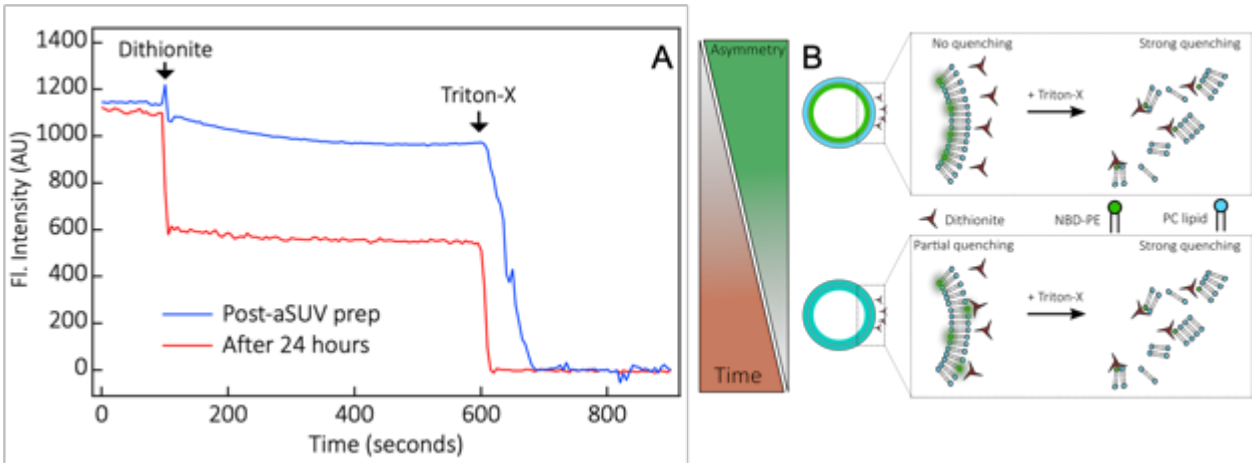

Figure 4.4. A fluorescence assay to determine the asymmetry of the synthesized liposomes. (A) Fluorescence quenching of NBD-PE by the reductant Sodium hydrosulfite (dithionite). In this case, NBD-PE was incorporated into the inner bilayer leaflet and POPC containing liposomes were used. (Experimental section). After a 24-hour incubation, the vesicles lose asymmetry due to lipid flip flop, and behave similarly to uniform vesicles (red trace). (B) A simplified schematic describing the assay.

proceeded to quantify the degree of asymmetry exhibited by the aSUVs. The quantification of asymmetry is important, as the fraction of fluorophores present in either leaflet will determine the fluorophore partitioning efficiency to one bilayer leaflet over the other, which in turn will be important in deconvoluting our stopped-flow results. The assay was based on the reduction of the fluorophore-NBD, once exposed to the reagent sodium hydrosulfite (25mM). In vesicles where NBD was targeted to the inner leaflet, we expect limited quenching (Figure 4.4A-blue trace) as the reducing agent cannot penetrate the membrane.[21] However, upon addition of a detergent (1% Triton-X), the inner

monolayer of the aSUVs get exposed to the reductant, leading to efficient quenching of the dye (Figure 4.4A, 4.4B).

Outer-leaflet composition	Inner-leaflet composition	Calculated % Asymmetry
POPC – Ni-NTA DGS	POPC – Ni-NTA DGS (NBD)	86 – 91%
POPC – Ni-NTA DGS (NBD)	POPC – Ni-NTA DGS	87 - 92%
DPPC – Ni-NTA DGS	DPPC – Ni-NTA DGS (NBD)	79 - 81%
DPPC – Ni-NTA DGS (NBD)	DPPC – Ni-NTA DGS	75 - 79%

Table 4.1. Quantification of asymmetry of the aSUV preparation protocol estimated by the fluorescence assay. The percentage asymmetry is calculated by dividing the difference in fluorescence signal upon addition of 25mM dithionite by the total fluorescence signal.

As seen in Table 4.1, we were consistently able to achieve 75-81% asymmetry when utilizing vesicles in the gel phase (DPPC-Ni-NTA-DGS) and 86-92% asymmetry when utilizing vesicles purely in the fluid phase (POPC-Ni-NTA-DGS). This is consistent with the previously reported literature values of exchange efficiency obtained by the catalyzed lipid-exchange method.[22]

4.2.4 Temporal separation of membrane thinning and membrane bending events by stopped flow fluorescence.

Having established a reproducible methodology for the synthesis of asymmetric vesicles, we turned our attention to quantifying the kinetics of membrane expansion by employing aSUVs. We reasoned that, by targeting our FRET probes to only the outer leaflet, (Figure 4.5B) any contributions to the fluorescence signal from energy transfer across the bilayer leaflets can be avoided. We estimated the aSUV concentration using our DLS based method (See Experimental Section). The starting concentration of the liposomes was maintained at 1 mM (DPPC with 20 mol% Ni-NTA DGS and 0.2mol% of NBD PE and

Rhodamine-PE) and the protein concentration was varied from 5 to 20μM. As discussed previously in Section 4.2.2, the bulk concentration of Ni-NTA DGS was maintained at a moderate excess relative to the total protein concentration. However, due to the limited surface area at the phase separated vesicle interface, significant steric crowding is expected.

Stopped flow transients reveal a similar time dependent increase in $F_{Donor}/F_{Acceptor}$ ratio while using aSUVs, in comparison to uniform vesicles, (Figure 4.5A) with a couple of notable exceptions.

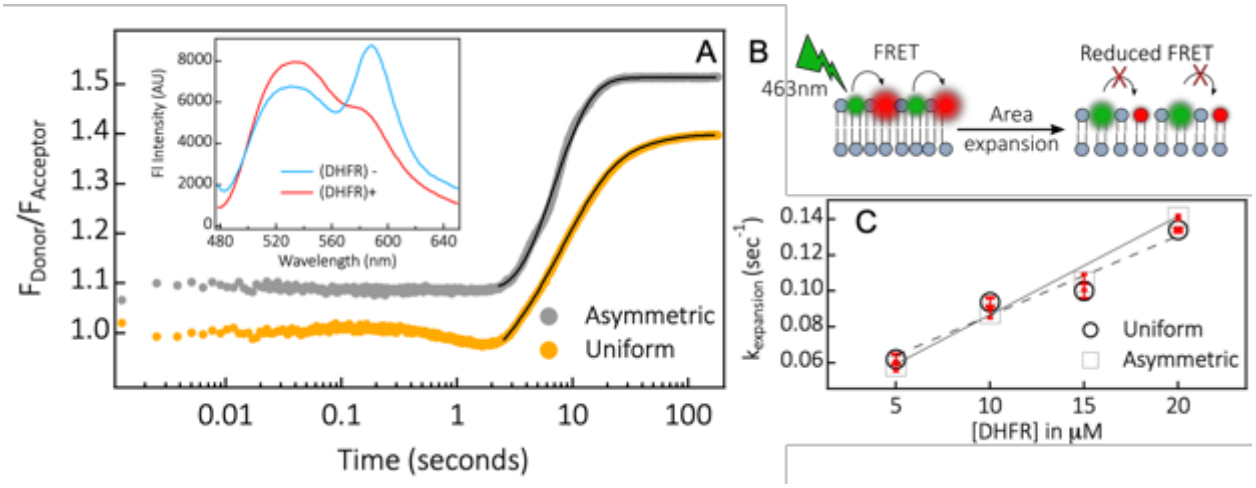

Figure 4.5. Comparison of membrane expansion kinetics of aSUVs vs uniform vesicles using stopped-flow fluorescence. (A) Representative stopped flow transients showing the ratio of donor fluorescence to acceptor fluorescence plotted as a function of time. 20 μM DHFR is used in both the equilibrium fluorescence measurement (Inset) and stopped flow measurement. The prominent negative feature is observed in the case of uniform vesicles, is greatly diminished in the case of aSUVs. The solid lines represent single exponential fits from t=2 seconds. The traces are offset for clarity (B) A schematic of the dequenching of NBD fluorescence upon membrane area expansion in case of aSUVs (C) Rate constants obtained from single exponential fits plotted as a function of DHFR concentration. Error bars represent standard deviation from three independent measurements. The linear fit is meant to guide the reader's eye.

First, the increase in $F_{Donor}/F_{Acceptor}$ ratio in the slower timescales, despite exhibiting similar rate constants (~$k_{expansion}$ ~0.6-1.4 sec^{-1}) appears to be steeper when using aSUVs, relative to the normal liposomes. This observation is puzzling as the time constants

should ideally increase as a function of increasing slopes. One possible explanation for this observation, is that the presence of a negative feature due to cross-bilayer FRET in the uniform vesicles can lead to convolution of the fluorescence transient, particularly at the faster timescales (<2 seconds). This might lead to artifacts while fitting the transients to an exponential function. Another possibility is that a single exponential is not adequate to fit the increase in relative donor fluorescence in the case of aSUVs. (Figure A4.2) It is possible that the membrane's outer leaflet is reporting on expansion events that would be difficult to discern by utilizing uniform vesicles. In the case of normal vesicles, the stopped flow transients report simultaneously on the expansion of both the leaflets through a relative increase in the donor fluorescence, apart from the additional cross-bilayer FRET that occurs at early timescales. Both of these hypotheses can be explored by using aSUVs with FRET pairs targeted to the inner bilayer leaflet.

Second, the magnitude of decrease in the relative fluorescence (using aSUVs) in the early timescales is extremely low, indicating that the origin of the negative feature in Figure 4.5A (yellow trace) is indeed due to cross-bilayer energy transfer. This noticeable decrease in the amplitude of the negative phase, suggests that the usage of aSUVs have severely diminished the quenching of donor fluorescence from cross-bilayer FRET (Figure 5.5B). In other words, by virtue of its asymmetry, the FRET pairs found only on the outer leaflet of aSUVs, are insensitive to fluctuations in the bilayer thickness upon protein association. This observation is interesting for a number of reasons. First, it adds more evidence to our initial hypothesis, that the thinning of membrane upon protein binding, indeed, is responsible for the initial decrease in $F_{Donor}/F_{Acceptor}$ ratio. Second, this observation suggests that the thinning of membranes upon protein association is a kinetic intermediate, that can be temporally separated from membrane expansion driven by

protein crowding. Third, membrane thinning occurs approximately in similar timescales (<4 seconds) as protein binding, indicating at least some temporal overlap between slowing of protein association at high densities (as discussed in chapter 3), and to the decrease in membrane thickness.

Interestingly, the idea of membrane thinning being a kinetic intermediate has been suggested independently, as a possible mechanism for α-Synuclein induced remodeling of membranes.[7] The study suggested that protein binding can cause enough disruption to the membrane surface, that leads to thinning of the overall membrane thickness. It was hypothesized that α-Synuclein might be able to squeeze the bilayer by applying a transverse vertical force to the membrane surface, leading to thinning, and subsequently lipid interdigitation. Given that membrane bending modulus and the thickness are intrinsically related, it is certainly possible that a thinned membrane intermediate can lower the energy cost of membrane bending. Our results seem to agree with these findings, though the membrane-binding interface is extremely different between both scenarios. It is certainly possible that a sudden jump in protein density, due to macromolecular association at the crowded protein-membrane interface can lead to strong changes in the bilayer structure as suggested by our stopped flow results. However, to validate our observations from analyzing aSUV expansion, and to probe molecular level changes in the bilayer structure, direct experimental validation of membrane thickness changes was necessary to arrive at accurate conclusions.

4.2.5 Characterization of change in membrane thickness by Small-Angle X-Ray Scattering.

To characterize the change in bilayer thickness upon protein binding to the liposome surface, we utilized Small Angle X-Ray Scattering (SAXS). SAXS is a useful methodology to study the bilayer structure at a molecular level despite its limited atomic resolution. We chose this methodology, because SAXS provides highly accurate and quantitative data on the size, shape and structural features of biological samples under relevant solution conditions, unlike most other techniques that involve harsh conditions such as freezing or drying.[25]

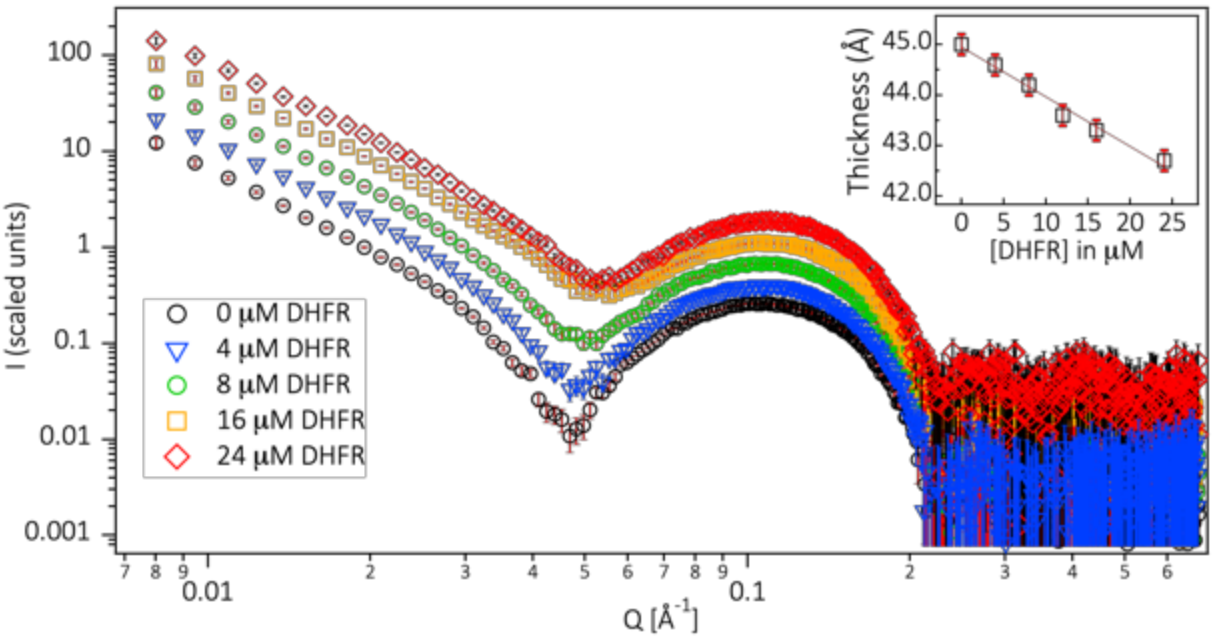

Figure 4.6. SAXS diffractograms of 6.5 mM aSUVs under different protein concentrations. It can be clearly seen that the minima at the lower Q values gradually shifts to higher Q-values with increasing protein concentrations. This indicates a significant thinning of the membrane bilayer upon protein binding. 12 scans were signal averaged, and reference corrected to yield the final diffractogram and error bars represent the standard deviation Inset shows the concentration dependence of change in the apparent bilayer thickness. Error bars represent the standard deviation.

SAXS is also an extremely useful tool to study lamellar structures of the liposomes. Typical SAXS diffractograms are sensitive to scattering signals that arise from transverse and longitudinal fluctuations from the lipid bilayers. Given that our liposomes are predominantly uni-lamellar, the scattering profile should ideally be diffuse without the presence of any appreciable Bragg's peaks.

As seen in Figure 4.6, a diffuse diffraction pattern is observed in case of aSUVs without the presence of any protein indicating a unilamellar vesicle structure without any major undulations (Black circles). The scattering profile from the lipid bilayer is characterized by the presence of the two major minima in the moderate Q ranges. The first minimum at Q ~ 0.05 $Å^{-1}$ is typically indicative of the electron density on the outer leaflet of the membrane, whereas the second minimum at the higher Q values (~ 0.2 $Å^{-1}$) is sensitive to the electron density at the inner leaflet of the bilayer. Upon addition of the protein to the aSUV samples, we notice a strong shift of the first minimum to higher Q-values indicating a significant decrease in the membrane thickness.

It is worthwhile noting that, due to high density of the protein binding to the outer layer of the membrane surface, (~ 0.05 $Å^{-1}$) the enhancement in electron density in this region complicates interpretation and the estimation of absolute values with regards to the bilayer thickness. Hence, for measuring the relative changes, only the changes to the hydrocarbon chain and inner headgroup layer of the vesicle will be considered. By modeling the SAXS diffractograms using a core-shell model,[26] we were able to determine the thickness changes of the bilayer as a function of protein concentration (Figure 4.6 Inset). We estimate a significant change in the average membrane thickness (from ~ 4.5nm to 4.27nm) upon addition of the protein samples. These values are

similar to those obtained in literature for α-Synuclein induced reduction in bilayer thickness,[6] despite our DHFR constructs not partitioning into the membrane directly through hydrophobic insertion. Apart from validating our initial interpretation of stopped-flow transients, the observation of membrane thinning leads to important insights into the mechanistic origins of membrane area expansion triggered by protein crowding.

In particular, the induction of asymmetry in the electron density profiles of the outer headgroup layer implies that the bilayer structure is modulated significantly upon protein binding. Asymmetric insertion of proteins into the outer leaflet of the bilayer surface has been proposed to be a crucial driving force for membrane bending in a number of previously established studies.[5, 27] It is certainly possible that asymmetric crowding of proteins, at very high densities on the outer leaflet of the bilayer surface can disrupt the bilayer's integrity, leading to re-arrangements that cause substantial thinning of the bilayer surface. However, it is a hypothesis yet to be tested experimentally.

Nonetheless, our observation that membrane thinning precedes membrane bending by protein crowding is a significant one. Conventional models that discuss the energy cost of membrane bending by protein association seldom consider the changes in bilayer thickness upon protein binding.[27] As discussed previously in section 4.2.4, the bending modulus of the lipid membranes are intrinsically related to the thickness of the bilayer. Any minor changes to the bilayer thickness will therefore severely affect the penalty associated with bending the membrane. The softening of the host cell membranes upon the interaction of HIV has been hypothesized to be critical for pore formation and

infectivity.[28] Also, a similar hypothesis was proposed for α-Synuclein induced remodeling of model membranes. Such studies imply that membrane thinning could be adopted universally by other membrane remodeling proteins as well.

4.3 Conclusion:

In summary, we provide direct experimental evidence to membrane thinning caused by protein crowding. By utilizing asymmetric vesicles, we also show that the membrane thinning and expansion processes are temporally separated from one another, indicating that membrane tubule formation is preceded by the initial membrane thinning process. Our results, not only complement previous observations about membrane deformation, but also provides a clear kinetic picture of the intermediates that precede membrane remodeling by protein association at high densities. We believe that the novel insights offered by this study greatly improves our understanding of the membrane bending process, and will inspire further quantitative investigation of protein crowding as a driver for membrane remodeling.

4.4 EXPERIMENTAL SECTION

4.4.1 Materials. DPPC, POPC and Ni-NTA-DGS were purchased from Avanti Polar Lipids (Alabaster, AL). NBD-PE and Rhodamine-PE were purchased from ThermoFisher Scientific (Waltham, MA). His-tagged DHFR was expressed and purified in house from a custom modified plasmid using protocols described in Chapter 3. EDTA, Sucrose, methyl-β–Cyclodextrin was obtained from Sigma-Aldrich (St. Louis, MO). MOPS, Sodium Chloride, and Amicon Ultra-0.5 mL centrifugal filters (10 kDa MWCO) were obtained from EMD Millipore (Billerica, MA).

4.4.2 Large unilamellar vesicles preparation. Large unilamellar vesicles (LUVs) were prepared by the extrusion method. Lipid mixtures (DPPC, 20 mol% Ni-NTA and 0.2 mol% NBD-PE and Rhod-PE) were dissolved in chloroform and dried under a stream of Argon gas on the inner wall of a small vial and then placed under vacuum overnight to form stable lipid cakes. For uniform liposomes, the lipid cakes were then rehydrated to a final liposome concentration of 1mM with MOPS buffer (50 mM MOPS, pH 7.2) for 1 hour at room temperature. For formation of acceptor liposomes for aSUV prep, similar protocol was followed, with minor changes to the buffer composition (25 mM NaCl). Every 15 minutes, the rehydrated lipid solution was vortexed thoroughly, and subsequently subjected to five freeze thaw cycles. The resulting multi-lamellar vesicle solutions were then extruded through a polycarbonate membrane (pore size 100nm; Whatman/GE Healthcare) 20 times to produce a clear solution of liposomes.

4.4.3 Dynamic light scattering measurements. Micromeritics Corporation's NanoPlus, a particle size analyzer was used to perform dynamic light scattering (DLS) to measure the hydrodynamic diameter of the liposomes with and without the presence of protein. A final liposome concentration of 1 mM was used in all experiments. A micro-volume glass cuvette capable of measuring sample volumes as low as 60μL was used for all measurements. Optimization of scattering intensity was performed by adjusting the cell-center, and by tuning the laser attenuation.

For quantifying aSUV concentrations upon purification, a standard curve was prepared by utilizing a highly monodisperse sample of polystyrene beads with diameters similar to the vesicle diameters (100nM). The laser attenuation was maintained constant, and the concentration of the beads were varied across a wide range. For a fixed laser attenuation,

the intensity of the scattered light correlates with the increasing concentration of the particles in the medium (See Appendix). Once the standard curve was constructed, liposome samples were measured under identical attenuation settings leading to a reliable approximation of the number of liposomes in solution.

4.4.4 Equilibrium fluorescence measurements. Steady state fluorescence measurements were performed by Horiba Fluorometer. A micro-volume cuvette capable of measuring solution volumes as low as 150 μL was used for all measurements. The final bulk concentration of Ni-NTA DGS in the liposome samples were maintained at 100 uM, and the protein solution was added at the reported concentrations. Determination of CDC, was performed in a high throughput fashion using BioTek Cytation 5 multi-mode microplate reader. Sample excitation was performed at the wavelength of 463 nm. Quantification of critical deformation concentration was performed by fitting the change in $F_{Donor}/F_{Acceptor}$ ratio as a function of protein concentration, to a sigmoidal function. Untreated, clear bottomed flat 96-well plates were used for all experiments. Quantification of bilayer asymmetry was performed by measuring the fluorescence emission, by manually adding the reductant and detergent at different time points as described in section 5.2.3.

4.4.5 Stopped flow fluorescence measurements. The membrane expansion kinetics upon protein binding to liposomes were quantified by using SX20 stopped flow apparatus (Applied Photophysics, UK). The starting concentration of the liposomes was maintained at 1mM (DPPC with 20mol% Ni-NTA DGS and 0.2mol% of FRET dyes) and the protein concentration was varied from 5 μM to 20 μM. Upon initiation of the stopped-flow, the two solutions were mixed in an observation chamber a short deadtime

(~ms) and the fluorescence was monitored by a Photomultiplier tube (PMT). For the donor fluorescence, a combination of a 495 nm Long-Pass filter along with a 550 nm short pass filter was used to eliminate any scattering of the excitation light (463 nm) and to eliminate contribution from the acceptor fluorescence from reaching the detector. For quantifying the acceptor fluorescence, a 561 nm long pass filter was used. The donor-fluorescence transients obtained from the stopped flow measurements were divided by the acceptor fluorescence transient, leading to the final $F_{Donor}/F_{Acceptor}$ trace (See Appendix). All measurements were performed at room temperature and curve fitting was performed using Igor Pro (Wavemetrics, Portland, OR).

4.4.6 Asymmetric vesicle preparation.

For preparation of aSUVs, a catalyzed lipid exchange protocol was followed as described elsewhere. Briefly, the donor vesicles were prepared by hydrating the donor lipid cake for at least 1 hour, with 20% w/w solution of sucrose at temperatures above the transition temperature of DPPC (>41°C). Donor MLVs were subsequently formed, by subjecting the solution to at least 5 freeze thaw cycles. The donor liposomes were then diluted by about 20-fold with water, and the supernatant was discarded. The first step of lipid exchange was initiated by incubating the donor pellet with mβCD solution. A mβCD/lipid ratio of 8:1 was used. After vigorous stirring for 2 hours, the template liposomes from section 5.4.2 was added to the donor- mβCD mixture. This mixture was gently stirred for at least 30 minutes, and subsequently diluted eightfold with de-ionized water, and centrifuged at 20,000 g for 30 minutes. Due to the presence of sucrose in the donor lamellae, the donor- mβCD mixtures precipitate at the bottom, leaving only the pure aSUVs in the supernatant. This solution was subjected to several rounds of

centrifugal filtration for removing the excess mβCD, and subsequently, used for our experiments.

4.4.7 Small Angle X-Ray Scattering measurements.

The SAXS experiments were performed on a Rigaku BioSAXS-2000 home-source system with a HF007 copper rotating anode with a Pilatus 100K Detector. SAXS data were collected at a fixed sample-to-detector distance using a silver behenate calibration standard. 6.5 mM aSUVs were loaded into the sample using the autosampler attachment. For measurements containing protein solutions, a standard reference containing equivalent concentrations of protein in buffer free of liposomes were used. At least 12 scans of individual samples were averaged and reduced using Rigaku SAXSlab data collection and processing software. The software - PRIMUS was used for initial analysis. Data fitting, and SLD analysis was performed using our in-house fitting routine described elsewhere.

4.5 References.

1. Stachowiak, J. C.; Schmid, E. M.; Ryan, C. J.; Ann, H. S.; Sasaki, D. Y.; Sherman, M. B.; Geissler, P. L.; Fletcher, D. A.; Hayden, C. C., Membrane bending by protein-protein crowding. *Nat Cell Biol* **2012,** *14* (9), 944-9.

2. Busch, D. J.; Houser, J. R.; Hayden, C. C.; Sherman, M. B.; Lafer, E. M.; Stachowiak, J. C., Intrinsically disordered proteins drive membrane curvature. *Nat Commun* **2015,** *6*, 7875.

3. Bassereau, P.; Jin, R.; Baumgart, T.; Deserno, M.; Dimova, R.; Frolov, V. A.; Bashkirov, P. V.; Grubmuller, H.; Jahn, R.; Risselada, H. J.; Johannes, L.; Kozlov, M. M.; Lipowsky, R.; Pucadyil, T. J.; Zeno, W. F.; Stachowiak, J. C.; Stamou, D.; Breuer, A.;

Lauritsen, L.; Simon, C.; Sykes, C.; Voth, G. A.; Weikl, T. R., The 2018 biomembrane curvature and remodeling roadmap. *J Phys D Appl Phys* **2018,** *51* (34).

4. Kozlov, M. M.; Campelo, F.; Liska, N.; Chernomordik, L. V.; Marrink, S. J.; McMahon, H. T., Mechanisms shaping cell membranes. *Curr Opin Cell Biol* **2014,** *29*, 53-60.

5. McMahon, H. T.; Boucrot, E., Membrane curvature at a glance. *J Cell Sci* **2015,** *128* (6), 1065-70.

6. Hahl, H.; Moller, I.; Kiesel, I.; Campioni, S.; Riek, R.; Verdes, D.; Seeger, S., alpha-Synuclein insertion into supported lipid bilayers as seen by in situ X-ray reflectivity. *ACS Chem Neurosci* **2015,** *6* (3), 374-9.

7. Shi, Z.; Sachs, J. N.; Rhoades, E.; Baumgart, T., Biophysics of alpha-synuclein induced membrane remodelling. *Phys Chem Chem Phys* **2015,** *17* (24), 15561-8.

8. Stachowiak, J. C.; Hayden, C. C.; Sasaki, D. Y., Steric confinement of proteins on lipid membranes can drive curvature and tubulation. *Proc Natl Acad Sci U S A* **2010,** *107* (17), 7781-6.

9. Heinrich, M.; Tian, A.; Esposito, C.; Baumgart, T., Dynamic sorting of lipids and proteins in membrane tubes with a moving phase boundary. *Proc Natl Acad Sci U S A* **2010,** *107* (16), 7208-13.

10. Baccanari, D. P.; Averett, D.; Briggs, C.; Burchall, J., Escherichia coli dihydrofolate reductase: isolation and characterization of two isozymes. *Biochemistry* **1977,** *16* (16), 3566-72.

11. Kozlowski, R.; Ragupathi, A.; Dyer, R. B., Characterizing the Surface Coverage of Protein-Gold Nanoparticle Bioconjugates. *Bioconjug Chem* **2018,** *29* (8), 2691-2700.

12. Struck, D. K.; Hoekstra, D.; Pagano, R. E., Use of resonance energy transfer to monitor membrane fusion. *Biochemistry* **1981,** *20* (14), 4093-9.

13. Chen, I. A.; Szostak, J. W., A kinetic study of the growth of fatty acid vesicles. *Biophys J* **2004,** *87* (2), 988-98.

14. Kucerka, N.; Nieh, M. P.; Katsaras, J., Fluid phase lipid areas and bilayer thicknesses of commonly used phosphatidylcholines as a function of temperature. *Biochim Biophys Acta* **2011,** *1808* (11), 2761-71.

15. Whiles, J. A.; Brasseur, R.; Glover, K. J.; Melacini, G.; Komives, E. A.; Vold, R. R., Orientation and effects of mastoparan X on phospholipid bicelles. *Biophys J* **2001,** *80* (1), 280-93.

16. Rai, D. K.; Qian, S., Interaction of the Antimicrobial Peptide Aurein 1.2 and Charged Lipid Bilayer. *Sci Rep* **2017,** *7* (1), 3719.

17. Mecke, A.; Lee, D. K.; Ramamoorthy, A.; Orr, B. G.; Banaszak Holl, M. M., Membrane thinning due to antimicrobial peptide binding: an atomic force microscopy study of MSI-78 in lipid bilayers. *Biophys J* **2005,** *89* (6), 4043-50.

18. Grage, S. L.; Afonin, S.; Kara, S.; Buth, G.; Ulrich, A. S., Membrane Thinning and Thickening Induced by Membrane-Active Amphipathic Peptides. *Front Cell Dev Biol* **2016,** *4*, 65.

19. Dietrich, C.; Schmitt, L.; Tampe, R., Molecular organization of histidine-tagged biomolecules at self-assembled lipid interfaces using a novel class of chelator lipids. *Proc Natl Acad Sci U S A* **1995,** *92* (20), 9014-8.

20. Markones, M.; Drechsler, C.; Kaiser, M.; Kalie, L.; Heerklotz, H.; Fiedler, S., Engineering Asymmetric Lipid Vesicles: Accurate and Convenient Control of the Outer Leaflet Lipid Composition. *Langmuir* **2018,** *34* (5), 1999-2005.

21. Pautot, S.; Frisken, B. J.; Weitz, D. A., Engineering asymmetric vesicles. *Proc Natl Acad Sci U S A* **2003,** *100* (19), 10718-21.

22. Doktorova, M.; Heberle, F. A.; Eicher, B.; Standaert, R. F.; Katsaras, J.; London, E.; Pabst, G.; Marquardt, D., Preparation of asymmetric phospholipid vesicles for use as cell membrane models. *Nat Protoc* **2018,** *13* (9), 2086-2101.

23. Lopez, C. A.; de Vries, A. H.; Marrink, S. J., Molecular mechanism of cyclodextrin mediated cholesterol extraction. *PLoS Comput Biol* **2011,** *7* (3), e1002020.

24. Zidovetzki, R.; Levitan, I., Use of cyclodextrins to manipulate plasma membrane cholesterol content: evidence, misconceptions and control strategies. *Biochim Biophys Acta* **2007,** *1768* (6), 1311-24.

25. Bouwstra, J. A.; Gooris, G. S.; Bras, W.; Talsma, H., Small angle X-ray scattering: possibilities and limitations in characterization of vesicles. *Chem Phys Lipids* **1993,** *64* (1-3), 83-98.

26. Grunewald, T. A.; Lassenberger, A.; van Oostrum, P. D.; Rennhofer, H.; Zirbs, R.; Capone, B.; Vonderhaid, I.; Amenitsch, H.; Lichtenegger, H. C.; Reimhult, E., Core-Shell Structure of Monodisperse Poly(ethylene glycol)-Grafted Iron Oxide Nanoparticles Studied by Small-Angle X-ray Scattering. *Chem Mater* **2015,** *27* (13), 4763-4771.

27. Stachowiak, J. C.; Brodsky, F. M.; Miller, E. A., A cost-benefit analysis of the physical mechanisms of membrane curvature. *Nat Cell Biol* **2013,** *15* (9), 1019-27.

28. Agrawal, H.; Zelisko, M.; Liu, L.; Sharma, P., Rigid proteins and softening of biological membranes-with application to HIV-induced cell membrane softening. *Sci Rep* **2016,** *6*, 25412.

Appendix 4: Membrane thinning precedes membrane bending by protein crowding.

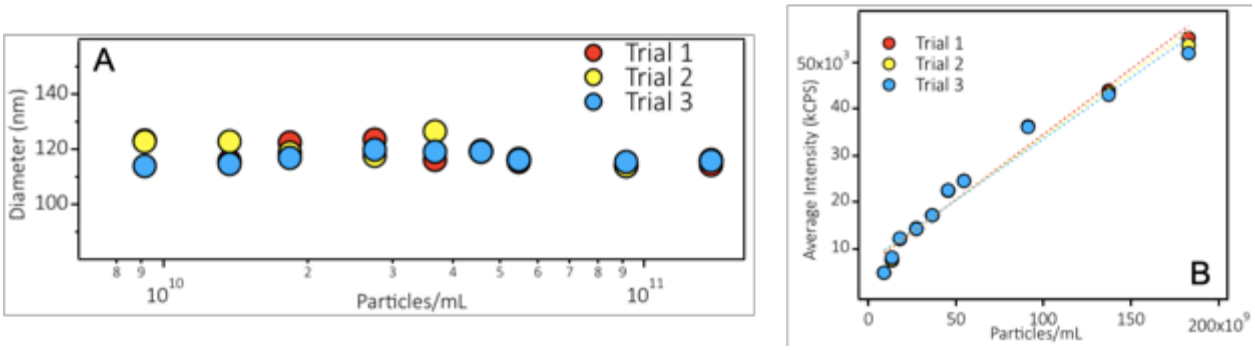

Figure A4.1. Determination of aSUV concentration by Dynamic Light Scattering. (A) 3 trials of polystyrene-latex beads measured at uniform laser attenuation. The hydrodynamic diameter reported, clearly indicates that only the scattering intensity (and, not the stokes radii) is sensitive to change in particle concentration (B) Standard curve generated by increasing particle concentration and the associated linear fit. We would like to note that all measurements were performed only in the linear regime of the standard curve, and the non-linear low concentration data was included in the graph purely for the reader's reference.

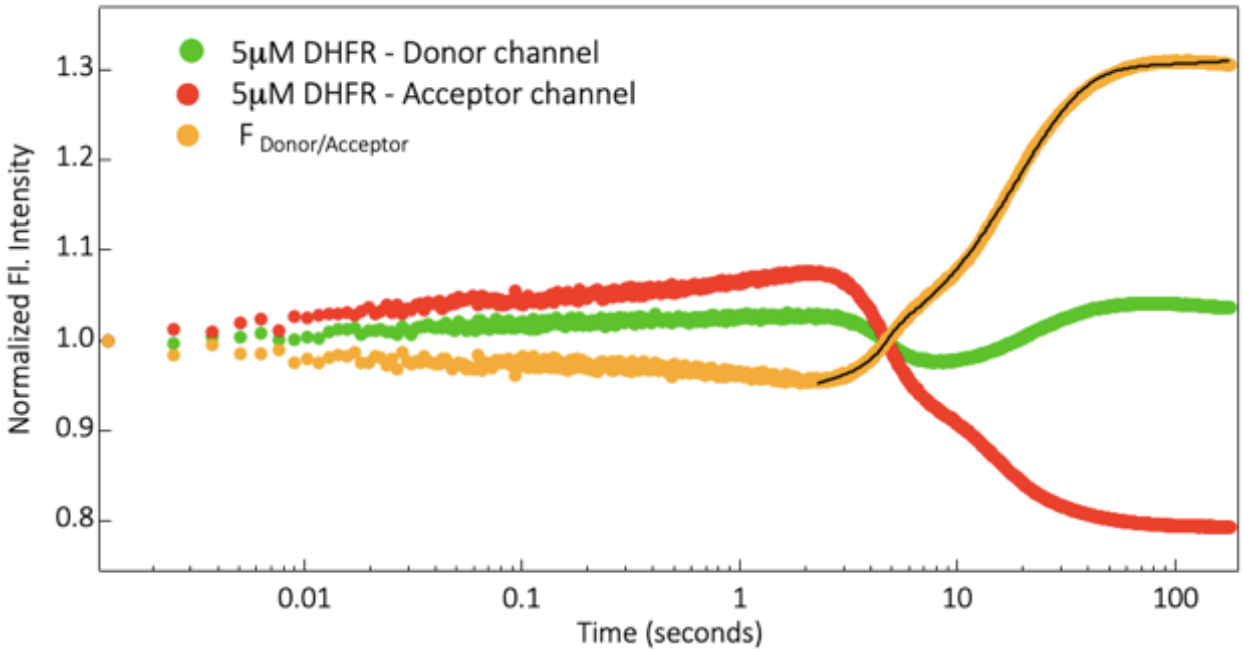

Figure A4.2. Treatment of the raw fluorescence transients obtained from stopped flow. Representative stopped flow fluorescence transients of the donor channel (green) and the acceptor channel (red). The two traces were divided to acquire the final $F_{Donor}/F_{Acceptor}$ transient (yellow). The solid line signifies a double sigmoidal fit at t>2 seconds. This is purely to guide the reader's attention to the presence of two distinct phases even during the membrane expansion process.

Chapter 5

Conclusion and Perspectives

5.1 Summary.

5.1.1 Exploring the physicochemical parameters that regulates membrane bending driven by protein crowding.

The single major aim of this dissertation was to perform a fundamental, mechanistic investigation of the biophysics underlying membrane bending triggered by protein crowding. Crowding induced membrane bending and lipid shape deformations has recently caught the attention of many.[1-3] The conformational flexibility and hydrodynamics of peripherally attached protein complexes have been attributed to be responsible for both membrane curvature sensing and curvature generation.[4-5] While a number of phenomenological observations have been made with regards to these systems, a thorough understanding of the role played by various physicochemical variables such as vesicle curvature, phase segregation, membrane thickness fluctuation, protein surface charge, etc., still remains under-characterized in the literature. Understanding the molecular origins of these parameters will be critical to constructing a thorough mechanistic picture, and to extrapolate in-vitro observations to biologically relevant processes.

To that end, we provide a quantitative biophysical investigation of membrane deformation driven by protein crowding. Using a multi-pronged approach, involving a combination of both equilibrium and kinetic spectroscopic techniques, we provide valuable insights into a number of critical factors that regulates membrane curvature generation in a multi-variate fashion. We find that steric pressure generated by the protein-unfolding transition of a surface-bound protein complex can lead to membrane deformation, by controlled chemical modification of the protein structure (Chapter 1).

In Chapter 2, we systematically investigated the coupling between the intrinsic vesicle curvature, vesicle phase segregation and the associated membrane bending capacity of the bound proteins and protein crowding. Using a spectroscopic approach, we were able to provide a quantitative handle on the membrane area expansion by using vesicles smaller than 200nm in diameter. We show very clearly, that bending membranes of higher mean vesicle curvatures requires a smaller concentration of proteins, than deforming vesicles with lower mean curvatures. We further explore the origin of this behavior by studying the curvature dependent changes in the liposome phase structure. We find that phase segregation of binary mixtures is exacerbated at lower vesicle radii, indicating that packing stress leads to favorable partitioning of the fluid lipid domains in the areas of extreme curvatures, thereby influencing, albeit, indirectly the spatial organization of the bound protein complexes.

5.1.2 Kinetic intermediates that precede membrane bending.

Our equilibrium measurements revealed new and novel insights into the physicochemical parameters that regulates membrane bending. However, we were able to acquire only limited mechanistic detail from steady state measurements. Given that protein association, crowding and membrane bending are dynamic processes, temporal separation of the critical steps leading to the final deformation of the membrane structure was necessary to understand such processes from a fundamental perspective.

In Chapter 3, we explored the kinetics of protein binding to liposome surface containing chelator lipids for convenient and reversible immobilization.[6] We find that, once steric crowding of the proteins occurs, the rate of protein association starts decreasing, indicating that major energetic bottlenecks have to be overcome at the protein-lipid

interface for the binding process to reach equilibrium. Through carefully constructed experiments, we were able to show that protein binding to the liposome surface, particularly, at high densities, follows a multi-phasic behavior characterized by protein orientational heterogeneity. Our results imply that, even when utilizing model systems comprised of chelator lipid- his tag complexes, the conformational flexibility of peripherally associated membrane proteins can dynamically regulate the protein density at the interface.

In Chapter 4, we explore the kinetics of membrane area expansion process by utilizing a spectroscopic approach. We show that membrane bending by area expansion is not a simple two-state process, as previously expected.[7] Instead, it is characterized by the presence of an intermediate that occurs on a timescale that is similar to the timescales of protein association as observed in Chapter 3. Using an array of biophysical techniques, we prove that thinning of the bilayer membrane is a kinetic intermediate that precedes the membrane deformation process. Membrane thinning has been hypothesized to play a critical role in membrane remodeling driven by physiologically relevant systems such as α-Synuclein.[8] However, direct experimental evidence has remained sparse. To our knowledge, this is the first report in literature to identify membrane thinning as an intermediate that leads to the bending of liposome surfaces. We believe that the relevance of this mechanism is far-reaching, and not just restricted to protein crowding driven membrane remodeling. Given that the thickness of the lipid bilayer is directly related to the bending rigidity of most biological membranes, small changes to the overall bilayer thickness by protein association can lead to a reduction of the energy cost associated with generating curvature.[8-9]

5.2 Future Outlook

5.2.1 Kinetics of vesicle fission and fusion.

A clear understanding of membrane bending kinetics is important for a number of reasons. For instance, the first steps of influenza viral invasion into the host cell, is characterized by membrane curvature generation by the viral surface protein-Hemagglutinin. [9-10] Generation of membrane curvature is a prerequisite for fusion, which leads to the viral genetic material being released into the host-cell. A number of non-pathological cellular processes, such as vesicle budding, lipid fission, etc., also require the generation of extremely high membrane curvatures driven by peripheral and integral membrane proteins.[11-12] While several crystallographic and steady state investigations have been conducted on these complicated machineries, very little is known about the dynamics of these systems. Particularly, we know little to nothing about the timescales of vesicle fission, or if the fission process has any kinetic bottlenecks. Understanding the dynamics of lipid fission and fusion, will therefore greatly enhance our knowledge of the factors that control cellular transport, sorting and pathology. We believe that our biophysical approach, detailed in Chapters 3 and 4, will guide future studies related to more complex biological processes

5.2.2 Rational design of modular bio-conjugates.

While the aim of the dissertation was to explore the mechanism of membrane bending process, the chelator lipid under study, is also a great platform for immobilization of target biomolecules. Lipid based biomaterials and bioconjugates have a unique advantage over other nano-carriers, in that, the antibody response against lipid-based

particles are often extremely muted. Additionally, liposomes are formed partially by self-assembly, opening up a lot of potential for drug delivery and targeting.[13]

Our results that explore the coupling between phase-separation and membrane curvature, offers new possible ways to modulate the spatial organization of specific lipids, and consequentially, conjugated biomolecules. For instance, by careful design, it is possible to achieve strong lipid-demixing by compositional variation, leading to unique architectures that will arise from self-assembly. Patterned nano-particles have been used for carrying out several functions. Recent studies have shown that, by producing two-faced Janus nanoparticles,[14] it is possible to chemo-osmotically accelerate the diffusion of the nano-carriers. With a thoughtful rational design, we can accomplish spatial control within a single liposome, to carry out similar functions with superlative modularity.

5.3 References.

1. Stachowiak, J. C.; Schmid, E. M.; Ryan, C. J.; Ann, H. S.; Sasaki, D. Y.; Sherman, M. B.; Geissler, P. L.; Fletcher, D. A.; Hayden, C. C., Membrane bending by protein-protein crowding. *Nat Cell Biol* **2012,** *14* (9), 944-9.

2. Chen, Z.; Atefi, E.; Baumgart, T., Membrane Shape Instability Induced by Protein Crowding. *Biophys J* **2016,** *111* (9), 1823-1826.

3. Stachowiak, J. C.; Hayden, C. C.; Sasaki, D. Y., Steric confinement of proteins on lipid membranes can drive curvature and tubulation. *Proc Natl Acad Sci U S A* **2010,** *107* (17), 7781-6.

4. Zeno, W. F.; Baul, U.; Snead, W. T.; DeGroot, A. C. M.; Wang, L.; Lafer, E. M.; Thirumalai, D.; Stachowiak, J. C., Synergy between intrinsically disordered domains and

structured proteins amplifies membrane curvature sensing. *Nat Commun* **2018,** *9* (1), 4152.

5. Zeno, W. F.; Thatte, A. S.; Wang, L.; Snead, W. T.; Lafer, E. M.; Stachowiak, J. C., Molecular Mechanisms of Membrane Curvature Sensing by a Disordered Protein. *J Am Chem Soc* **2019,** *141* (26), 10361-10371.

6. Dietrich, C.; Schmitt, L.; Tampe, R., Molecular organization of histidine-tagged biomolecules at self-assembled lipid interfaces using a novel class of chelator lipids. *Proc Natl Acad Sci U S A* **1995,** *92* (20), 9014-8.

7. Stachowiak, J. C.; Brodsky, F. M.; Miller, E. A., A cost-benefit analysis of the physical mechanisms of membrane curvature. *Nat Cell Biol* **2013,** *15* (9), 1019-27.

8. Shi, Z.; Sachs, J. N.; Rhoades, E.; Baumgart, T., Biophysics of alpha-synuclein induced membrane remodelling. *Phys Chem Chem Phys* **2015,** *17* (24), 15561-8.

9. Edinger, T. O.; Pohl, M. O.; Stertz, S., Entry of influenza A virus: host factors and antiviral targets. *J Gen Virol* **2014,** *95* (Pt 2), 263-77.

10. Harrison, S. C., Viral membrane fusion. *Virology* **2015,** *479-480*, 498-507.

11. Roux, A.; Antonny, B., The long and short of membrane fission. *Cell* **2008,** *135* (7), 1163-5.

12. Shnyrova, A. V.; Bashkirov, P. V.; Akimov, S. A.; Pucadyil, T. J.; Zimmerberg, J.; Schmid, S. L.; Frolov, V. A., Geometric catalysis of membrane fission driven by flexible dynamin rings. *Science* **2013,** *339* (6126), 1433-6.

13. Sercombe, L.; Veerati, T.; Moheimani, F.; Wu, S. Y.; Sood, A. K.; Hua, S., Advances and Challenges of Liposome Assisted Drug Delivery. *Front Pharmacol* **2015,** *6*, 286.

14. Ma, X.; Jannasch, A.; Albrecht, U. R.; Hahn, K.; Miguel-Lopez, A.; Schaffer, E.; Sanchez, S., Enzyme-Powered Hollow Mesoporous Janus Nanomotors. *Nano Lett* **2015,** *15* (10), 7043-50.